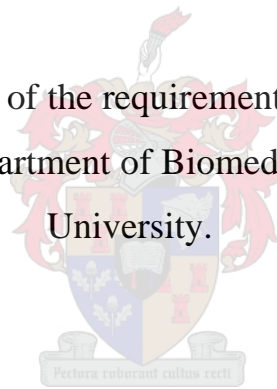


THE COMPARATIVE FUNCTIONAL ANATOMY OF THE  
FORELIMB IN TWO AFRICAN MOLE-RAT SPECIES,  
*BATHYERGUS SUILLUS* AND *HETEROCEPHALUS GLABER*

by

Narusa Suria Doubell

Thesis presented in fulfilment of the requirements for the degree of *Master of Science (Anatomy)* in the Department of Biomedical Sciences at Stellenbosch University.



Supervisor: Prof Sanet H. Kotzé

Co-supervisor: Dr Lauren Sahd

December 2021

## **DECLARATION:**

By submitting this thesis/dissertation electronically, I declare that the entirety of the work contained therein is my own, original work, that I am the sole author thereof (save to the extent explicitly otherwise stated), that reproduction and publication thereof by Stellenbosch University will not infringe any third-party rights and that I have not previously in its entirety or in part submitted it for obtaining any qualification.

Date: 31 Augustus 2021

## ABSTRACT

Different digging and communication methods are observed in various subterranean mole-rat species. Seismic signalling in the form of hind foot-drumming is the main communication method in most solitary mole-rat species, such as the scratch-digging *Bathyergus suillus*. The aim of the present study was to determine if hind foot-drumming and scratch-digging influence the morphology of the fore limb muscles in a drumming, scratch-digging species, *B. suillus*, belonging to the family Bathyergidae and a non-drumming, chisel-tooth digging species, *Heterocephalus glaber* belonging to the family Heterocephalidae. Furthermore, the secondary aim was to determine if somatosensory mechanisms that may be responsible for the detection of seismic signals could be identified histologically in the foot pads and lateral aspect of the feet in both species.

Four muscle architecture parameters were measured and compared in 40 formalin-fixed muscles from the right forelimb of each species (n=6). The composition of type I and II fibres as well as the glycolytic, oxidative glycolytic and oxidative fibres in 21 forelimb muscles were histochemically and immunohistochemically determined in six fresh *B. suillus* and six fixed *H. glaber* specimens. The densities of Pacinian corpuscles, Merkel cells, Ruffini corpuscles and Meissner corpuscles were determined within the footpads and the morphology of the robust hairs on the lateral aspect of the feet was described.

Muscles involved in the power stroke of digging had higher muscle mass percentage, force output and shortening capacity in *B. suillus* compared to *H. glaber*. Significantly higher percentages of glycolytic fibres were observed in the scapular elevators and digital flexors of *B. suillus*. These results suggest that the forelimb muscles involved in digging in *B. suillus* provide fast and powerful motions for effective burrowing. The *m. sternohyoideus* had significantly more oxidative fibres in *H. glaber* compared to *B. suillus*. Furthermore, the *m. sternocleidomastoideus* in *H. glaber* had significantly higher physiological cross-sectional area (PCSA) and fascicle length values compared to *B. suillus*. Regionalisation of type I and II fibres was observed in the *m. claviculo-scapularis* of *B. suillus* and *m. triceps brachii caput medialis* in *H. glaber*. Significantly higher densities of Meissner corpuscles in the drumming *B. suillus* suggests that this somatosensory mechanism in their footpads may be responsible for detecting seismic signals. The hairs on the lateral aspect of the feet did not have the typical follicle-sinus complex seen in sensory hairs. However, Merkel cells within the outer root sheath and the nervous tissue surrounding the hairs in both species are indicative of functioning either as tactile perception for movement in burrows or moving loosened soil around within the burrows.

In conclusion, the differences in the muscle architecture and muscle fibre typing between the two species may reflect adaptations for scratch-digging and production of seismic signals in *B. suillus*. Additionally, the muscle architecture and fibre type compositions in the neck muscles of *H. glaber* may point toward faster contractions for chisel-tooth digging. However, the phylogeny of the two species may also be responsible for these differences and not just behavioural demands such as hind foot-drumming and digging methods.

## OPSOMMING

Verskillende grawe en kommunikasie metodes is waargeneem in verskeie ondergrondse mol-rot spesies. Die doel van die huidige studie was om vas te stel of die produksie van seismiese seine en die gebruik van voorpote om te grawe, die morfologie in die spiere van die voorste ledemaat in twee mol-rot spesies beïnvloed. *Bathyergus suillus* is 'n drommende, alleenlopende mol-rot spesie, wat aan die Bathyergidae familie behoort en gebruik hoofsaaklik sy voorpote om tunnels te grawe. *Hetercephalus glaber* is 'n nie-drommende, eusosiale spesie wat aan die familie Heterocephalidae behoort en gebruik sy tande om tunnels te grawe. Die sekondêre doelwit was om die meganoreseptore in die voetsole te analiseer om vas te stel of 'n somatosensoriese meganisme verantwoordelik is vir die waarneming van seismiese seine. Daarbenewens is die laterale aspek van die voete ook ondersoek vir 'n moontlike somatosensoriese meganisme vir die waarneming van seismiese seine.

Vier spierargitektuur parameters is gemeet en vergelyk in 40 formalien-gefikseerde voorpoot spiere van elke monster (n=6). Die samestelling van tipe I en II spiervesels asook die glikolitiese, oksidatiewe glikolitiese en oksidatiewe spiervesel is histochemies en immunohistochemies bepaal in 21 spiere. Die samestelling van Paciniese korpusse, Merkel-selle, Ruffini-korpusse en Meissner -korpusse in die plantêre oppervlak van die voete is histologies bepaal en die morfologie van robuuste hare op die laterale aspek van die voete is beskryf.

Van die hoofspiere wat gebruik word om te grawe met die voorpote, het 'n hoër spiermassa persentasie, kragopbrengs en verkortings kapasiteit in *B. suillus* gehad, in vergelyking met *H. glaber*. Aansienlike hoër persentasies glikolitiese vesels is ook waargeneem in die skapulêre stabiliseerders en digitale fleksor spiere van *B. suillus*. Verder het die *m. sternocleidomastoideus* in *H. glaber* aansienlike hoër fisiologiese deursnee-oppervlakte (PCSA) en fassikellengte waardes gehad in vergelyking met *B. suillus*. Die opeenhoping van tipe I spiervesels in die dieper gedeeltes (regionalisation) van die spier is waargeneem in die *m. claviculo-scapularis* van *B. suillus* en *m. triceps brachii caput medialis* in *H. glaber*. Aansienlike hoër digtheid van Meissner-korpusse in *B. suillus* dui daarop dat hierdie somatosensoriese meganisme binne hul voete verantwoordelik kan wees vir die waarneming van seismiese seine. Die hare op die laterale aspek van die voete in beide spesies het nie die tipiese follikel-sinus-kompleks gehad wat tipies in sensoriese hare gevind word nie. Merkel-selle binne die buitenste wortelskede asook die senuweeweefsel rondom die hare in beide spesies dui op 'n tasbare funksie vir óf persepsie in hulle tunnels óf om losgemaakte grond in die gate rond te beweeg.

Ten slotte kan die verskille in die spierargitektuur en spierveseltipes tussen die twee spesies aanpassings weerspieël in *B. suillus* om met die voorpote te grawe en vir die vervaardiging van seismiese seine met hulle agterpote vir die vervaardiging van seismiese seine. Boonop kan die spierargitektuur en veseltipe samestellings in die nekspiere van *H. glaber* dui op vinniger kontraksies om te grawe met hulle tande. Die filogenie van die twee spesies kan egter ook verantwoordelik wees vir hierdie verskille en nie net gedragsvereistes soos agtervoet-trommel en grawemetodes nie.

## ACKNOWLEDGEMENTS

Firstly, and most importantly I want to thank God and give Him all the glory for giving me the strength, knowledge and patience to finish this research. Without Him I would not have been here.

Thank you to my supervisor, Prof. Sanet Kotzé, for all the guidance throughout my post-grad years. Thank you for giving me the opportunity to work under you and for all the learning experiences. A special thank you to my co-supervisor and friend, Dr. Lauren Sahn. Thank you for always being there for any and all questions I had, regardless of the day and time. I will always cherish our chats in the laboratory as we waited for our slides to incubate. I am grateful for all the emotional support and/or technical assistance I received from the following people: Reggie Williams, Chantelle Marais, Ruan Lochner, Arno Volschenk and Luke Daniels.

Thank you to Prof. Martin Kidd for all the help and patience with the statistics of my project. The financial assistance of the National Research Foundation (NRF) towards this research is hereby acknowledged. Opinions expressed and conclusions arrived at, are those of the author and are not necessarily to be attributed to the NRF.

## TABLE OF CONTENTS

ABSTRACT .....	iii
OPSOMMING .....	v
ACKNOWLEDGEMENTS.....	vii
FIGURES .....	x
TABLES .....	xiv
ADDENDA .....	xv
EQUATIONS .....	xvi
ABBREVIATIONS .....	xvii
1 INTRODUCTION.....	1
1.1 Research topic .....	1
1.2. Aim .....	1
1.3 Objectives.....	2
1.4 Hypothesis.....	2
2 LITERATURE REVIEW .....	4
2.1 Species .....	4
2.1.1 Phylogeny .....	4
2.1.2 Physical appearance .....	5
1.3 Habitat and ecology.....	7
2.1.4 Burrowing .....	8
2.1.6 Seismic signalling .....	9
2.2 Muscle architecture.....	10
2.2.1 Overview.....	10
2.2.2 Muscle architecture in various animals .....	13
2.3 Muscle fibre typing.....	14
2.4 Somatosensory mechanisms in the feet .....	19
2.4.1 General structure of mammalian skin .....	19
2.4.2 Cutaneous mechanoreceptors.....	19
2.4.2 Hair .....	22
3 MATERIALS AND METHODS.....	28
3.1 Sample information.....	28
3.2 Muscle architecture.....	28
3.2.1 Dissection .....	28
3.2.2 Muscle architecture measurements .....	29
3.2.3 Statistical analysis .....	32

3.2.4 Functional space plots .....	32
3.3 Muscle fibre typing.....	33
3.3.1 Specimen preparation.....	33
3.3.2 Staining methods.....	34
3.3.3 Morphometric and statistical analysis .....	36
3.4 Somatosensory mechanisms in the feet of <i>Bathyergus suillus</i> and <i>Heterocephalus glaber</i> .....	39
3.4.1 Sample preparation.....	39
3.4.2 Histochemical staining .....	40
3.4.3 Quantification of mechanoreceptors .....	41
3.4.4 Statistical analysis .....	44
3.4.5 Hairy skin on the lateral aspect of the manus and pes.....	44
4 RESULTS.....	45
4.1 Muscle architecture.....	45
4.1.1. Muscle architecture comparisons of muscle groups.....	45
4.1.2 Muscle architecture comparison of individual muscles .....	51
4.2 Muscle fibre typing.....	61
4.2.1 Slow myosin stain: Type I and II fibres .....	61
4.2.2 NADH and PAS stains: Oxidative, oxidative glycolytic and glycolytic fibres .....	68
4.3 Cutaneous mechanoreceptors .....	76
4.3.1 Merkel cell density .....	76
4.3.2 Ruffini corpuscles (RC) density.....	77
4.3.3 Meissner corpuscle (MC) density .....	77
4.3.4 Pacinian corpuscles .....	78
4.4 Sensory hairs .....	80
5 DISCUSSION.....	85
5.1 Muscle architecture and muscle fibre typing .....	85
5.2 Somatosensory mechanisms in the fore- and hind feet.....	90
5.2.1 Cutaneous mechanoreceptors.....	90
5.2.2 Sensory hairs.....	92
5.3 Limitations, strengths and future research .....	93
6 CONCLUSION.....	96
7 REFERENCES .....	98

## FIGURES

<b>Figure 2.1:</b> Genus-level phylogeny of Bathyergidae and Heterocephalidae that diverged into separate families ~31.2 Mya. (Drawn based on image of Seney <i>et al.</i> , 2009).....	5
<b>Figure 2.2:</b> <i>Bathyergus suillus</i> . Reproduced with permission from author (Bennett <i>et al.</i> , 2009).....	6
<b>Figure 2.3:</b> Digging chain of <i>Heterocephalus glaber</i> colony members. Reproduced with permission from photographer, J. O’Riain (Griffin, 2008). .....	7
<b>Figure 2.4:</b> Three main types of muscle. Skeletal muscle fibres may be orientated parallel to the force-generating axis (A, longitudinal architecture), at a fixed angle relative to the force-generating axis (B, pennate architecture), or at multiple angles relative to the force-generating axis (C, multipennate architecture), (drawn based on image from Lieber & Ward, 2011).....	11
<b>Figure 2.5:</b> Characterization of muscle fibre types of the fin whale ( <i>Balaenoptera physalus</i> ) according to the myosin heavy chain (MHC) isoform they express. Reproduced with permission from Journal of Experimental Biology (Rivero, 2018).....	17
<b>Figure 2.6:</b> Schematic depiction of four mechanoreceptors in the skin: Tactile/Meissner corpuscles, lamellated/Pacinian corpuscles, tactile discs/Merkel cells and Ruffini corpuscles. Permission to use image from website, Blausen.com (Blausen Medical, 2014). .....	20
<b>Figure 2.7:</b> Illustration of the general structure of a single hair unit. Permission to use image from website, Blausen.com (Adapted from Blausen Medical, 2014). .....	23
<b>Figure 2.8:</b> The various components of a hair follicle. Longitudinal section of a H&E-stained hair follicle (A) (Dartmouth.edu, 2021, used with permission from R. Swenson) and a cross-sectioned illustration of a hair follicle (B) (Drawn based on image from Dellmann & Eurell, 1998). .....	25
<b>Figure 2.9:</b> Diagrammatic illustration of the vibrissal structure (A) and H&E cross-section of vibrissal hairs located near the feet in mice (B). (Drawn based on image from Marotte <i>et al.</i> , 1992; Mutant Mouse Skin Database, 2021). .....	26
<b>Figure 3.1:</b> Slide layout for muscle fibre staining.....	34
<b>Figure 3.2:</b> The settings used on the Qupath interface for the detection of positively stained muscle fibres which appear white on the optical density sum image. ....	37
<b>Figure 3.3:</b> The Qupath interface showing the NADH staining with the settings used for the detection and classification of the muscle fibres. The polygon tool was used to quantify fibres within a specific area (yellow line).....	38
<b>Figure 3.4:</b> Lateral view of the pes of <i>Bathyergus suillus</i> , as representation of both species, with the red line indicating the skin with sensory hairs that were harvested and analysed. Scale bar=1 cm. ....	40
<b>Figure 3.5:</b> Plantar surface of the left foot of <i>Bathyergus suillus</i> (A) and the right foot of <i>Heterocephalus glaber</i> (B). Footpads were cut into a proximal, middle and distal section in <i>B. suillus</i> (A) and a proximal and distal section in <i>H. glaber</i> (B). Scale bars=5mm. ....	40
<b>Figure 3.6:</b> Qupath interface showing the measured length along the apical surface of the epithelium (yellow polyline) with the counting tool that is used to quantify the four different mechanoreceptors. ..	43

- Figure 4.1:** Mean ( $\pm$  standard deviation) of the angle of pennation (A) and maximum isometric force (B) of the muscle groups in *B. suillus* (blue) and *H. glaber* (orange). ..... 46
- Figure 4.2:** The muscle mass distribution of each muscle group to the total front limb muscle mass of *B. suillus* (blue) and *H. glaber* (orange). The summed muscle mass of all the individual muscles was used to calculate the total front limb mass. The muscle mass is expressed as percentages with the bars indicating the mean percentage of each muscle group. Biarticular muscles were included in more than one group (see Table 3.1). ..... 47
- Figure 4.3:** Physiological cross-sectional area, normalized to body mass (PCSA/Mb<sup>0.67</sup>) as a function of resting fascicle length normalized to body mass (Lf/Mb<sup>0.33</sup>) of the muscle groups in *B. suillus* (blue) and *H. glaber* (red). The force capability is represented by the horizontal dashed line (high-above line; low-below line), while the vertical dashed line separates muscles with high (right) and low (left) shortening capability. Muscles located in the upper right quadrant have both high force and high shortening capabilities and are therefore adapted for high-power outputs. .... 49
- Figure 4.4:** The mean ( $\pm$  standard deviation) architectural index of muscle fascicle length/muscle belly length (Lf/LM) for the proximal (A) and distal (B) individual muscles of *B. suillus* (blue) and *H. glaber* (orange). \* indicates a significant difference of  $p < 0.05$  between species. Muscle abbreviations as detailed in Table 4.2 and 4.3. .... 58
- Figure 4.5:** Physiological cross-sectional area, normalized to body mass (PCSA/Mb<sup>0.67</sup>) as a function of resting fascicle length normalized to body mass (Lf/Mb<sup>0.33</sup>) of all the individual muscles (A) and an enlarged representation of the lower left quadrant of panel A (B) for *B. suillus* (blue) and *H. glaber* (red). In panel A the force capability is represented by the horizontal dashed line (high-above line; low-below line), while the vertical dashed line separates muscles with high (right) and low (left) shortening capability. For panel B the muscles are shown separately from panel A to make referencing easier. Muscle abbreviations as detailed in Table 4.2 and 4.3. .... 60
- Figure 4.6:** The mean ( $\pm$  standard deviation) of the slow myosin composition (%) of individual muscles in *Bathyergus suillus* (blue) and *Heterocephalus glaber* (orange). ..... 62
- Figure 4.7:** The mean ( $\pm$  standard deviation) of the slow myosin composition (%) of muscle groups in *Bathyergus suillus* (blue) and *Heterocephalus glaber* (orange). Muscle group abbreviations: SE- scapular elevators/stabilisers/retractors; LR- limb retractors; EEX- elbow extensors; DF- digital flexors. .... 65
- Figure 4.8:** Regionalisation of muscle fibres (A-C) illustrated in the myosin heavy chain-stained *m. triceps brachii caput longum* of *Bathyergus suillus* (A; scale bar= 1 mm), *m. deltoideus pars scapularis* (B; scale bar=400  $\mu$ m) and *m. pectoralis superficialis* (C; scale bar= 500  $\mu$ m) in *Heterocephalus glaber*. Regionalisation in these three muscles were present in both species. .... 66
- Figure 4.9:** Myosin heavy chain-stained muscles displaying regionalisation (A & D) compared to muscles with no regionalisation (B & C) in *Bathyergus suillus* (A & C) and *Heterocephalus glaber* (B & D). *Musculus claviculo-scapularis* (A & B) with regionalisation of fibres in *B. suillus* (A; scale bar= 1mm) and no regionalisation in *H. glaber* (B; scale bar= 250  $\mu$ m). *Musculus triceps brachii caput*

<i>medialis</i> (C & D) with no regionalisation in <i>B. suillus</i> (C; scale bar= 1 mm) and regionalisation of fibres in <i>H. glaber</i> (D; scale bar= 400 $\mu$ m).....	67
<b>Figure 4.10:</b> Two serial sections of the <i>m. latissimus dorsi</i> of <i>Bathyergus suillus</i> (A & B) stained with MHCs (A) and NADH (B) illustrates that the MHC-positive fibres did not necessarily have a high oxidative capacity (darkly stained fibres with NADH) but were rather stained with a medium to dark intensity. Type I muscle fibre (I); oxidative fibres (O); oxidative glycolytic fibres (OG); glycolytic fibres (G). Scale bar= 200 $\mu$ m.....	68
<b>Figure 4.11:</b> Two serial sections of <i>m. latissimus dorsi</i> of <i>Bathyergus suillus</i> stained with MHCs with heat-induced epitope retrieval (A) and PAS (B). Type I muscle fibre (I). Scale bar= 100 $\mu$ m.....	69
<b>Figure 4.12:</b> Frozen NADH-stained (A; scale bar= 400 $\mu$ m) and fixed PAS-stained (B; scale bar=50 $\mu$ m) sections of <i>m. latissimus dorsi</i> of <i>Bathyergus suillus</i> (A & B). O- oxidative fibres (yellow); OG- oxidative glycolytic fibres (orange); G- glycolytic fibres (red).....	69
<b>Figure 4.13:</b> The mean percentages ( $\pm$ standard deviation) of the oxidative (A), oxidative glycolytic (B) and glycolytic (C) fibres in the individual muscles of <i>Bathyergus suillus</i> (blue) and <i>Heterocephalus glaber</i> (orange).....	71
<b>Figure 4.14:</b> The mean ( $\pm$ standard deviation) of the oxidative, oxidative glycolytic and glycolytic stained fibres as an indication of oxidative capacity in the functional muscle groups of <i>Bathyergus suillus</i> (blue) and <i>Heterocephalus glaber</i> (orange).....	75
<b>Figure 4.15:</b> General structure of Merkel cells in the forefeet of <i>Heterocephalus glaber</i> (A), Meissner corpuscle (B) and a Ruffini corpuscle (C) in the forefeet of <i>Bathyergus suillus</i> . Arrows= Merkel cells; Square= Meissner corpuscle; Oval= Ruffini corpuscle. Scale bars: A= 20 $\mu$ m; B= 50 $\mu$ m; C= 20 $\mu$ m.....	76
<b>Figure 4.16:</b> Total mechanoreceptor densities in the fore- and hindfeet of <i>Bathyergus suillus</i> and <i>Heterocephalus glaber</i> .....	77
<b>Figure 4.17:</b> Pacinian corpuscles (A and B) and peripheral nerve (C) observed in the glabrous skin of the distal sections of the hindfeet (A, C) and forefeet (B) in <i>Heterocephalus glaber</i> . Scale bars: A, B= 20 $\mu$ m; C= 50 $\mu$ m.....	78
<b>Figure 4.18:</b> Sections from the lateral aspect of the skin of the feet in <i>Bathyergus suillus</i> (A) and <i>Heterocephalus glaber</i> (B) stained with H&E. Multiple hair follicles observed in the pes of <i>B. suillus</i> (A) and a single hair follicle in the pes of <i>H. glaber</i> (B). Hair follicles indicated with arrows. Scale bars: A= 500 $\mu$ m; 200 $\mu$ m.....	80
<b>Figure 4.19:</b> Haematoxylin and Eosin (A) and Masson's trichrome (B) stain of a cross section of a sensory hair follicle in <i>Bathyergus suillus</i> with a sebaceous gland indicated in black. Scale bars= 20 $\mu$ m.....	81
<b>Figure 4.20:</b> Nervous tissue observed surrounding the hairs of the skin on the lateral aspect of the pes of <i>Bathyergus suillus</i> (A, B, D) and <i>Heterocephalus glaber</i> (C, E); stained with H&E. A hair follicle from the manus of <i>B. suillus</i> (B) surrounded by a single section of nervous tissue. Images D and E are	

enlarged sections from images A and C, respectively. Merkel cells are indicated by the arrows and accumulation of nerve tissue is indicated by the circles. Scale bars: A, D, E= 50µm; B, C= 100µm ..... 83

**Figure 4.21:** Haematoxylin and Eosin stain of a longitudinal section of a hair follicle on the lateral aspect of the hindfeet of *Bathyergus suillus* as representative of both species. Note the absence of a cavernous and ring sinus in between the outer root sheath and dermal capsule, which are both typically seen in sensory hairs. A= inner root sheath; b= outer root sheath; c= dermal capsule. Scale bar= 200 µm.

..... 84

## TABLES

<b>Table 3.1:</b> Information on the specimens, original ethical approval numbers, capture site and mean body mass for muscle architecture ( $\pm$ standard deviation). .....	28
<b>Table 3.2:</b> List of muscle function groups.....	31
<b>Table 3.3:</b> Inclusion criteria for the quantification of the four mechanoreceptors in <i>Bathyergus suillus</i> and <i>Heterocephalus glaber</i> . .....	42
<b>Table 4.1:</b> The analysis of covariance (ANCOVA) results of the comparisons of the muscle groups between species. ....	50
<b>Table 4.2:</b> The mean and standard deviation ( $\pm$ ) of the architecture parameters of the front limb muscles of <i>Bathyergus suillus</i> .....	52
<b>Table 4.3:</b> The mean and standard deviation ( $\pm$ ) of the architecture parameters of the front limb muscles of <i>Heterocephalus glaber</i> .....	54
<b>Table 4.4:</b> The analysis of covariance (ANCOVA) results of the comparisons of the individual muscles between species. ....	56
<b>Table 4.5:</b> The mean percentage and standard deviation ( $\pm$ ) of the type I and type II fibres in the individual muscles of <i>Bathyergus suillus</i> and <i>Heterocephalus glaber</i> . .....	63
<b>Table 4.6:</b> The mean percentage and standard deviation ( $\pm$ ) of the type I and type II fibres in the muscle groups of <i>Bathyergus suillus</i> and <i>Heterocephalus glaber</i> .....	64
<b>Table 4.7:</b> The mean percentage and standard deviation ( $\pm$ ) of the oxidative, oxidative glycolytic and glycolytic stained fibres in the individual muscles of <i>Bathyergus suillus</i> and <i>Heterocephalus glaber</i> ....	73
<b>Table 4.8:</b> The mean percentage and standard deviation ( $\pm$ ) of the oxidative, oxidative glycolytic and glycolytic stained fibres in the individual muscles of <i>Bathyergus suillus</i> and <i>Heterocephalus glaber</i> ....	74
<b>Table 4.9:</b> Average mechanoreceptor densities ( $\pm$ standard deviation) quantified in the footpads of <i>Bathyergus suillus</i> (BS) and <i>Heterocephalus glaber</i> (HG).....	79

## ADDENDA

<b>Addendum A:</b> Slow myosin immunohistochemical staining procedure .....	116
<b>Addendum B:</b> NADH staining protocol .....	117
<b>Addendum C:</b> Periodic Acid Schiff (PAS) staining protocol .....	118
<b>Addendum D:</b> Masson's Trichrome staining protocol.....	119
<b>Addendum E:</b> Histological processing protocol .....	121
<b>Addendum F:</b> Plagiarism report.....	122

## EQUATIONS

Equation 1:  $PCSA (mm^2) = [MM (g) * \cos\theta] / [Lf (mm) * \rho (g/mm^3)] \dots\dots\dots 12$

## ABBREVIATIONS

ADV	<i>M. abductor digiti V</i>	EP	<i>M. extensor pollicis</i>
AI	architectural index	FCR	<i>M. flexor carpi radialis</i>
ANCOVA	analysis of covariance	FCU	<i>M. flexor carpi ulnaris</i>
ANOVA	analysis of variance	FDP	<i>M. flexor digitorum profundus</i>
APL	<i>M. abductor pollicis longus</i>	FDPU	<i>M. flexor digitorum profundus</i> (ulnar head)
ATPase	adeno-triphosphatase	FDS	<i>M. flexor digitorum superficialis</i>
BB	<i>M. biceps brachii</i>	FL	fibre length
Br	<i>M. brachialis</i>	FSC	follicle-sinus complex
CAS	Chemical Abstracts Service	GPDH	glyceraldehyde 3-phosphate dehydrogenase
CB	<i>M. coracobrachialis</i>	H&E	Haematoxylin and Eosin
CE	Carpal extensors	HH	Head extensors and hyoid bone depressors
CF	Carpal flexors	HIER	heat induced epitope retrieval
DA	<i>M. deltoideus pars acromialis</i>	IF	<i>M. infraspinatus</i>
DAB	diaminobenzidine tetrahydrochloride	LD	<i>M. latissimus dorsi</i>
DB	Digital abductors	L <sub>f</sub>	fibre length
DC	<i>M. deltoideus pars clavicularis</i>	L <sub>M</sub>	muscle length
DEX	Digital extensors	LP	Limb protractors
DF	Digital flexors	LR	Limb retractors
DS	<i>M. deltoideus pars scapularis</i>	LSD	Least Significant Difference
ECD	<i>M. extensor digitorum communis</i>	m	meter
ECR	<i>M. extensor carpi radialis</i>	M <sub>b</sub>	body mass
ECU	<i>M. extensor carpi ulnaris</i>	MCs	Meissner corpuscles
EE	Elbow extensors		
EF	Elbow flexors		

MHC	Myosin heavy chain	SDH	succinate dehydrogenase
ML	muscle length	SDS-PAGE	Sodium dodecyl sulfate-polyacrylamide gel electrophoretic
mm	millimeter	SE	Scapular elevators/stabilizers/retractors
Mya	Million years ago	SH	<i>M. sternohyoideus</i>
NADH	nicotinamide adenine dinucleotide, reduced disodium salt hydrate	SS	<i>M. supraspinatus</i>
NCL	NovoCastra Lyophilized	Su	<i>M. supinator</i>
ORO	oil red O	SuS	<i>M. subscapularis</i>
OT	<i>M. omotransversarius</i>	SV	<i>M. serratus ventralis</i>
P	Pronators	TBS	tris-buffered saline
PAS	periodic acid-Schiff	TFA	<i>M. tensor fasciae antebrachium</i>
PCs	Pacinian corpuscles	TLa	<i>M. triceps brachii caput laterale</i>
PCSA	physiological cross-sectional area	TLo	<i>M. triceps brachii caput longum</i>
PL	<i>M. palmaris longus</i>	TM	<i>M. teres major</i>
PS	<i>M. pectoralis superficialis</i>	TMe	<i>M. triceps brachii caput mediale</i>
PT	<i>M. pronator teres</i>	TPC	<i>M. trapezius pars cervicales</i>
RA	rapidly adapting	TPT	<i>M. trapezius pars thoracica</i>
RC	<i>M. rhomboideus cervicis</i>	TRIS	trisaminomethane
RCa	<i>M. rhomboideus capitis</i>	⊖	pennation angle
RCs	Ruffini corpuscles	ρ	muscle density
S	Supinators		
SA	slowly adapting		
SB	<i>M. subclavius</i>		
SC	<i>M. claviculo-scapularis</i>		
SCM	<i>M. sternocleidomastoideus</i>		

# 1 INTRODUCTION

## 1.1 Research topic

The musculoskeletal anatomy of various subterranean rodent species has been described in various studies. Multiple authors have suggested that species-specific behaviours such as hind foot-drumming, chisel-tooth digging and scratch-digging, may influence the morphology of their limbs (Lehmann, 1963; Hildebrand, 1985; Fransescoli, 2000; Rose, Sandefur, Huskey, Demler & Butcher, 2013; Sahd, Doubell, Bennett & Kotzé, 2021). The two mole-rat species in the present study, *Bathyergus suillus* and *Heterocephalus glaber*, are species with different sociality, phylogenetic family, digging and communication methods. *Bathyergus suillus* is a solitary species that produce seismic signals to communicate (hind foot-drumming) and uses its forelimbs to burrow (scratch-digging; Bennett & Jarvis 1988; Bennett, Faulkes, Hart & Jarvis, 2009). *Heterocephalus glaber* is a eusocial species that communicates through tactile or touch signalling (non-drumming) and uses its incisors to burrow (chisel-tooth digging; Jarvis, 1981; Pepper, Braude, Lacey & Sherman, 1991; Jarvis & Sherman, 2002). The qualitative morphology of the forelimb in both of these species has been previously described (Doubell, Sahd & Kotzé, 2020), however quantitative research on their forelimbs remains underreported. The current research project will focus on the muscle architecture and fibre type composition of the muscles in the forelimb of *B. suillus* and *H. glaber*. The results may reveal if the differences between the two species are a result of their different digging and communication methods or due to phylogenetic differences. Furthermore, somatosensory mechanisms, such as mechanoreceptors and sensory hairs, within the footpads of the feet and the hairy skin on the lateral aspect of the feet will be histologically analysed. Significant differences may indicate a somatosensory mechanism for the detection of seismic signals within the feet of *B. suillus* or *H. glaber*.

## 1.2. Aim

The aim of the study is to provide quantitative data on the muscles in the forelimb of two African mole-rat species, *Bathyergus suillus* and *Heterocephalus glaber*. Muscle architecture as well as the fibre type composition within the muscles will be analysed which may reflect adaptations for digging behaviour within the species, scratch-digging and chisel-tooth digging respectively. Furthermore, the footpads of the fore- and hindfeet and row of coarse hairs on the lateral edges of the manus and pes will be analysed histologically in order to determine possible adaptations for the detection of seismic signals or for tactile perception.

### 1.3 Objectives

- Muscle architecture of 40 muscles in the forelimb and neck will be analysed by measuring the following parameters: fascicle length, pennation angle, muscle mass, physiological cross-sectional area (PCSA) and maximum isometric force. Some of these parameters will be scaled and compared to each other within and between predetermined functional muscle groups.
- Different types of muscle fibres in each muscle will be determined histologically by performing a slow-myosin immunohistochemical staining protocol to visualise the type I fibres and the NADH and PAS staining protocols, which are metabolic stains and will indicate the oxidative capacity of the fibres. These results will be calculated as percentages of the total fibre types within the specific muscles and muscle groups. This data will be compared between species and will further reflect the functionality of the various muscles and muscle functional groups with regards to possible adaptations for scratch-digging and/or stabilisation for hind foot-drumming (*B. suillus*) and stabilisation for chisel-tooth digging (*H. glaber*).
- The footpads of the forefeet in *B. suillus* and both the fore- and hindfeet in *H. glaber* will be stained using three different staining protocols: H&E and Masson's trichrome. Mechanoreceptor densities in the footpads will be an indication of a somatosensory mechanism present for detection of seismic signals. Additionally, H&E staining will be performed on the hairy skin of the lateral aspect of the feet to determine if the row of robust hairs have a somatosensory mechanism for the detection of seismic signals.

### 1.4 Hypothesis

Hypothesis: The morphology of the forelimb muscles in *Bathyergus suillus* reflects adaptations for scratch-digging. Additionally, the footpads will reveal somatosensory mechanisms for the detection of seismic signals.

The morphology of the forelimb in *Heterocephalus glaber* does not reflect adaptations for scratch-digging and hind foot-drumming, but rather chisel-tooth digging within the neck muscles. Additionally, the footpads will reflect a lack of somatosensory mechanisms for detection of seismic signals in the non-drumming *H. glaber*.

Null hypothesis: Both *B. suillus* and *H. glaber* will have similar forelimb and footpad morphology. The scratch-digging behaviour and the detection of seismic signals in *B. suillus* are not reflected in its forelimb and footpad morphology while chisel-tooth digging, and the

absence of seismic signalling is not reflected in the forelimb and footpad morphology of *H. glaber*.

## 2 LITERATURE REVIEW

### 2.1 Species

#### 2.1.1 Phylogeny

Mole-rats are burrowing rodents that permanently live underground with some species going above ground to forage for food. These mammals belong to the Old World hystricomorph suborder within the Rodentia order (Bennett & Faulkes, 2000). The general morphology of mole-rats reflects adaptations for life in a subterranean habitat. For example, their cylindrical bodies allow them to move within their narrow and confined burrow system (Hildebrand, 1985; Fransescoli, 2001). The eyes in subterranean rodents have regressed, with the eye diameter reduced to only around 2mm in pocket gophers, due to the fact that vision becomes less useful in their subterranean habitat (Hildebrand, 1985).

*Bathyergus suillus* and *Heterocephalus glaber* belong to the same phylogenetic family, Bathyergidae, also called African mole-rats. However, recent studies on the phylogeny and biogeography of *H. glaber* place this species into a separate family of hystricomorphs, Heterocephalidae (Patterson & Upham, 2014; Patterson, 2016; Tavares & Seuánez, 2018; Burgin, Colella, Kahn & Upham, 2018; D'Elia, Fabre & Lessa, 2019). In the early Oligocene (31.2 Mya), *H. glaber* diverged from the other African mole-rats and evolved independently. Further research revealed multiple cranial, dental, postcranial, external, and ecological characters that differentiates *Heterocephalus* from the other bathyergids (Figure 2.1; Patterson & Upham, 2014). Externally, the body of *H. glaber* is nearly hairless (vs. other African mole-rats that are hairy), and an ear conch is absent (vs. some mole-rats that have remnants of an ear conch); the tail is longer than the hindfoot (vs. tail always shorter than hindfoot), the third digit of the manus is longer than digit four (vs. always shorter). Cranial characteristics include a palate that does not extend behind molars and is not extremely constrained between the cheek-teeth, and both or either of the upper or lower molars are present (Ellerman, 1940; De Graaff 1971; Woods, 1984). Postcranially *H. glaber* lacks papillae within their colonic groove, the caecum is uncoiled and they have an unlooped ascending colon (Kotzé, Van der Merwe, Ndou, O'Riain & Bennett, 2009; Kotzé, Van der Merwe, Bennett & O'Riain 2010). These features as well as their lack of pain-related neuropeptides (Park *et al.*, 2008) and resistance to cancer (Seluanov *et al.*, 2009) distinguish them further from other Bathyergids. The magnitude of these autapomorphies (distinct feature unique to a taxon) accentuates its distinction from other African mole-rats (Patterson & Upham, 2014).

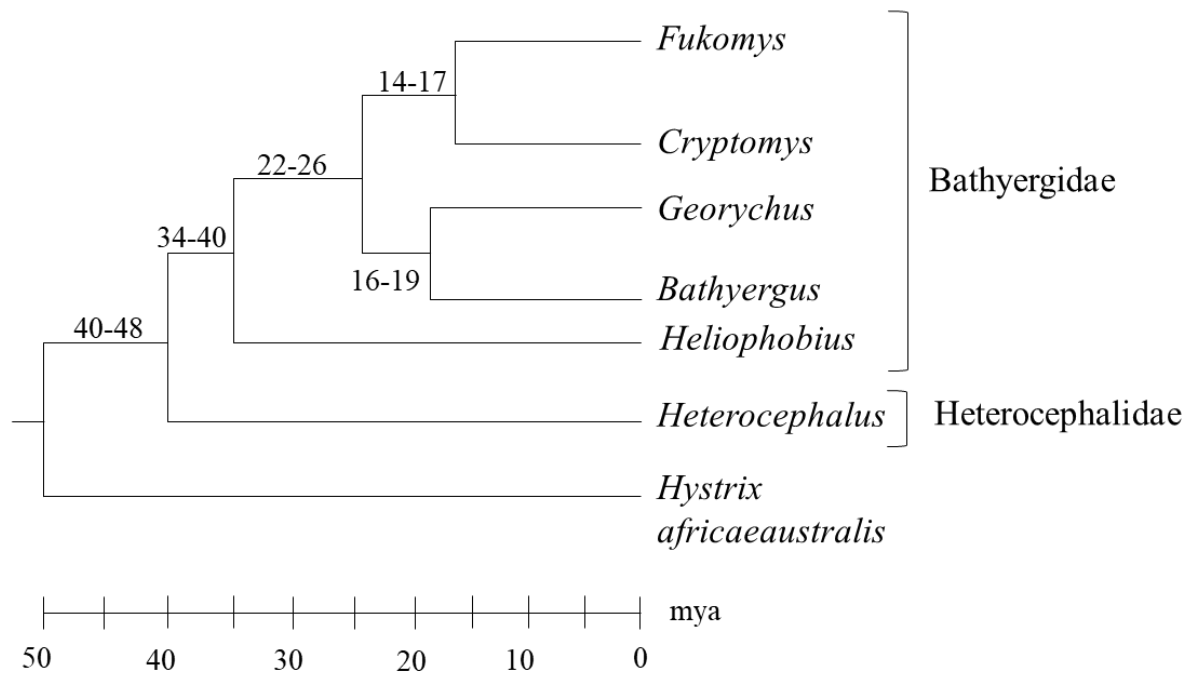


**Figure 2.1:** Genus-level phylogeny of Bathyergidae and Heterocephalidae that diverged into separate families ~31.2 Mya. (Drawn based on image of Seney *et al.*, 2009)

### 2.1.2 Physical appearance

*Bathyergus suillus* (Cape dune mole-rat) is one of two species belonging to the *Bathyergus* genus and is the largest African mole-rat, weighing up to 2kg (Jarvis, 1969; Bennett *et al.*, 2009; Davies & Jarvis, 1986). Their average head and body measurements of the males and females are 311 mm and 305 mm, respectively (Hart, Chimimba, Jarvis, O’Riain & Bennett, 2007). The Cape dune mole-rat has a cinnamon-brown dorsal pelage and grey ventral pelage with beige to white patches on the snout and around the eyes and ears (Bennett *et al.*, 2009) (Figure 2.2). They have small, black eyes with a cylindrical torso and short, stout limbs with prominent claws on the forefeet that they use to excavate their burrowing systems (Skinner & Smithers 1990; Bennett *et al.*, 2009).



**Figure 2.2:** *Bathyergus suillus*. Reproduced with permission from author (Bennett *et al.*, 2009).

*Heterocephalus glaber* has wrinkled skin that is a brown pinkish colour with pale-coloured hairs scattered across its body and tail (Nowak & Paradiso, 1983). The body mass of adults ranges from 30 to 50 grams with no sexual dimorphism between males and females (Jarvis, 1978). During digging they use their white, ungrooved incisors as the main digging apparatus to burrow (Jarvis, 2002). Their procumbent incisors and naked-like appearance are depicted in Figure 2.3.



**Figure 2.3:** Digging chain of *Heterocephalus glaber* colony members. Reproduced with permission from photographer, J. O’Riain (Griffin, 2008).

### 1.3 Habitat and ecology

*Bathyergus suillus* is found in the coastal regions of the Cape Peninsula in South Africa, in the southwestern parts of the Western Cape Province (Skinner & Smithers, 1990; Bennett & Faulkes, 2000). They are found in mesic regions with sandy soils and are found in areas with an altitude less than 300m above sea level (De Graaff, 1981) with a high annual rainfall (>500mm).

Naked mole-rats are endemic to dry regions of eastern Africa that has high temperatures and irregular rainfall (200-400mm/year; Brett, 1991). These regions include central Ethiopia, most of Somalia and the northern and eastern parts of Kenya (Meester & Setzer, 1971; Honeycutt, Allard, Edwards & Schlitter, 1991). *Heterocephalus glaber* is found most frequently in hard, compact, lateritic soils but prefer living in soft and sandy soils. The *H. glaber* colonies inhabiting lateritic soils have difficulty digging and constructing burrows due to large amounts of quartz and crystalline material found within the soil. During dry seasons, the soft soils that some colonies live in, become hard, only softening after rain. With these areas having an irregular rainfall, it would make foraging and burrowing difficult for these eusocial animals (Jarvis & Bennett, 1991; Brett, 1993).

#### 2.1.4 Burrowing

*Bathyergus suillus* use their well-developed claws and short front limbs to dig their burrow systems or to loosen soil within their burrows (Bennett & Faulkes, 2000). The Cape dune mole-rat starts burrowing after rains when the soil is moist and easily workable. They are scratch-diggers and use their short forelimbs with well-developed claws to loosen the soil. After loosening the soil, they use their forefeet to sweep the soil underneath their bodies and push it behind them with their hindfeet. The pile of loosened soil behind the mole-rat is then pushed along the burrow and expelled onto the surface to form a molehill (Genelly, 1965; Jarvis & Sale, 1971; Bennett & Faulkes, 2000). This solitary species rarely leave their burrows, therefore their tunnels are completely sealed and can stretch between 50 and 420 metres (Davies & Jarvis, 1989).

*Heterocephalus glaber* is a chisel-tooth digger and use its procumbent incisors to burrow, and does not use its forefeet like *B. suillus* (Genelly, 1965; Jarvis & Sale, 1971; Bennett & Faulkes, 2000). The burrow systems they excavate are more extensive and longer compared to *B. suillus*, with burrows sometimes exceeding 3km (Brett, 1991). During the digging process the members of a colony form digging chains where the soil is swept backwards along the burrow, after the first individual loosened or gnawed the soil at the blind end of a tunnel (Figure 2.3). The loosened soil is moved by the last individual of the chain, onto the surface where it creates a volcano-shaped mound with a hole in the centre (Jarvis & Sale, 1971; Braude 1991). Thereafter, the colony quickly seals the volcano hole to avoid predators such as snakes and driver ants from having access into their burrows (Brett 1991; Braude, Schilder & Muli, 1999).

#### 2.1.5 Sociality

The social organization of a species is defined as the tendency of animals to associate in social groups or form cooperative societies and is considered a survival response to evolutionary stresses such as competition, predation and climate change (Smelser & Baltes, 2001). The sociality in subterranean animals is not a consequence of their subterranean niche as much as the niche imposing similar constraints on the animals (Nevo, 1979). Therefore, the degree of sociality is a result of the divergent, convergent or parallel evolutionary histories amongst the various animals. The spectrum of sociality exhibited by the family Bathyergidae is of interest due to the fact that it ranges from strictly solitary to cooperative breeding and eusociality (Jarvis & Bennett, 1991; Bennett & Faulkes, 2000). Cape dune

mole-rats are solitary animals and individual adults inhabit extensive burrow systems that are much longer and less branched, than other bathyergids (Davies & Jarvis, 1986; Bennett & Faulkes, 2000).

*Heterocephalus glaber* is an eusocial burrowing rodent which is characterised by three criteria namely, labour is reproductively divided, overlapping of generations and cooperative caring of the young (Jarvis, 1981; Jarvis & Bennett, 1993). Their colonies consist of an average of 80 animals and have the largest colony of all the members of Bathyergidae. Within each colony there is one female, the queen, and two to three males that are reproductively active (Jarvis, 1981; Faulkes, Abbott & Jarvis, 1991; Faulkes & Abbott, 1997). The rest of the colony consist of members of both sexes, subordinates, that do not participate in reproduction but provide structured support in burrowing, foraging, defending the colony and taking care of the queen's pups (Faulkes, Abbott & Jarvis, 1991; Faulkes & Abbott, 1997).

#### **2.1.6 Seismic signalling**

Behavioural and ecological specialisations of species can include specific eating behaviour, locomotion and communication between individuals of both conspecific and heterospecific species. Communication methods include seismic signalling where the individuals convey information by creating vibrations by drumming or striking a part of the body on the ground, or by producing low frequency vocalisations (Bennett & Jarvis, 1988; Mason & Narins, 2001; Randall, 2001). In fossorial animals such as mole-rats, the subterranean environment is not favourable for the use of vision or producing airborne sounds as a means of long-distance perception and communication. Furthermore, due to the aggressive nature of some solitary fossorial species, seismic signals are produced to avoid conflict and burrowing in overlapping areas between intraspecific individuals (Mason & Narins, 2001). Therefore, most of the subterranean rodent species produce seismic vibrations by repeatedly striking the ground with their feet, head or teeth to communicate within their burrow systems. The two African mole-rat species studied here differ in the methods of seismic signalling they use to communicate. Hind foot-drumming occurs in the solitary *Bathyergus suillus* with the males drumming at higher speeds compared to the females (Jarvis, 1969; Jarvis & Bennett, 1991). Detection of these seismic signals produced by hind foot-drumming in *B. suillus* remains unproven. A few authors suggest that somatosensory pathways, such as lamellated receptors in the feet are responsible for signal detection of hind foot-drumming, especially in scratch-digging species where the limbs are used for burrowing (Fransescoli, 2000; Mason & Narins, 2001). In the

eusocial species, *Heterocephalus glaber*, hind foot-drumming does not occur. Within the burrow system of this eusocial species, the colony members are constantly in close proximity and therefore long-distance communication might not be needed between individuals. Instead, low-frequency vocalisations are produced by this species (Bennett & Jarvis, 1988; Pepper *et al.*, 1991).

## **2.2 Muscle architecture**

### **2.2.1 Overview**

Skeletal muscle architecture is defined as the macroscopic arrangement of muscle fibres within a muscle relative to the axis of force generation. Furthermore, muscle architecture is a determinant and reflection of the muscle function as well as the force by which the muscle contracts and are both important for understanding the structure-function relationship of muscles (Sacks & Roy, 1982; Lieber & Fridén, 2000; Eng, Smallwood, Rainiero, Ward & Lieber, 2008; Rupert, Rose, Organ & Butcher, 2015). There are three main types of architectural arrangements that are used to describe skeletal muscle fibre arrangements: parallel/longitudinal, unipennate or multipennate muscle architecture (Figure 2.4; Lieber & Fridén, 2000; Lieber & Ward, 2011). While a combination of these designs may occur within a muscle, they are inclined towards only one type of architecture (Lieber & Ward, 2011).

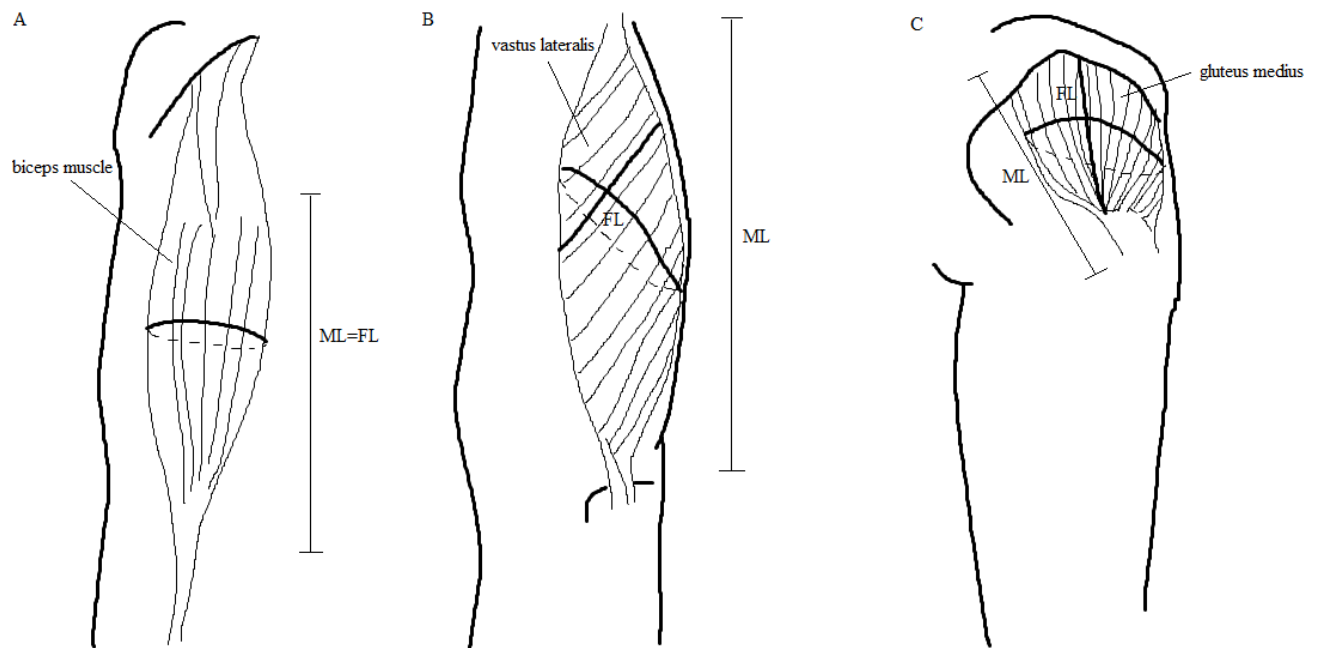


**Figure 2.4:** Three main types of muscle. Skeletal muscle fibres may be orientated parallel to the force-generating axis (A, longitudinal architecture), at a fixed angle relative to the force-generating axis (B, pennate architecture), or at multiple angles relative to the force-generating axis (C, multipennate architecture), ML-muscle length, FL-fibre length (drawn based on image from Lieber & Ward, 2011).

In order to analyse muscle architecture, multiple parameters are required which includes muscle length ( $L_M$ ), fibre length ( $L_f$ ), pennation angle (fibre angle relative to the force-generating axis,  $\theta$ ), and physiological cross-sectional area (PCSA) (Gans & Bock, 1965; Gans & De Vries, 1987). The pennation angle is measured by determining the angle between the force-generating axis and the muscle fibres on the superficial muscle surface (Lieber & Fridén, 2000).

Fibre length is described as the distance between the origin of the most proximal muscle fibres and the insertion of the most distal muscle fibres (Lieber, 1992). According to various studies the muscle fibre length is directly proportional to the muscle excursion (the displacement of the myotendinous junction throughout the range of motion). A longer muscle fibre will have a larger number of serial sarcomeres that acts as a single muscle fascicle when activated, which leads to higher maximum muscle velocity and ultimately permits a greater muscle excursion (Bodine, Roy, Meadows, Zernicke, Sacks, Fournier & Edgerton, 1982; Winters, Takahashi, Lieber & Ward, 2010; Lieber & Ward, 2011). Most studies report resting muscle fibre fascicle length and not the fibre length (Lieber & Fridén, 2000; Moore, Budny, Russell & Butcher, 2013; Rupert *et al.*, 2015; Olson, Womble, Thomas, Glenn & Butcher, 2016). This is due to muscle fibres terminating end to end and not running the length of the

entire muscle belly, making the methodology of fibre measuring extremely challenging (Lieber & Fridén, 2000). However, muscle fascicles contain multiple fibres and act as single functional units which can be easily visualised and analysed using macro dissection and imaging software.

After the parameters mentioned above are measured, the physiological cross-sectional area (PCSA) is calculated using the equation described by Sacks and Roy (1982); Charles, Cappellari, Spence, Hutchinson & Wells (2016). The PCSA is the sum of the cross-sectional areas of all the muscle fibres within the muscle and is also directly proportional to the maximum isometric force capacity of a muscle (Powell, Roy, Kanim, Bello & Edgerton, 1984; Lieber & Fridén, 2000). Mathematically PCSA is calculated using Equation 1:

$$\text{Equation 1: } PCSA (mm^2) = [MM (g) * \cos\theta] / [Lf (mm) * \rho (g/mm^3)]$$

The muscle density is  $0.0010597 \text{ g}\cdot\text{mm}^{-3}$  which is a constant for mammalian skeletal muscle density determined by Mendez & Keyes (1960) and Ward & Lieber (2005). As previously discussed, muscle fascicle length is directly proportional to the muscle excursion while PCSA is directly proportional to the maximum isometric force of the muscle. The isometric force-velocity relationship suggests that a higher shortening velocity would lead to lower force production. As the velocity increases from zero to a finite number, the probability of actin-myosin crossbridge interaction decreases which ultimately leads to decreased muscle force. Therefore, muscles with high shortening velocities do not produce high forces (Lieber & Ward, 2010).

The maximum isometric force of the muscle can be calculated by multiplying the PCSA with a conversion factor of  $22.5 \text{ N}\cdot\text{m}^{-2}$ . This is the value that has been experimentally verified as a constant for the tension of normal mammalian muscle (Lieber & Fridén, 2000; Arnold, Ward, Lieber & Delp, 2010). The maximum isometric force of the muscle is an indicator of the functional performance of a muscle (Moore *et al.*, 2013). Therefore, a high PCSA and long fascicle length would be indicators of a powerful muscle (Lieber & Ward, 2011). Muscle fibre size has also been suggested as a factor that determines the force production of a muscle. However, it has been shown that there is little to no variation in muscle fibre size between muscles. Force production is better predicted by the architectural differences between muscles (Lieber & Fridén, 2000).

### 2.2.2 Muscle architecture in various animals

Anatomical analyses of the forelimb in scratch-digging mammals and more specifically subterranean scratch-digging rodents, have described large and powerful muscles with skeletal adaptations to provide mechanical advantage for the excavation of soil. Musculoskeletal adaptations for scratch-digging burrowing rodents include robust humeri, the *m. triceps brachii* heads attaching to an elongated olecranon process, robust digital and carpal flexors and prominent and long claws which all provide mechanical advantage for the power-stroke during scratch-digging (Lehmann, 1963; Hildebrand, 1985; Lessa & Stein, 1992; Fransescoli, 2000; Morgan & Verzi, 2011). However, according to Lieber & Ward (2011) muscle size (mass and volume) is not an accurate predictor of the functional properties of a muscle. Therefore, quantifying the muscle architecture in addition to the muscle size of the forelimb muscles would provide more accurate results regarding the function-structure relationship of the muscles.

In the forelimbs of scratch-digging mammals such as badgers (*Taxidea taxus*; Moore *et al.*, 2013) and armadillos (*Dasypus novemcinctus*; Olson *et al.*, 2016) the humeral retractors and elbow extensors are the largest functional groups according to their muscle mass, which reflects the powerful stroke motions during scratch-digging. In badgers (Moore *et al.*, 2013) a proximal-to-distal increase in muscle mass of the forelimb was seen in comparison with cursorial mammals such as the hare (Williams, Payne & Wilson, 2007) and the horse (Brown, Kawcak, McIlwraith & Pandy, 2003), where there is a reduction in proximal-to-distal muscle mass. According to Zajac (1992) muscles that are specialised to produce high forces usually have a pennate fibre architecture with a high PCSA to muscle mass ratio. Alternatively, muscles with a parallel fibre structure and long fibres, have a greater capacity of shortening and producing high forces over a large range of joint motion (Peters & Rick, 1977; Zajac, 1992).

Muscles involved in the power stroke during scratch-digging typically have a high PCSA value. For example, the long head of *m. triceps brachii* in various scratch-digging mammals, has a high PCSA which provides greater forces for digging (Moore *et al.*, 2013; Rose, Sandefur, Huskey, Demler & Butcher, 2013; Rupert *et al.*, 2015; Olson *et al.*, 2016). In burrowing rodents such as the Eastern mole (*Scalopus aquaticus*; Rose *et al.*, 2013) and the groundhog (*Marmota monax*; Rupert *et al.*, 2015) the carpal and digital flexors have a high PCSA to muscle mass ratio, allowing for high force production through the digits and resistance to overextension of the carpal joints in order to excavate the soil.

### 2.3 Muscle fibre typing

Muscle fibres are generally classified according to their metabolic activity as type I, IIA, IIB and IIX (Brooke & Kaiser, 1970; Eng, Smallwood, Rainiero, Lahey, Ward & Lieber, 2008; Talbot & Maves, 2016). Type I fibres are slow-contracting fibres, resistant to fatigue, with a high mitochondrial density and an oxidative metabolism. Types IIX and IIB are fast-twitch fibres reliant on anaerobic glycolysis to metabolise glucose but type IIB has a lower fatigue resistance compared to type IIX. Type IIA fibres are fast oxidative glycolytic fibres and represent a hybrid fibre type of type I and IIB fibres but with a higher mitochondrial density (Peter, Barnard, Edgerton, Gillespie & Stempel, 1972; Talbot & Maves, 2016). Furthermore, each fibre type expresses a specific myosin heavy chain (MHC) gene and hybrid MHC expression can result in subtypes of muscle fibres such as I/IIA or IIA/IIX with some expressing predominance for one of the two MHCs forming the hybrid fibre type. For example, a hybrid fibre co-expressing MHC I and IIA, can have a predominance of MHC-IIA on MHC-I or a dominance of MHC I versus MHC IIA (Rivero, 2018). Multiple components determine the fibre type identities and not just the metabolic properties of a muscle fibre (Talbot, & Maves 2016). Therefore, combining muscle fibre type composition and other muscle components such as muscle architecture can contribute to the understanding of muscle function (Eng *et al.*, 2008).

The metabolic properties and MHC's can be detected or visualised in order to identify muscle fibre types within a specific muscle. Sodium dodecyl sulphate-polyacrylamide gel electrophoretic (SDS-PAGE) separation of MHC isoforms is a more direct method of acquiring the fibre type percentages within a muscle (Figure 2.5 A, B). However, due to the high costs of this method when having a large sample size, histological methods are used for fibre typing. Several fibre typing methods can be applied to acquire the fibre type composition within a muscle. Myosin adeno-triphosphatase (ATPase) histology tests the sensitivity of each myosin ATPase on myosin heavy chains (MHC) to pH pre-incubation (Figure 2.5 G; Song, Ahn & Kim, 2019). Furthermore, two or more muscle fibre types can be subdivided according to different activities of the metabolic enzymes in muscles, such as succinate dehydrogenase (Figure 2.5 I), used as an oxidative indicator and glycerol-3-phosphate dehydrogenase (Figure 2.5 J), used as a glycolytic indicator (Martin *et al.*, 1985; Blanco *et al.*, 1988). Enzyme activities are required for these methods and therefore biopsies or fresh tissue samples (from post-slaughtered specimens) are needed.

When tissue undergoes fixation, all biological processes, including enzyme activities, are terminated. Therefore, any histological technique that identifies muscle fibre types according to its metabolic enzyme activities, cannot be applied to formalin fixed tissue. Intracellular lipid droplets and glycogen particles are stored within skeletal muscle. These two substances can be measured in order to differentiate between fibre types by using histochemical methods. The oil red O (ORO) and periodic acid-Schiff (PAS) stains are the most common histology stains used to assess skeletal muscle lipid and glycogen stores (Prats, Gomez-Cabello, Nordby, Anderson, Helge, Dela, Baba & Ploug, 2013). It is important to note that these histology stains can also be applied on fresh tissue, however due to the development of more accurate fibre type classification methods, such as immunohistochemistry techniques (see below), the importance of histological methods have decreased (Faqi, 2017). Oil red O is a fat-soluble dye that stains neutral lipids within the intracellular lipid droplets and the lipids forming part of the intracellular membranes (Figure 2.5 K). Therefore, it is important to present representative images of the stains when publishing work that analyses intramuscular lipid droplets using the ORO stain. The use of the PAS stain presents a similar problem when one is measuring skeletal muscle glycogen. Besides staining glycogen, the PAS stain also stains glycoproteins and proteoglycans. Therefore, diastase, such as  $\alpha$ -amylase, is used to digest glycogen to differentiate it from the other stained structures (Figure 2.5 L) (Thompson & Hunt, 1966; Young, Woodford & O'Dowd, 2006; Prats *et al.*, 2013).

Hybrid fibre types cannot be distinguished using enzymatic and non-enzymatic histology staining methods and therefore immunohistochemistry methods are applied. Immunohistochemistry of muscle tissue depends on antibody to antigen specificity where several antibodies specific to MHC isoforms (antigens), referred to as primary antibodies, are used to identify pure and hybrid muscle fibre types (Figure 2.5 C-F, M) (Young *et al.*, 2006; Kim *et al.*, 2014). To visualise the primary antibody, the antibody is pre-linked to an indicator substance, referred to as the secondary antibody. The secondary antibody can be a fluorescent substance in which case the staining method is referred to as immunofluorescence and it can be visualised using a fluorescence microscope. To visualise the antibody using a light microscope, an enzyme, such as horseradish peroxidase, is applied that binds to the primary antibody. The enzyme chosen must be able to convert a colourless substrate to a coloured product, such as diaminobenzidine tetrahydrochloride (DAB), PermaBlue, PermaRed and PermaGreen (Young *et al.*, 2006). The coloured product stains the primary antibody and the remaining fibres remain colourless (Figure 2.5).

However, myosin ATPase histology and immunohistochemical staining of a specific MHC are both time consuming and does not identify and visualise all the pure and hybrid fibres at once. Bloemberg and Quadrilatero (2012) suggested immunofluorescence (Figure 2.5 C-F) analysis as an improved method for rapid analysis of MHC-based muscle fibre types. This method is time efficient because a cocktail of the primary antibodies specific to each MHC isoform as well as the secondary antibodies are used. This method allows identification of the hybrid fibre types as well as the pure muscle fibre types (Song, Ahn & Kim, 2019).

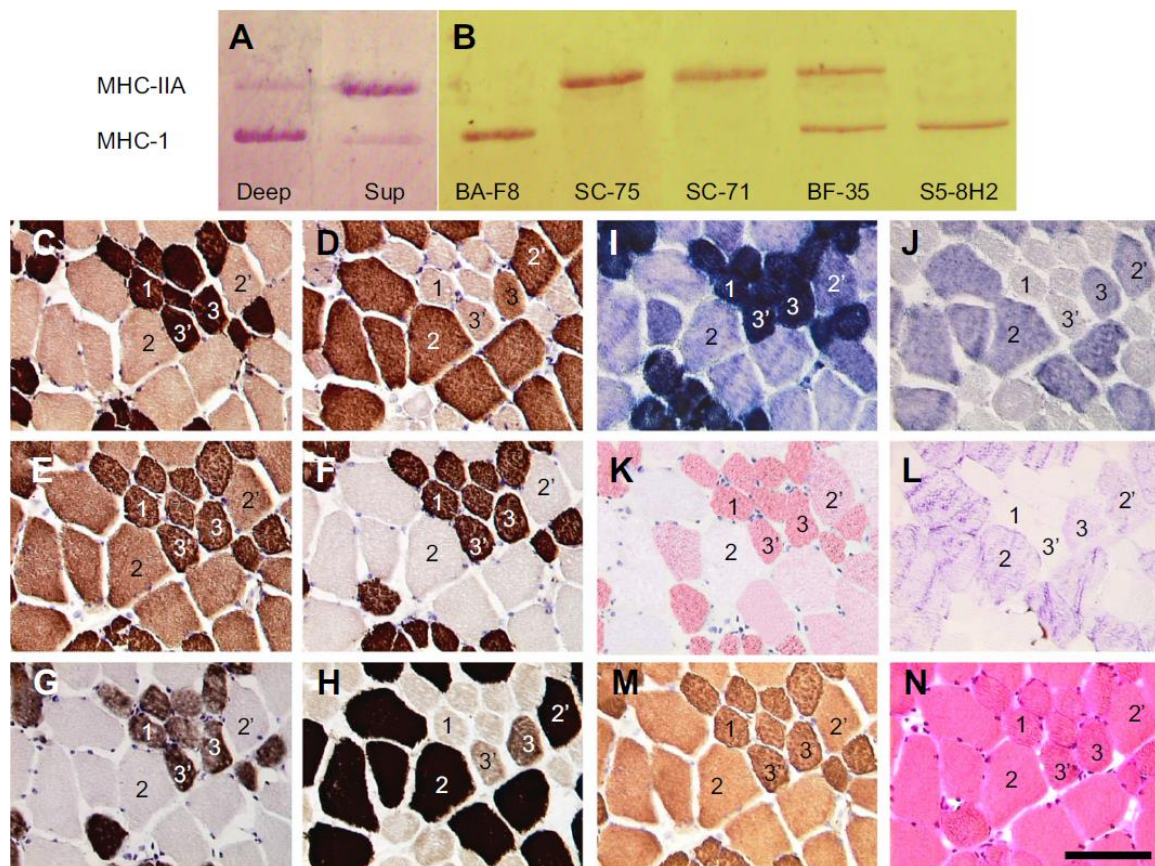


**Figure 2.5:** Characterization of muscle fibre types of the fin whale (*Balaenoptera physalus*) according to the myosin heavy chain (MHC) isoform they express. (A) 8% SDS-PAGE of representative deep ('Deep') and superficial ('Sup') muscle samples showing two MHC bands with different migrating speeds. (B) Immunoblots stained with specific anti-MHC monoclonal antibodies [BA-F8 (anti MHC I), SC-75 (anti MHC IIA+IIX+IIB), SC-71 (anti MHC IIA), BF-35 (anti MHC I+IIA+IIB) and S5-8H2 (anti MHC I+IIX+IIB)], revealing that the two electrophoretically separated bands are identified as MHC-IIA and MHC-I isoforms going from the slowest (top) to the fastest (bottom) migrating bands. (C–N) Serial sections of a representative superficial sample of the longissimus dorsi muscle of *B. physalus* were stained for immunohistochemistry (C–F,M), enzyme histochemistry (G–J) and histology (K,L,N) of MHC-based fibre types: monoclonal antibodies BF-F8 (C), SC-71 (D), BF-35 (E) and S5-8H2 (F); acidic (G) and alkaline (H) pre-incubations of myosin adeno-triphosphatase (ATPase); succinate dehydrogenase (SDH; I) and glycerol-3-phosphate dehydrogenase (GPDH; J) histochemical enzyme activities; oil red O (ORO; K) and periodic acid–Schiff (L); immunohistochemistry with the antimyoglobin monoclonal antibody MG-1 (M); and haematoxylin and Eosin (N). Scale bar, 100  $\mu\text{m}$ . The muscle fibres labelled '1' and '2' are pure fibres expressing MHCs I and IIA, respectively; the fibre labelled '2'' is a pure MHC-IIA fibre showing high SDH activity (I); the fibre labelled '3' is a hybrid fibre co-expressing MHC I +IIA with predominance of MHC-IIA on MHC-I; the fibre labelled '3'' is also a hybrid I+IIA fibre with dominance of MHC I versus MHC IIA, and showing weaker GPDH and PAS staining compared with previous hybrid fibre phenotype. Reproduced with permission from Journal of Experimental Biology (Rivero, 2018).

Several studies indicated that the muscle fibre type composition differs towards the deeper layers of the limb muscles and may reflect the functional complexity of the specific muscle.

The percentage of oxidative muscle fibres (Type I) is usually higher towards the deeper layers of the muscle while the percentage of glycolytic fibres (Type II) is higher towards the superficial muscle layers (Figure 2.5A). This heterogeneous intermuscular fibre type distribution is termed regionalisation (Burke, 1981; Armstrong, Saubert, Sherman & Taylor, 1982; McConathy, Giddings & Gonyea, 1983; McIntosh, Ringqvist & Schmidt, 1985; Acosta & Roy, 1987; von Mering & Fischer, 1999; Eng *et al.*, 2008). Armstrong and colleagues (1982) noted that the extensor muscles tend to show more regionalisation than the flexor muscles. Von Mering & Fischer (1999) further showed that the high fibre type regionalisation in *m. triceps brachii* and the significant role that this muscle plays in joint stabilisation may point towards a correlation between fibre type regionalisation and joint stabilisation. Furthermore, selective activation within these regionalised muscles has been shown in electromyographic studies (English, 1984, Hoffer, Loeb, Sugano, Marks, O'Donovan & Pratt, 1987). Low-level activation of a regionalised muscle, such as isometric contractions for slow walks or standing, indicates that the slow fibres are recruited first (Walmsley, Hodgson & Burke, 1978; von Mering & Fischer, 1999). Regionalised muscles as isotonic lever-arms indicate that the intramuscular architecture is optimised for the superficial fast glycolytic fibres, which produce fast and energetic actions (Walmsley, Hodgson & Burke, 1978). The joint-stabilising *mm. supraspinatus* and *triceps brachii* in the common yellow-toothed cavy (*Galea musteloid*) and the Northern treeshrew (*Tupaia belangeri*) showed intramuscular fibre type regionalisation (von Mering & Fischer, 1999) and further reflected the functional segregation principle within muscles (Windhorst, Hamm & Stuart, 1989; English, 1993). Furthermore, von Mering & Fischer (1999) found that all the muscles analysed in the common yellow-toothed cavy and the Northern treeshrew showed an increase in slow fibres from superficial to deep except for *m. triceps brachii caput mediale* which consisted mostly of type II fibres.

Similarly, a study on the functional morphology of the scratch-digging nine-banded armadillo (*Dasypus novemcinctus*; Olson *et al.*, 2016) determined the fibre type composition of 29 forelimb muscles. The muscles were placed into functional groups based on the main function of the specific muscles. Olson and colleagues (2016) found that the limb retractors and intrinsic and extrinsic muscles mainly consisted of type IIX fibres. In the brachium and antebrachium muscles there was a proximal-distal decrease in type IIX fibres and an increase in type I fibres towards the manus. Functionally the limb retractors play an important role during the power stroke of scratch-digging and therefore the high percentage of type IIX

fibres would provide high force and power output for the power stroke. In contrast the low percentage of type IIX fibres and high percentage type I fibres in the digital flexors reflect the high fatigue resistance provided by these muscles in order to sustain carpal and digital flexion throughout the entire digging stroke of the forelimb.

## **2.4 Somatosensory mechanisms in the feet**

### **2.4.1 General structure of mammalian skin**

The general structure of the skin in mammals consists of three anatomical layers: the epidermis, dermis and hypodermis (Kanitakis, 2002; Young *et al.*, 2006). The epidermis is the outer most layer of the skin and is made up of stratified squamous epithelial cells and contains receptor cells (Young *et al.*, 2006; Boulias & Misery, 2008). This layer produces a protein, keratin, which protects the underlying tissues from chemical, physical and biological insults (Young *et al.*, 2006; Brandner, Haftek & Niessen 2010). Furthermore, the epidermis is specialised to form skin appendages such as hair, sebaceous glands, sweat glands and specialised glandular structures (Dellmann & Eurell, 1998). The dermis consists of fibrocollagenous and elastic tissue and has a rich network of blood vessels, nerves and sensory receptors (Young *et al.*, 2006). The irregular connective tissue in the dermis provides nutrients and structural support to the epidermis and plays an important role in thermoregulation (Braverman, 2000). The deepest layer of skin, the hypodermis contains loose connective tissue and a pad of adipose fat cells which provide energy, protection and thermoregulation to the body (Avram, Avram & James, 2005; Young *et al.*, 2006). The skin of all mammals consists of these three layers; however, inter- and intraspecific differences can occur in the skin thickness, content and pigmentation of the epidermis and dermis (Sokolov, 1982; Dellman & Eurell, 1998). For the purposes of the current study, cutaneous mechanoreceptors and hairs found in the fore- and hindfeet of mammals will be described in the following section.

### **2.4.2 Cutaneous mechanoreceptors**

Cutaneous mechanoreceptors are defined as sense organs or cells situated within the dermis and epidermis of the skin and these receptors respond to mechanical stimuli such as touch, temperature or vibrations (Munger, 1971). The morphologies of four primary mechanoreceptors have been described and can be identified in different locations within the glabrous or hairy skin of mammals (Figure 2.6; Paré, Smith & Rice, 2002). The two most superficial mechanoreceptors are the Merkel cells and Meissner corpuscles (MCs). Merkel cells or complexes are comprised of clusters of specialised cells with disc-like endings and

can be seen in the basal lamina of the intermediate epidermal ridges (Smith, 1970). Meissner corpuscles are situated within dermal papillae that bud off from the dermal papillary ridges between the intermediate epidermal ridges (Cauna, 1956). The other two mechanoreceptors situated deeper in the dermis are the Pacinian corpuscles (PCs) and the Ruffini corpuscles (RCs). Pacinian corpuscles are ellipsoid structures that consist of a neurite terminal that are wrapped in multiple layers of lamellar cells and are only found in the hairless skin deep to the level of sweat glands (Chouchkov, 1971; Munger 1971). Ruffini corpuscles are described as long spindle-shaped structures arranged and intertwined with dermal collagen bundles which are supplied by two to three large axon fibres (Miller, Ralston & Kasahara; 1958; Chambers, Andres, Duering & Iggo, 1972).

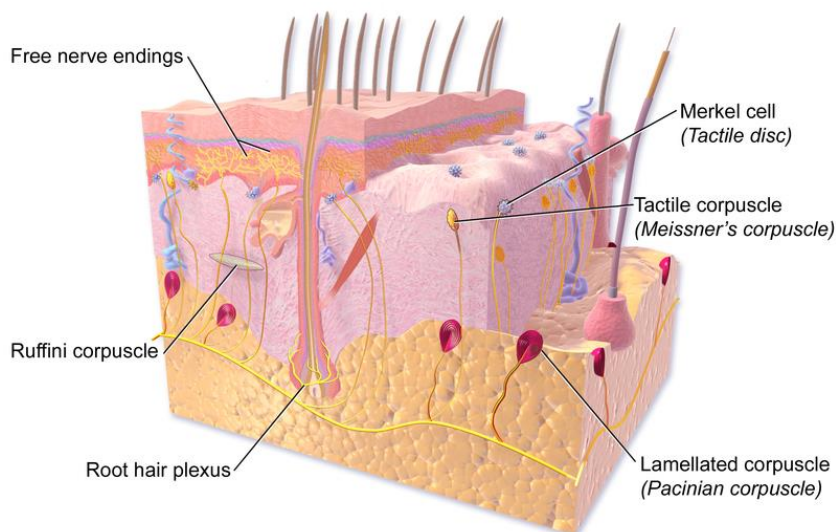


**Figure 2.6:** Schematic depiction of four mechanoreceptors in the skin: Tactile/Meissner corpuscles, lamellated/Pacinian corpuscles, tactile discs/Merkel cells and Ruffini corpuscles. Permission to use image from website, Blausen.com (Blausen Medical, 2014).

These primary mechanoreceptors are innervated by the afferent axons of sensory neurons which can be classified according to the signalling characteristics of the mechanoreceptors (Chambers *et al.*, 1972; Iggo & Ogawa, 1977; Munger, Page & Pubols, 1979). Two categories have been established based on their response to stimuli: rapidly and slowly adapting primary afferents. Type I rapidly adapting (RAI) primary afferents supply MCs. These respond to bending of hairs, gentle friction of the skin or low force stimulation of the glabrous or hairy skin by inducing a rapidly adapting discharge. Meissner corpuscles are also sensitive to light discriminatory touch, with the degree of discrimination depending on the density of MCs within the dermis (Young *et al.*, 2006). Pacinian corpuscles are supplied by

type II rapidly adapting (RAII) primary afferents and respond to vibration. The rapidly adapting primary afferents only respond to temporary tactile stimuli while type I (SAI) and type II (SAII) slowly adapting primary afferents respond to maintained low-force tactile stimuli to the hairy and glabrous skin. Merkel cells are supplied by SAI afferents while SAII afferents supply RCs with the additional capacity of the SAII afferents responding to dermal stretch (Chambers *et al.*, 1972; Edin & Abbs, 1991; Edin, 1992; Leem, Willis, Weller & Chung, 1993; Hamann, 1995; Ollausson, Wessberg & Kakuda, 2000; Paré *et al.*, 2002).

Currently no studies could be found on the mechanoreceptor density and composition in the glabrous or hairy skin of the feet in subterranean rodents such as the African mole-rats. However, a study performed on the glabrous skin of the feet in a ground and a tree squirrel species (Brenowitz, 1980) indicated how the proportional representation of the different mechanoreceptors between the species reflect their ecological and behavioural specialisations. The results indicated that the forepaws of the tree squirrel had higher differentiated mechanoreceptors in the digital and palmar areas compared to the ground squirrels. This suggested that the palm and digits of the tree squirrel might play highly differentiated roles in performing behavioural movements that are species-specific. Furthermore, the forepaw receptor densities did not differ between the tree and ground squirrel species and therefore, it proved difficult to predict receptor densities in one part of the body alone (Brenowitz, 1980). Additionally, the mechanoreceptor density of the palmar skin was higher than the digits in both species and therefore the palmar region would represent a more accurate presentation of the mechanoreceptor differentiation. For the current research project, the palmar regions of both the fore- and hindfeet will be analysed to produce significant results.

Bouley and colleagues (2007) performed a histomorphological study on the foot of the Asian elephant and found that the Pacinian corpuscles (PCs) located in the soles of their feet are responsible for the detection of seismic waves. The study also indicated that the PCs were localised to areas in the feet that correlate with specific foot postures which are exhibited when the elephants respond to seismic signals. Similarly, in primates the PCs and Meissner corpuscles (MCs) are responsible for detection of vibrations between 10 and 400Hz (Merzenich & Harrington, 1969) whereas in wallabies (Gregory, McIntyre & Proske, 1986) and cats (Hunt, 1961) the PCs detect vibrational frequencies up to 1.3kHz and between 50 and 800Hz, respectively. In these animals the MCs and PCs may function to detect ground-borne vibrations; which provides sensory perception for cats (Hunt, 1961) and intra- and

interspecific communication through seismic signals for primates and wallabies (Merzenich & Harrington, 1969; Gregory *et al.*, 1986).

Subterranean animals also produce seismic signals for perception and navigation within their burrows, in order to forage for food and to detect predators (Mason & Narins, 2001). The role of somatosensory receptors in seismic signalling has not been documented thoroughly in fossorial species such as the bathyergids. The nose pad of the lesser mole-rat (*Spalax ehrenbergi*) contains PCs and MCs within the dermal papillae which may be sensitive to seismic vibrations (Klauer, Burda & Nevo, 1997). A study on the brain cortex of the star-nosed mole (*Condylura cristata*) revealed a large representation of the forepaw which can possibly suggest that the receptors within the forelimb are sensitive to seismic vibrations (Catania & Kaas, 1995).

To visualise mechanoreceptors within glabrous and hairy skin, various staining methods can be used. Silver impregnation of tissue is the more accurate method for visualising peripheral nerves, especially in its ability to identify changes within unmyelinated fibres and nerve endings. However, due to the high cost and complexity, and time-consuming process of reduced silver techniques, alternative staining methods can be used for serial sections in studies using large specimens and where budget is a limiting factor (Bodian, 1936). Alternative methods include Masson's trichrome and H&E stains. Masson's trichrome is not often used for histological analysis of peripheral nervous tissue since it is not possible to accurately identify the myelin sheaths of the nerves (Carriel, Garzon, Alaminos & Cornelissen, 2014). However, this method is considerably better than H&E according to Raimondo and colleagues (2014). In a study where mechanoreceptors are analysed and not structures specific to peripheral nerves, the staining of myelin sheaths is not required. Therefore, a combination of histochemical stains such as Masson's trichrome and H&E can be used to visualise and accurately identify mechanoreceptors within tissue.

#### **2.4.2 Hair**

Mammalian hair is a derivative of the epidermis, consisting of keratinized epidermal cells that grow from a hair follicle situated within the dermis (Sokolov, 1982; Erdoğan, 2017). The typical structure of hair consists of two distinct structures: the hair root, which is situated within the hair follicle in the dermis and contains the terminal hair bulb, and the hair shaft, which is the free end of the hair that protrudes above the surface of the skin (Figure 2.7) (Dellmann & Eurell, 1998; Young *et al.*, 2006). There are multiple differences in the shape,

texture, length, thickness, density and colour of hairs between species but also within the same animal within the different areas of the body (Otberg, Richter, Schaefer, Blume-Peytavi, Sterry & Lademann, 2004; Davis, Brummer & Shivik, 2010). Ultimately, mammalian hair can be categorized into four types based on the structure of the hair follicle, shaft and root: guard hairs, intermediate hairs, fur /under hairs and vibrissae/sensory hairs, (Hausman, 1920; Loo & Halata, 1991; Tridico, 2005). The pelage or coat of mammals is formed by the guard, intermediate and fur hairs. Guard hairs are the longest hairs and usually protrude from the rest of the pelage. The morphology of guard hairs in different regions of the body can vary in most mammals (Stains, 1958). The intermediate hairs are shorter and thinner than the guard hairs, but longer and thicker than the under hairs. Fur hairs are short and fluffy hairs, usually closest to the skin and are efficient for trapping air to insulate the animal (Sokolov, 1982; Knecht, 2012). Vibrissae, or whiskers, are specialised stiff hairs utilized for tactile sensation (Sokolov, 1982; Dellmann & Eurell, 1998; Feldhamer, Drickamer, Vessey, Merritt & Krajewski, 2007; Knecht, 2012). They are usually longer and thicker compared to other hair types. Vibrissae are found in various regions of the face but mostly around the nostrils and above the lips and sometimes they grow on the forelegs and feet of some mammal species (Knecht, 2012).

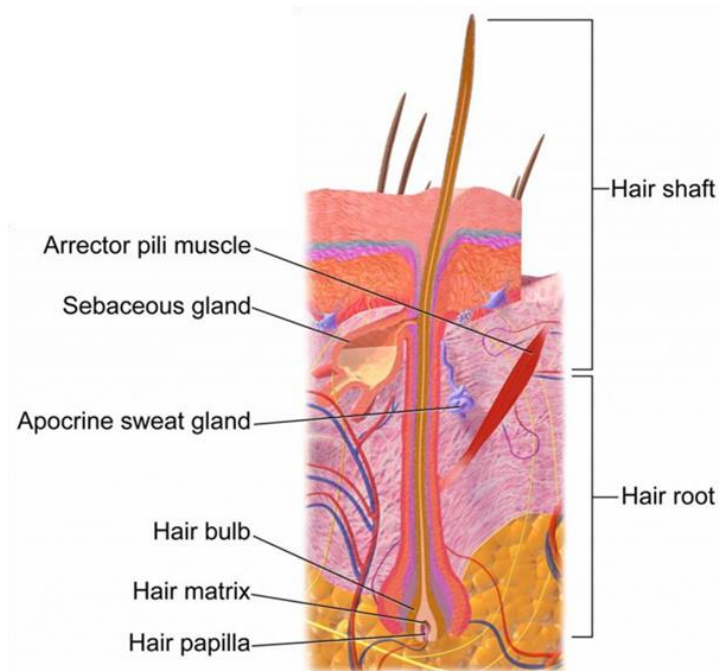


**Figure 2.7:** Illustration of the general structure of a single hair unit. Permission to use image from website, Blausen.com (Adapted from Blausen Medical, 2014).

Hair follicles can be classified as primary, secondary, simple or compound hair follicles (Delman & Eurell, 1998; Oznurlu, Celik, Sur, Telatar & Ozparlak, 2009). Primary hair follicles have roots that extend deep into the dermis with a thick diameter whereas secondary hair follicles have a smaller diameter and are rooted more superficially in the dermis, closer to the surface (Dellmann & Eurell, 1998; Meyer, 2009). Simple hair follicles consist of a single hair emerging from the dermis whereas compound hair follicles are a cluster of hair follicles (Meyer, 2009; Oznurlu *et al.*, 2009).

In all mammals, hair follicles consist of the external and internal root sheath, the dermal papilla and the hair matrix (Figures 2.7 and 2.8) (Eroschenko, 2008). The external root sheath comprises of epidermal cells and is surrounded by a homogenous glassy membrane with an outer connective tissue layer, the dermal sheath, that envelopes the entire hair follicle (Figures 2.7 and 2.8) (Dellmann & Eurell, 1998). The internal root sheath is the innermost layer, next to the hair root. The dermal papilla is situated at the base of the hair follicle, covered by the hair matrix, and consists of connective tissue and a capillary loop (Figure 2.7) (Robley *et al.*, 2002; Pawlina & Ross, 2018). Bundles of smooth muscle, arrector pili muscles, are commonly associated with most hair follicles and attaches to the dermal sheath and extends into the epidermis (Figure 2.7) (Poblet *et al.*, 2004). When contracted, the arrector pili muscles cause air to be trapped between the erected body hairs, thereby providing heat insulation to the animal (Pascalau, Raluca, Kuruvilla & Rejji, 2020). Animals such as sea otters (*Enhydra lutris*), Pinnipeds (seals and sea lions) and Cetaceans (whales and dolphins), lack arrector pili muscles (Sokolov, Khams *et al.*, 2012; Yochem & Stewart, 2018; da Silva, Machado, Le Bas, Silva, dos Anjos Silva & Hernandez-Blazquez, 2020).

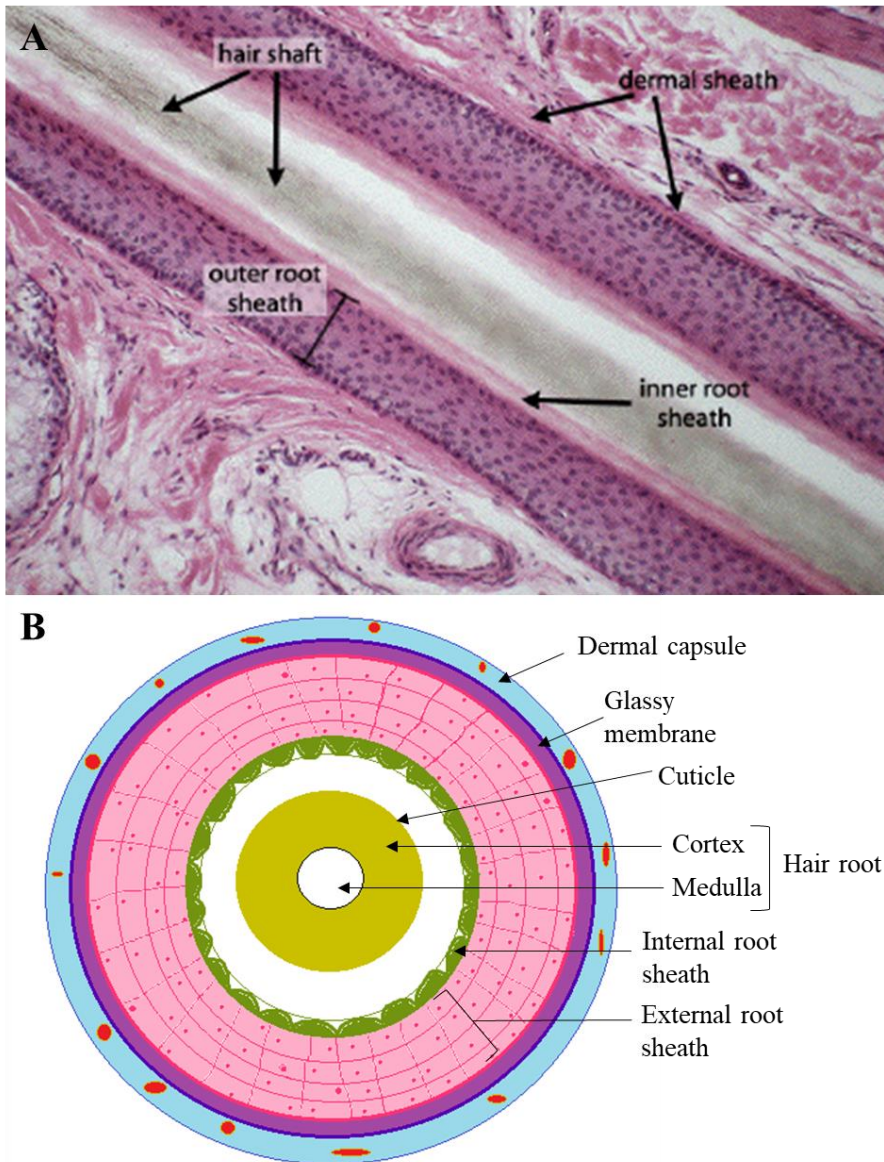


**Figure 2.8:** The various components of a hair follicle. Longitudinal section of a H&E-stained hair follicle (A) (Dartmouth.edu, 2021, used with permission from R. Swenson) and a cross-sectioned illustration of a hair follicle (B) (Drawn based on image from Dellmann & Eurell, 1998).

The hair follicles of all hair types have the same basic structure, except vibrissal follicles. The hair follicles of vibrissae are large, lack arrector pili muscles and are characterized by a follicle-sinus complex (FSC; Rice, Mance & Munger, 1986). The follicle is surrounded by a venous sinus that is situated within the dermal sheath. The FSC is divided into an upper non-trabecular cavernous sinus, a middle ring sinus and a lower trabecular cavernous sinus (Figure 2.9) (Rice & Munger, 1986; Marshall, Amin, Kovacs & Lydersen, 2006). The dermal sheaths of vibrissae contain numerous penetrating nerve bundles with skeletal muscles attached to the dermal sheath (Rice, Fundin, Arvidsson, Aldskogius & Johansson, 1997).

There are multiple differences in the structure of vibrissal follicles between different mammal species. For example, the vibrissal hairs in the tammar wallaby (*Macropus eugenii*) lack a ring sinus and the in horses and ruminants, the upper cavernous sinus is trabeculated (Marotte, Rice & Waite, 1992; Dellmann & Eurell, 1998).

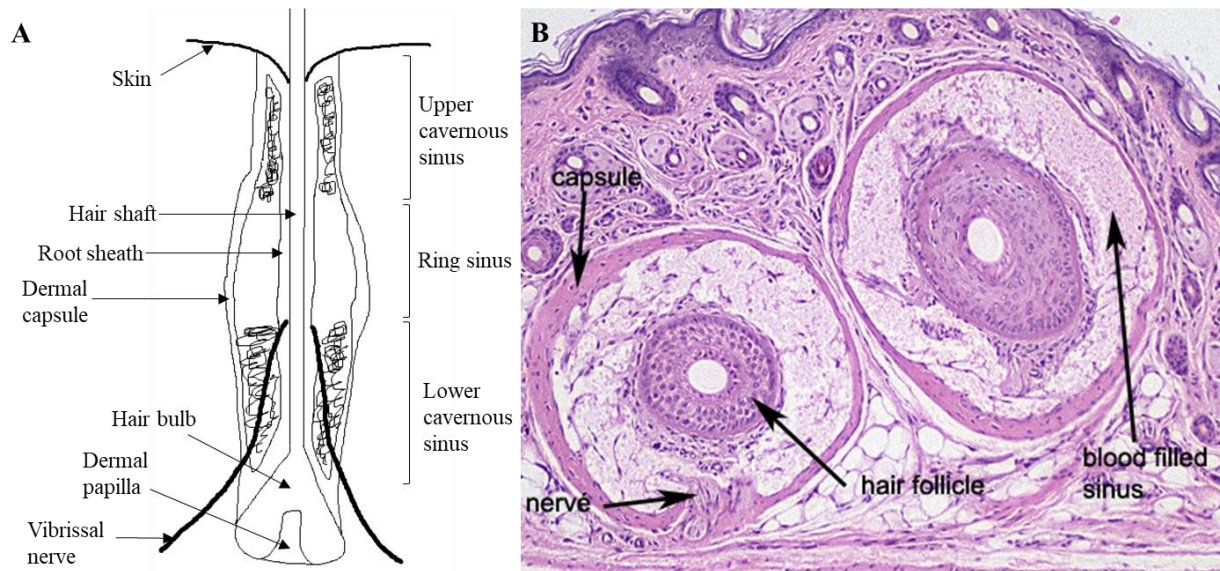


**Figure 2.9:** Diagrammatic illustration of the vibrissal structure (A) and H&E cross-section of vibrissal hairs located near the feet in mice (B). (Drawn based on image from Marotte *et al.*, 1992; Mutant Mouse Skin Database, 2021).

All rodent species have three main hair types: vibrissae, guard hairs and fur (Sokolov, 1982), with four different groups of cranial vibrissae namely supraorbital (above the eyes), genal (on the cheeks), mystacial (between the nose and snout) and mandibular (inferior to the snout) vibrissae (Wallace, Chen, Chorev & Brecht, 2013). Sensory hairs play a significant role in sensory perception and communication and is present in nearly all fossorial rodent species (Jarvis & Bennett, 1991; Klauer *et al.*, 1997; Nowak, 1999). Crish, Rice, Park and Comer (2003) observed that head and body orientation responses were triggered when the vibrissae of naked mole-rats were artificially deflected. The vibrissae in the Cape dune mole-rat or behavioural responses to tactile stimuli is underreported. Therefore, the sensory hairs located on the lateral skin of the feet as well as the hairless skin of the feet may reflect behavioural adaptations related to seismic signalling and sensory perception of the specific species.

In conclusion, the mechanoreceptors that are in the footpads of various mammalian species play a role in detecting seismic signals. Additionally, sensory hairs located in the lateral skin

of the feet may have surrounding mechanoreceptors within the skin that detect vibrations and movement of the hairs and could contribute towards detection of seismic signals.

### 3 MATERIALS AND METHODS

#### 3.1 Sample information

Ethical clearance was obtained for the use of animal tissue from the Research Ethics Committee: Animal Care and Use of Stellenbosch University (SU-ACUM 16-00005). Ethical clearance was extended for the present study under a new number, ACU-2020-19344. The animals were obtained from previous unrelated studies (Table 3.1) and were not specifically killed for the present study. The previous ethical approval numbers for the animals of each species as well as the mean body mass and capture sites are detailed in Table 3.1.

**Table 3.1:** Information on the specimens, original ethical approval numbers, capture site and mean body mass for muscle architecture ( $\pm$  standard deviation).

Species	Ethical approval	n	Capture site	Mean body mass
<i>Bathyergus suillus</i>	Stellenbosch University: 10NP_VAN01; University of Cape Town: 200/V7/JOR	6	Darling, Western Cape	Muscle architecture: 798.23 $\pm$ 431.67 Muscle fibre typing: 842.79 $\pm$ 335.18 Cutaneous mechanoreceptors: 768.73 $\pm$ 386.95
<i>Heterocephalus glaber</i>	University of the Western Cape: ScR1RC2007/3/30	6	University of the Western Cape	40.76 $\pm$ 6.6

#### 3.2 Muscle architecture

##### 3.2.1 Dissection

Twelve mole-rat specimens (N=12) were used for muscle architecture analysis of which six thawed *B. suillus* halves (n=6) were fixed in 10% buffered formalin and six *H. glaber* specimens that were already fixed in buffered formalin (n=6). The forelimb joints of the *B. suillus* specimens were placed at a 90° angle prior to fixation in order to keep the limb in a resting position and to maintain the fibre integrity of the muscles during analysis. The origin and insertion sites of 40 muscles were dissected on each limb, as previously described by Doubell and colleagues (2020), after which the muscles were removed and placed into labelled plastic tubes containing 10% buffered formalin for further analysis. In both species

the left forelimb was dissected, however if one or more muscles were damaged on the left forelimb, the right forelimb was used.

### 3.2.2 Muscle architecture measurements

Techniques similar to that described by Payne, Hutchson, Robilliard, Smith & Wilson (2005) and Martin, Warburton, Travouillin & Fleming (2019) were used to measure four architectural parameters of 40 front limb muscles in each species. A digital scale (*Ohaus Adventurer Pro AV3102, Nanikon, Switzerland*) was used to measure the muscle mass ( $M_M$ ) to the nearest 0.001g. The muscle belly length ( $L_M$ ; length between the origin of the most proximal muscle fibres and the insertion of the most distal fibres) was measured to the nearest 0.01mm using a digital sliding calliper. A Leica MZ67 Stereomicroscope (*Leica Biosystems, Wetzlar, Germany*) was used to take high magnification photographs of each muscle. Image Composite Editor (Microsoft 2.0.3) was used to produce composite images after which six to eight random fascicles per muscle were chosen to measure the fascicle length ( $L_f$ ) using the ‘segmented line tool’ in ImageJ (Java 1.8.0\_112; Schneider, Rasband & Eliceiri, 2012). Additionally, using the ‘angle tool’ in ImageJ, five random fascicles per muscle were chosen to measure the pennation angle ( $\theta$ ). Correction factors for fixed muscle tissue were used to correct the muscle mass and fascicle length of all muscles (an increase of 14% and 11%, respectively; Kikuchi & Kuraoka, 2014). The mammalian skeletal muscle density ( $\rho$ ) was determined as 0.001056 g/mm<sup>3</sup> according to Mendez & Keys (1960) and Ward & Lieber (2005). The physiological cross-sectional area (PCSA) of each muscle was calculated using the following formula (Equation 1) (Sacks & Roy, 1982; Charles *et al.*, 2016):

$$\text{Equation 1: } PCSA (mm^2) = [MM (g) * \cos\theta] / [L_f (mm) * \rho (g/mm^3)]$$

In addition, the PCSA (mm<sup>2</sup>) was multiplied by a maximum isometric stress of 0.3 N/mm<sup>2</sup> (Medler, 2002) to estimate the maximum isometric force of contraction ( $F_{max}$ ) of each muscle. This is only an estimation of the maximum isometric force because of the variation in muscle excursion (displacement of the myotendinous junction throughout the range of motion) as the tension changes across the tendon and muscle (Fukunaga, Roy, Shellock, Hodgson & Edgerton, 1996). Furthermore, the architectural index (AI) was determined by calculating the fibre length to muscle length ratio ( $L_f/L_M$ ), which is proportional to the velocity of muscle contraction (Sharir, Milgram & Shahar, 2006; Charles *et al.* 2016).

Forty muscles were categorised according to their main functions into thirteen functional muscle groups for statistical analysis (Table 3.2) (Olson *et al.*, 2016; Martin *et al.*, 2019). Biarticular muscles were included in more than one functional group (Table 3.2). There are species differences in the absence and presence of specific muscles. *Musculus coracobrachialis*, *tensor fasciae antebrachium* and *abductor pollicis longus*, were absent in *H. glaber* while *m. deltoideus pars clavicularus* was absent in *B. suillus* (Doubell *et al.*, 2020).

**Table 3.2:** List of muscle function groups

<b>Muscle group</b>	<b>Muscle</b>
Head extensors and hyoid bone depressors (HH)	<i>M. sternocleidomastoideus</i> <i>M. sternohyoideus</i>
Scapular elevators/stabilizers/retractors (SE)	<i>M. trapezius pars cervicales</i> <i>M. trapezius pars thoracica</i> <i>M. rhomboideus cervicis</i> <i>M. rhomboideus capitis</i> <i>M. serratus ventralis</i> <i>M. subclavius</i> <i>M. omotransversarius</i> <i>M. claviculo-scapularis</i>
Limb retractors (LR)	<i>M. latissimus dorsi</i> <i>M. pectoralis superficialis</i> <i>M. infraspinatus</i> <i>M. teres major</i> <i>M. deltoideus pars acromialis</i> <i>M. deltoideus pars scapularis</i> <i>M. deltoideus pars clavicularis</i> <i>M. triceps brachii caput longum</i>
Limb protractors (LP)	<i>M. subscapularis</i> <i>M. supraspinatus</i> <i>M. coracobrachialis</i> <i>M. biceps brachii</i>
Elbow extensors (EE)	<i>M. triceps brachii caput longum</i> <i>M. triceps brachii caput laterale</i> <i>M. triceps brachii caput mediale</i> <i>M. tensor fasciae antebrachium</i>
Elbow flexors (EF)	<i>M. biceps brachii</i> <i>M. brachialis</i>
Carpal flexors (CF)	<i>M. palmaris longus</i> <i>M. flexor carpi ulnaris</i> <i>M. flexor carpi radialis</i>
Carpal extensors (CE)	<i>M. extensor carpi radialis</i> <i>M. extensor carpi ulnaris</i>
Digital flexors (DF)	<i>M. flexor digitorum superficialis</i> <i>M. flexor digitorum profundus</i>
Digital extensors (DEX)	<i>M. extensor pollicis</i> <i>M. extensor digitorum communis</i>
Digital abductors (DB)	<i>M. abductor pollicis longus</i> <i>M. abductor digiti V</i>
Supinators (S)	<i>M. supinator</i>
Pronators (P)	<i>M. pronator teres</i>

### 3.2.3 Statistical analysis

The mean and standard deviation as well as other descriptive statistics were reported for all measurements and calculations for each species. To obtain significant differences from the results, a minimum of three samples per muscle had to be used. All four parameters of each muscle and muscle group were  $\log_{10}$ -transformed and plotted against  $\log_{10}$  body mass to calculate the scaling co-efficients. The two species studied were scaled allometrically to body mass for all the parameters. The  $\log_{10}$  body mass was used as the covariate to compare the  $\log_{10}$ -transformed data. A one-way analysis of covariance (ANCOVA) was performed to determine significant differences within the muscle groups as well as the individual muscles between the two species (Sahd, Bennett & Kotzé, 2020). Fischer's Least Significant Difference (LSD) *post-hoc* test was used to determine the p-values with a  $p < 0.05$  indicating statistically significant results. Statistica 13.5 (*TIBCO software, Palo Alto, California, USA*) was used to perform all statistical analyses. All graphs were created in Statistica and Microsoft Excel 2010.

### 3.2.4 Functional space plots

The scatter plots of the mean PCSA (normalized to body mass,  $PCSA/M_b^{0.67}$ ) of each individual muscle and muscle group were plotted against mean  $L_f$  (normalized to body mass,  $L_f/M_b^{0.33}$ ) in both species (Martin *et al.*, 2019). The normalization of parameters to body mass allowed comparison between species as there was a large variation in body size between species.

### 3.3 Muscle fibre typing

#### 3.3.1 Specimen preparation

The right forelimbs of six frozen *B. suillus* specimens and six formalin fixed *H. glaber* specimens were used for the muscle fibre typing. The mid-bellies of specific forelimb muscles were harvested from each limb from the specimens of both species. These specific muscles were chosen according to a similar study on the nine-banded armadillo (Olson *et al.*, 2016). A layout was designed of the muscle arrangement on the histology slides to ensure accurate identification of specific muscles (Figure 3.1).

##### a.) Fresh tissue preparation

The frozen *B. suillus* specimens were thawed one at a time and a small section from the mid-belly of each muscle was harvested and snap-frozen in liquid nitrogen (-170°C). The muscles were stored in a -80°C freezer overnight to allow for optimal cryostat sectioning of samples. Cross-sections of the mid-belly of each muscle were positioned onto labelled squares of cork and tissue freezing medium (OCT, *Leica Biosystems: Wetzlar, Germany*) was placed around the section of muscle to keep it in the correct orientation. The freezing medium and muscle tissue were sprayed with Pellox freezing spray (*Cell Path Services, Midrand, South Africa*) to keep the tissue frozen during sectioning. The muscles were sectioned at -15°C using a Leica CM1520 Cryostat (*Leica Biosystems, Wetzlar, Germany*) and one 7µm section of each muscle was placed onto positively charged slides according to the slide layout. Three slides of the exact same slide layout were produced: one slide for each staining method and a backup slide which was stored in a dust-free container in a -20°C freezer.

##### b.) Fixed tissue preparation

The right forelimbs of six *H. glaber* specimens, which were previously fixed in 10% buffered formalin, were used. The muscles were harvested, processed in an Automated Vacuum Tissue Processor (ASP6025; *Leica Biosystems, Wetzlar, Germany*; Addendum E) and the cross-sections of the mid-belly of each muscle were embedded into Paraplast® paraffin wax blocks using a Leica EG 116 Embedder (*Leica Biosystems, Wetzlar, Germany*) according to the slide layout. Three 5µm sections of each wax block were sectioned using a Leica RM 2125 RT microtome (*Leica Biosystems, Wetzlar, Germany*) onto positively charged slides. Furthermore, three additional muscles (*mm. latissimus dorsi, anconeus* and *flexor carpi ulnaris*) of *B. suillus* were harvested and fixed in 10% buffered formalin for a minimum of 24 hours after which the muscles were processed (Addendum E) and embedded into paraffin wax blocks with Paraplast® paraffin wax and a Leica EG 116 Embedder (*Leica*

*Biosystems: Johannesburg, South Africa*). The fixed *B. suillus* muscles were placed into two wax blocks (1-*m. latissimus dorsi*; 2- *mm. flexor carpi ulnaris* and *triceps brachii caput medialis*) and were sectioned onto positively charged slides. These additional three muscles served as a test which compared the staining of the muscle fibres between the fresh and the fixed muscle tissue and also served as the positive control for the slow myosin staining of the *H. glaber* tissue.

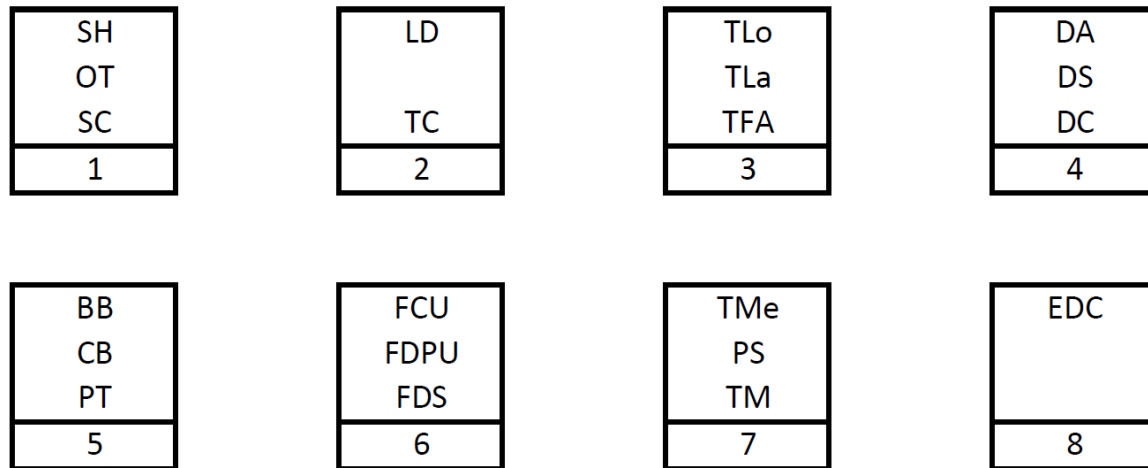


**Figure 3.1:** Slide layout for muscle fibre staining. SH-*m. sternohyoideus*; OT- *m. omotraversarius*; SC- *m. claviculoscapularis*; LD- *m. latissimus dorsi*; TC- *m. trapezius pars cervicales*; TLo- *m. triceps brachii caput longum*; TLa- *m. triceps brachii caput lateralis*; TFA- *m. tensor fasciae antebrachia*; DA- *m. deltoideus pars acromialis*; DS- *m. deltoideus pars scapularis*; DC- *m. deltoideus pars clavicularis*; BB- *m. biceps brachii*; CB- *m. coracobrachialis*; PT- *m. pronator teres*; FCU- *m. flexor carpi ulnaris*; FDP- *m. flexor digitorum profundus* (ulnar head); FDS- *m. flexor digitorum superficialis*; TMe- *m. triceps brachii caput medialis*; PS- *m. pectoralis superficialis*; TM- *m. teres major*; EDC- *m. extensor digitorum communis*.

### 3.3.2 Staining methods

#### a.) Fresh tissue staining

Immunohistochemically the NovoCastra Lyophilized Mouse Monoclonal Antibody Myosin Heavy Chain (slow; CAS: NCL-MHCs; LOT: 6065928; *Leica Biosystems: Wetzlar, Germany*) was used to label the slow myosin heavy chains within the type I fibres. A Novolink Polymer detection system (CAS: RE7150-CE; LOT: 6029001; *Leica Biosystems: Wetzlar, Germany*) and diaminobenzidine tetrahydrochloride (DAB; LOT: 6072346; *Leica Biosystems: Wetzlar, Germany*) were used to detect positive staining of the type I fibres. This staining protocol, as seen in Addendum A is similar to the protocol described by Kalmar, Blanco & Greensmith (2012). After storing the prepared slides in a -20°C freezer, the frozen

slides had to reach room-temperature before staining. The slides were washed in TRIS buffered saline (TBS, pH 7.6) for two increments of five minutes each after which each individual tissue section was circled using a Novopen (NCL-Pen; *Leica Biosystems: Wetzlar, Germany*) reagent pen, which kept the reagents within the circled area. After applying 50µl of primary antibody onto each tissue section (MHCs: TRIS; 1:40 dilution), the slides were placed in a plastic humidity chamber and incubated for one hour at 37°C (TC2323 SHEL LAB CO<sub>2</sub> Incubator, *Sheldon Manufacturing Inc.: Cornelius, Oregon, United States*). Between each step the slides were washed in TBS for two increments of five minutes each. Three to five drops of Novalink post-primary antibody were applied to each section and incubated for 15 minutes at room temperature. The same procedure was followed for the Novalink Polymer (3-5 drops; 15 minutes incubation). After the last TBS wash; 50µl of DAB solution (1:20 dilution of Novalink DAB chromogen and Novalink DAB substrate buffer) was applied to each tissue section and incubated for five minutes at room temperature. Slides were counterstained with Meyer's haematoxylin for one minute before washing the slides in tap water. After counterstaining, the slides were washed in running tap water for five minutes and dehydrated in a series of ethanol, cleared in xylene and mounted using DPX mounting media. Cross sections of the *m. biceps femoris* of a rat were used as a positive control for all runs.

For the second staining method for the *B. suillus* muscle tissue, β-nicotinamide adenine dinucleotide, reduced disodium salt hydrate (β-NADH; CAS: 606-68-8; *Sigma-Aldrich: Missouri, United States*) was used to detect the levels of oxidative enzymes within the muscle fibres. Fibres with a high oxidative capacity will stain dark blue and fibres with low oxidative capacity will have a light blue stain. Prepared slides were removed from the -20°C freezer and allowed to reach room temperature. Five to seven drops of NADH solution (see Addendum B) were applied to each tissue section after which the slides were placed in a humidity chamber and incubated at 37°C for 35 minutes. The slides were rinsed in distilled water and mounted with glycerine jelly.

#### b.) Formalin fixed tissue staining

For the fixed *H. glaber* muscle tissue, antigen retrieval was necessary (Behan, Cossar, Madden & McKay, 2002) and this was achieved through heat induced epitope retrieval (HIER) by using an AEG Electrolux Digital Pressure Cooker (*AEG: Frankfurt, Germany*). The prepared slides were first deparaffinised from xylene and taken through a series of ethanol for 10 minutes in each solution. Thereafter, the slides were placed into a metal slide

rack and submerged into Leica BOND Epitope Retrieval Solution (X10 concentrate, pH 6; *Leica Biosystems: Wetzlar, Germany*) within the pressure cooker. The slides were cooked on high pressure for one minute after which steam was released. Once all the steam was released the pressure cooker was switched off and the slides were allowed to cool down for twenty minutes before opening the lid of the pressure cooker. The slide rack was removed and placed into a container with warm water (60-80°C) before slowly washing the slides with running tap water. This allowed the slides to gradually cool down to prevent tissue damage. The slow myosin immunohistochemical staining proceeded as described above for the *B. suillus* tissue. For each run, one of the *B. suillus* slides with fixed tissue was stained and used as a positive control.

For the second staining method for the *H. glaber* tissue, Periodic Acid Schiff (PAS) was applied to demonstrate the glucose content within muscle fibres. However, to differentiate between glycogen and other structures such as capillaries and polysaccharides within the sarcolemma, amylase digestion was done using Sigma  $\alpha$ -amylase type VI-B (CAS: 9000-90-2; *Sigma-Aldrich: Missouri, United States*). The prepared slides were rehydrated in xylene and through a series of ethanol for five minutes in each solution. Thereafter, five to eight drops of 0.35% amylase solution were applied to each tissue section and incubated in a plastic humidity chamber at 38°C for 20 minutes (TC2323 SHEL LAB CO<sub>2</sub> Incubator, *Sheldon Manufacturing Inc.: Cornelius, Oregon, United States*). The slides were washed in tap water and staining continued according to the adjusted PAS stain protocol described in Addendum C. For each run, one of the *B. suillus* slides with fixed tissue was stained and used as to compare the results of the PAS stain with the NADH stain.

### 3.3.3 Morphometric and statistical analysis

The slides were scanned using the 40X objective of an Olympus V120-100L (*Olympus Corporation, Tokyo, Japan*) slide scanner at the University of Cape Town, Pathology Learning Centre. The images had a final resolution of 16 $\mu$ m per pixel and quantification of the positively stained fibres per muscle cross section and the staining intensity of both the NADH and PAS stains were done using Qupath version 0.2.3 (Bankhead, Loughrey, Fernández *et al.*, 2017). Before analysis of the slow myosin slides, the image type was set to 'Brightfield (H-DAB)' and the stain vectors of each slide were set for the positive and negative cells in the Qupath programme. The percentage of type I fibres for each section was determined by using the polygon tool to select the muscle tissue area (folded and longitudinal tissue areas were avoided) and then using the positive cell detection function to determine the

positively stained cell percentages. The negative cells or fibres that were not stained positively were considered to be type II fibres. The settings for the positive cell detection are detailed in Figure 3.2.

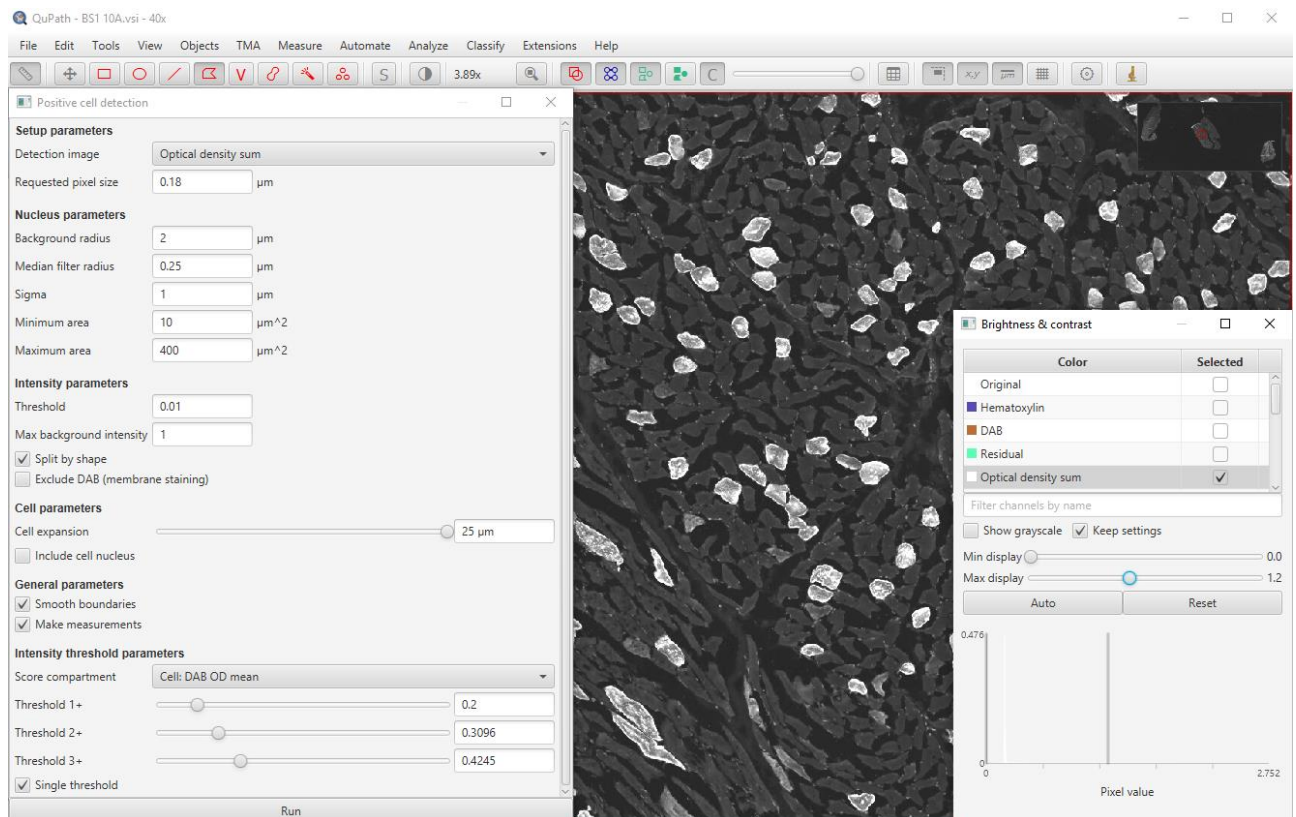


**Figure 3.2:** The settings used on the Qupath interface for the detection of positively stained muscle fibres which appear white on the optical density sum image.

The differences in the oxidative capacity (NADH) between fibre types were quantified by using the polygon tool to select the muscle tissue area and the cell detection function to determine the area for cell classification (Figure 3.3). Thereafter, the cell intensity threshold setting was used to classify the cells according to its stain intensity based on the three thresholds automatically determined by the Qupath software. The number of cells per threshold was determined via this setting which were then calculated as the percentage of light, medium and dark fibres per muscle per species. The same method was applied for the quantification of the glycogen content (as a reflection of oxidative capacity) of the PAS stain slides. The settings for cell detection and stain intensity thresholds are detailed in Figure 3.3. Both the positive cell detection and cell detection functions had a maximum cell parameter of 25  $\mu\text{m}$ . Due to the cell size of both species being much larger than the maximum cell parameter of Qupath, the software counted each cell as an average of 2-3 cells.

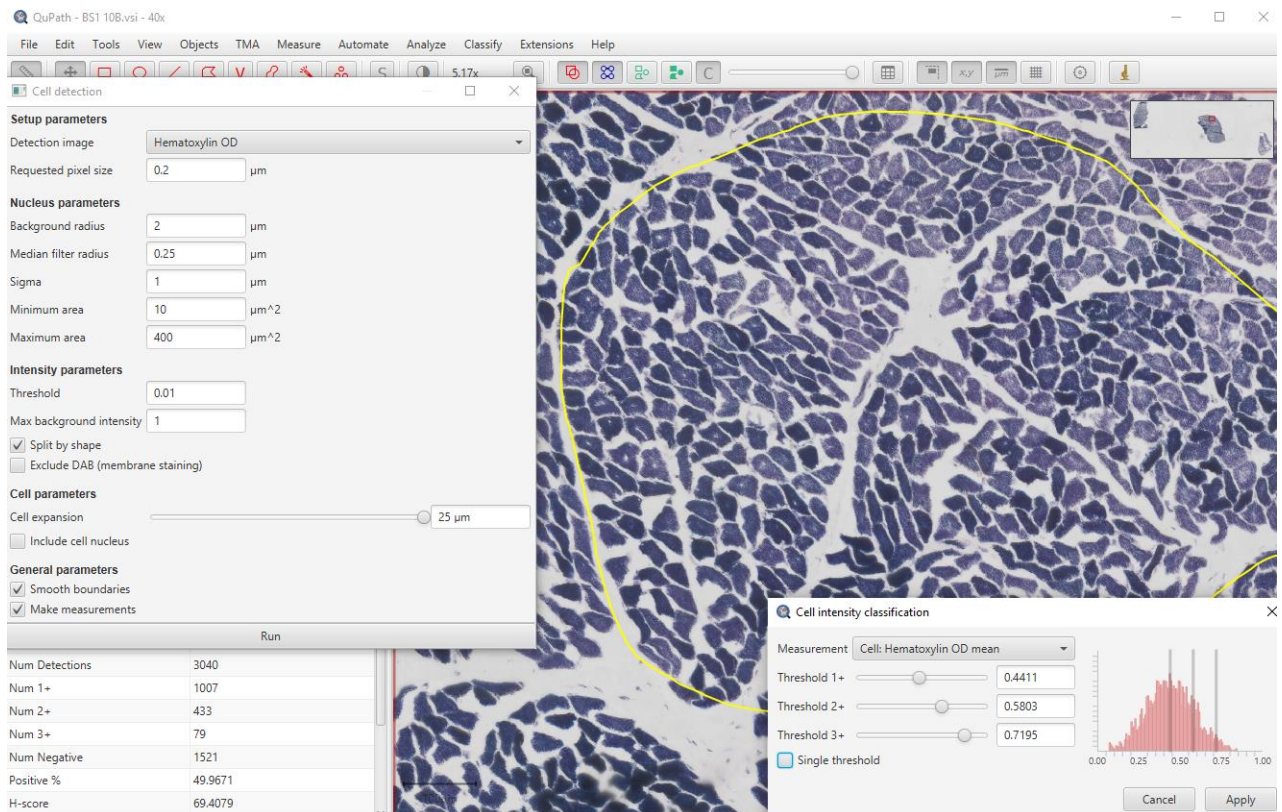


**Figure 3.3:** The Qupath interface showing the NADH staining with the settings used for the detection and classification of the muscle fibres. The polygon tool was used to quantify fibres within a specific area (yellow line)

Optimization of counting the cells of the different stains (NADH and PAS) was done by comparing the results of the three additional fixed *B. suillus* muscles (PAS stain) against the three fresh muscles of the same *B. suillus* animal (NADH stain).

The inclusion criteria for muscle fibre regionalisation were qualitatively defined as a muscle where type I fibres congregate in the deeper regions of the muscle while they are scattered among the type II fibres in a random pattern in the superficial areas of the muscles.

Descriptive statistics were reported per species which include the mean and standard deviation. Significant differences between the muscles of each species were determined through a one-way analysis of variance (ANOVA). Fischer's Least Significant Difference (LSD) *post-hoc* test was used to determine the p-values. A p-value less than 0.05 was considered as statistically significant. Statistica 13.5 (TIBCO software, Palo Alto, California, USA) was used to create most of the graphs and to perform all statistical analyses. The rest of the graphs were created in Microsoft Excel 2010.

### 3.4 Somatosensory mechanisms in the feet of *Bathyergus suillus* and *Heterocephalus glaber*

#### 3.4.1 Sample preparation

The front limbs of six *B. suillus* and six *H. glaber* specimens were fixed in 10% buffered formalin. The footpads of both the left and right front feet were harvested from both species. Similarly, skin containing a row of course hairs on the lateral aspect of the left and right manus, extending from the carpal area to the level of the middle phalanx of the fifth digit, was harvested (Figure 3.4). In addition to the forefeet, the footpads of the pes in *H. glaber* were also harvested. Furthermore, the row of course hair on the lateral aspect of both the manus and pes were harvested as one section with the footpads in the *H. glaber* specimens. This was done due to the small size of the *H. glaber* specimens. Prior to processing the tissue, the footpads were cut into sections as illustrated in Figure 3.5 A and B and wrapped in labelled lint-free papers to be placed within perforated cassettes. All the samples were processed in a Leica Biosystems Automated Vacuum Tissue Processor (ASP6025; *Leica Biosystems: Wetzlar, Germany*) according to the protocol described in Addendum E and then embedded into Paraplast® paraffin wax blocks with a Leica EG 116 Embedder (*Leica Biosystems: Johannesburg, South Africa*). Prior to processing, the distal, middle and proximal footpad sections were wrapped in separate pieces of pencil labelled gauze and placed into plastic cassettes. The sections of each footpad were embedded into one wax block, with the most proximal section placed closest to the labelled part of the cassette and the distal section on the opposite side. The left and right hairy skin sections from the lateral aspect of the manus and pes of the same animal were embedded into one block. The wax blocks were trimmed and sectioned at 7µm with a Leica RM 2125 RT microtome (*Leica Biosystems, Wetzlar, Germany*) and mounted onto frosted microscope slides. Two slides of each wax block were sectioned for staining.



**Figure 3.4:** Lateral view of the pes of *Bathyergus suillus*, as representation of both species, with the red line indicating the skin with sensory hairs that were harvested and analysed. Scale bar=1 cm.

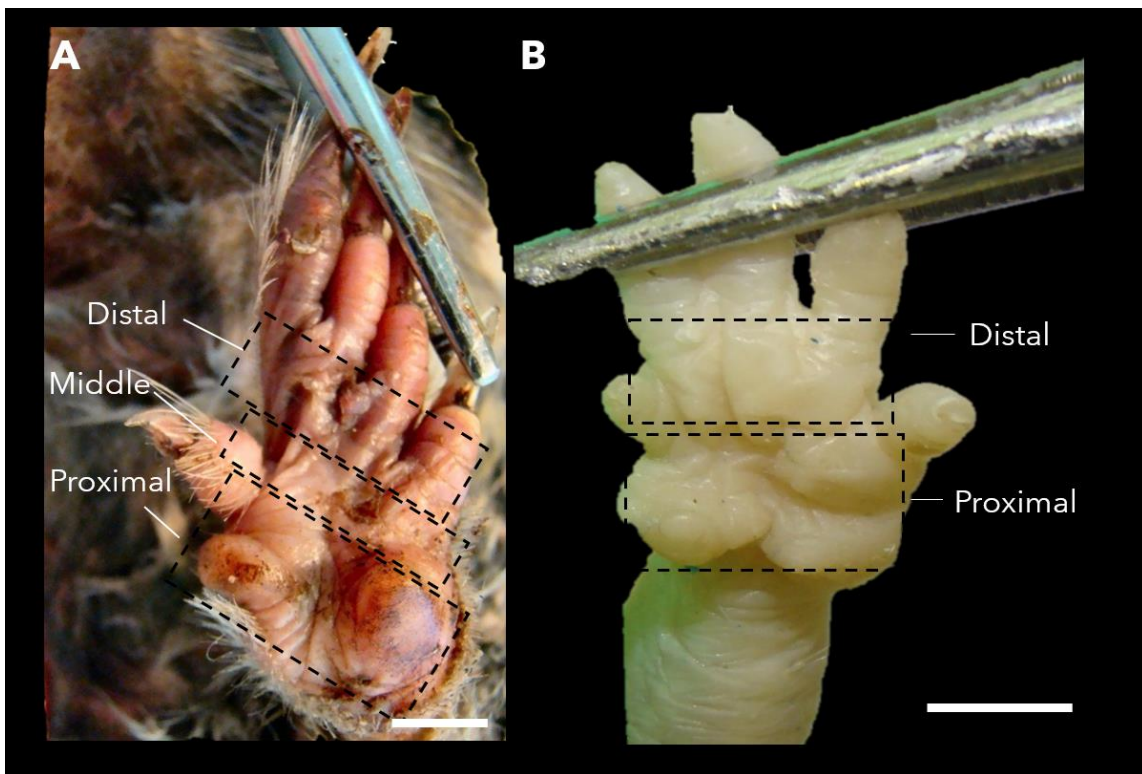


**Figure 3.5:** Plantar surface of the left foot of *Bathyergus suillus* (A) and the right foot of *Heterocephalus glaber* (B). Footpads were cut into a proximal, middle and distal section in *B. suillus* (A) and a proximal and distal section in *H. glaber* (B). Scale bars=5mm.

### 3.4.2 Histochemical staining

The prepared slides were deparaffinised through xylene and a series of ethanol (99%, 99%, 99%, 96%, 96% and 70%) for 5-minute intervals and were stained with haematoxylin and

eosin (H&E) using a Leica Autostainer XL (*Leica Biosystems: Weztlar, Germany*). To confirm the types of mechanoreceptors, ten slides were additionally stained with the Masson's trichrome stain according to the protocol outlined in Addendum D. After staining, the slides were dehydrated in a series of ethanol, cleared in xylene and mounted using DPX mounting media.

### **3.4.3 Quantification of mechanoreceptors**

The slides were scanned at the University of Cape Town, Pathology Learning Centre using an Olympus VS120-L100 (*Olympus Corporation, Tokyo, Japan*) slide scanner. The images were taken with the 40x objective with a final resolution of 16µm per pixel. The composition of mechanoreceptors within the footpads and sensory hairs were analysed and counted using Qupath 0.2.3 software (Bankhead, Loughrey, Fernández *et al.*, 2017). Firstly, a section of tissue was chosen without any tears and with visible epithelium and submucosal layers. The 'Polyline' tool in Qupath was then used to determine the length of the area by measuring the apical surface of the epithelial layer. Once the length of the area was obtained, mechanoreceptors were counted using the 'Counting' tool (Figure 3.6). Inclusion criteria for the four mechanoreceptors are outlined in Table 3.3.

**Table 3.3:** Inclusion criteria for the quantification of the four mechanoreceptors in *Bathyergus suillus* and *Heterocephalus glaber*.

Mechanoreceptor	Inclusion criteria		Source
	Location	Structure	
Merkel cell	Basal layer of epithelium	Clear and oval shaped with a peripheral protein; single cells or clusters and usually in contact with terminal nerve	Iggo & Muir, 1969; Erovic & Erovic, 2013
Ruffini corpuscle	Throughout dermal layer of hairy and glabrous skin.	Small partially encapsulated structure with singular or cluster proteins.	Rein, Hanisch, Zwipp, Fieguth, Lwowski & Hagert, 2013
Meissner corpuscle	Dermal ridges of epidermis.	Coiled structure with stacked disc-like laminar cells and a thin collagenous capsule	Cauna & Ross, 1960
Pacinian corpuscle	A structure with a central terminal neurite surrounded by multiple concentric lamellae and an external capsule	Deep within hairless/ glabrous skin at the level of sweat glands or in the subcutaneous layer of the skin	Cauna, 1965; Bell, Bolanowaki & Holmes, 1994

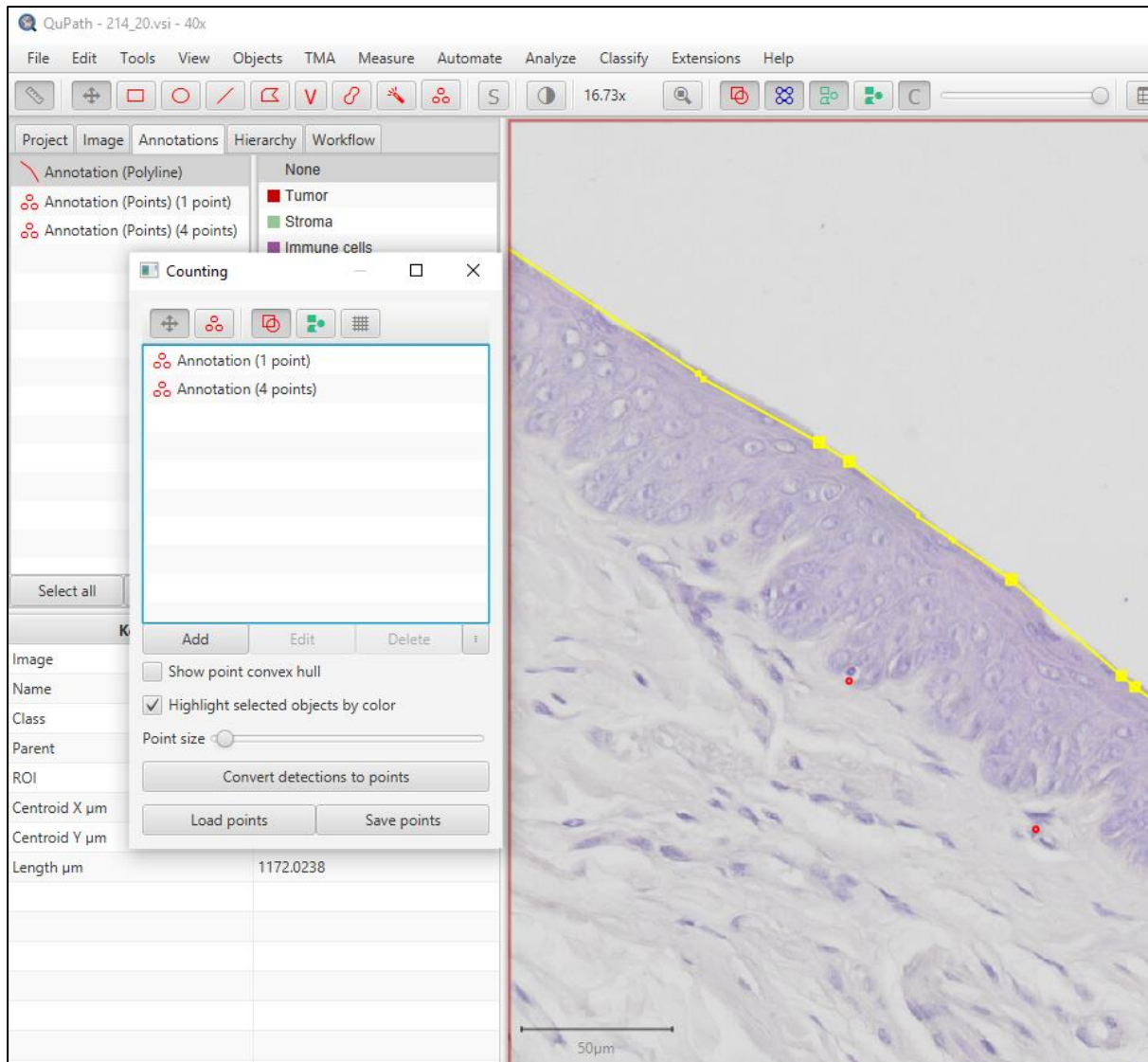


**Figure 3.6:** QuPath interface showing the measured length along the apical surface of the epithelium (yellow polyline) with the counting tool that is used to quantify the four different mechanoreceptors.

In order to compare the mechanoreceptor densities of the fore- and hindfeet between the two studied species, micrographs of the footpads of the hindfeet of *B. suillus* were obtained and re-analysed from a previous unpublished study which used the exact same staining and scanning procedures as described for the present study.

Once all of the data was obtained, the mechanoreceptor densities were calculated by dividing the number of mechanoreceptors by the surface area. The surface area was measured by multiplying the length of the analysed section with the thickness of the tissue section, which was a constant of  $7\mu\text{m}$  for all sections. Thereafter the density of each mechanoreceptor was calculated by dividing the number of mechanoreceptors per tissue section, with the tissue surface area. All calculations were done on Microsoft Excel 2010.

#### **3.4.4 Statistical analysis**

A mixed model analysis of covariance was used to determine significant differences between the two species as well as between the various areas of the footpads within a species. The p-values were determined by using the Fischer's Least Significant Difference *post-hoc* test with statistically significant results determined with a  $p < 0.05$ . All statistical analysis was performed using Statistica 14.0 (TIBCO software, Palo Alto, California, USA). All graphs were created using Microsoft Excel 2010.

#### **3.4.5 Hairy skin on the lateral aspect of the manus and pes**

The hairs observed on the lateral aspect of the skin of the manus and pes of both species were compared and the differences were described based on general histological terminology of the skin. The hairs were identified as sensory or tactile hairs using the following characteristics (Hyvärinen, Kangasperko and Peura 1977; Fundin, Arvidsson & Rice, 1995):

- Merkel cells within the basal layer of the outer root sheath
- Follicle-sinus complex with a trabecular cavernous and ring sinus
- Sebaceous and tubular glands within the upper cavernous sinus

## 4 RESULTS

### 4.1 Muscle architecture

The mean and standard deviation of multiple architectural parameters of each individual muscle are detailed in Tables 4.2 and 4.3 per species. The results of the ANCOVA analyses, including the  $p$ -values of the muscle groups and individual muscles are detailed in Tables 4.1 and 4.4.

#### 4.1.1. Muscle architecture comparisons of muscle groups

The differences in the muscle groups between the species are detailed in Table 4.1 which include the results of the ANCOVA analysis as well as the  $p$ -values. The mean summed isometric force and mean angle of pennation of each muscle group are illustrated in Figure 4.1. The percentage muscle mass to the total front limb muscle mass of each muscle group is illustrated in Figure 4.2.

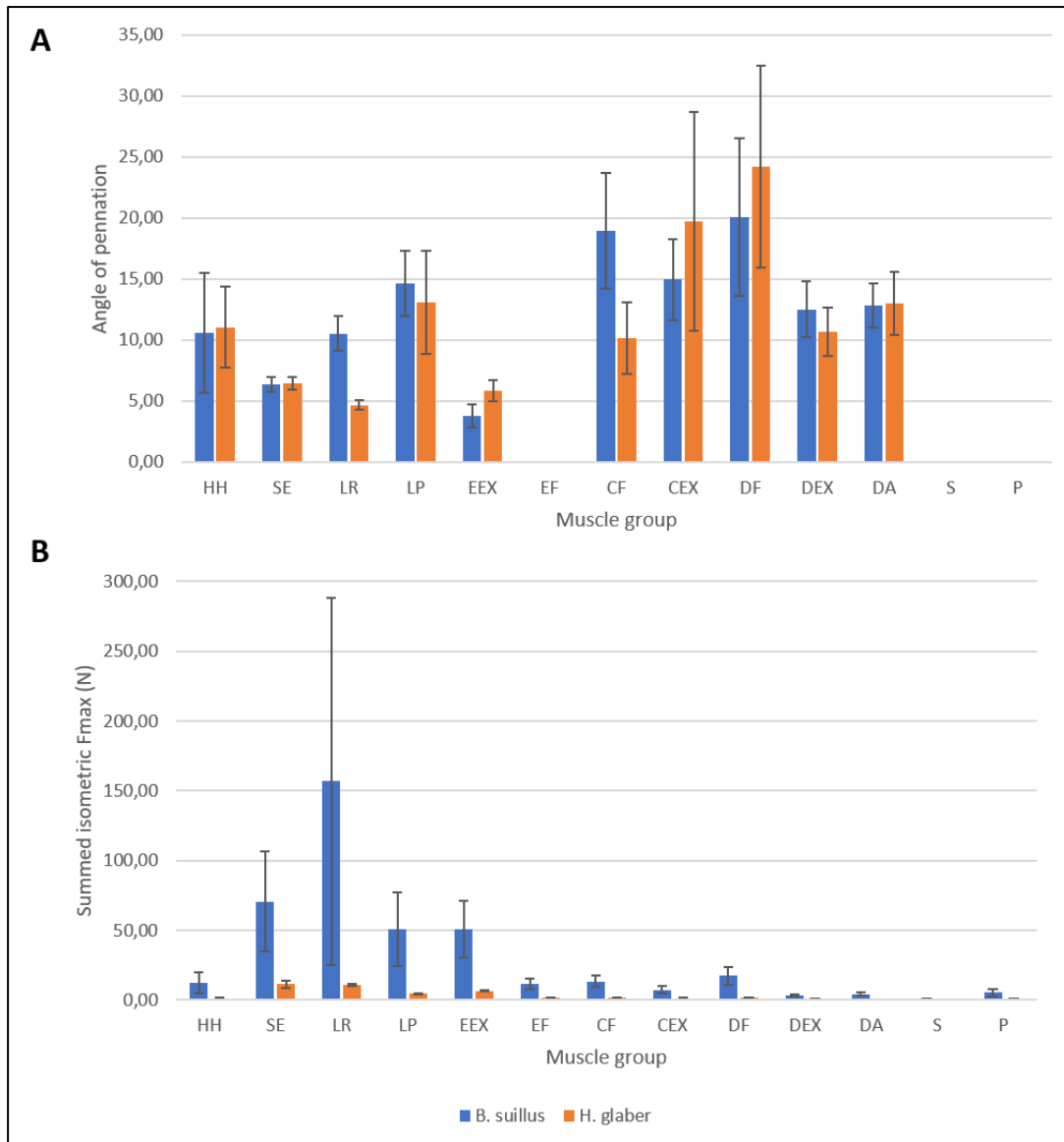


**Figure 4.1:** Mean ( $\pm$  standard deviation) of the angle of pennation (A) and maximum isometric force (B) of the muscle groups in *B. suillus* (blue) and *H. glaber* (orange). Muscle group abbreviations: HH- head extensors and hyoid bone depressors; SE- scapular elevators; LR- limb retractors; LP- limb protractors; EEX- elbow extensors' EF- elbow flexors; CF- carpal flexors; CEX- carpal extensors; DF- digital flexors; DEX- digital extensors; DB- digital abductors; S- supinators; P- pronators

#### a.) Muscle mass

In both species a proximal to distal reduction in muscle mass was seen in the forelimb. The forelimb muscle mass consists of  $\sim 75\%$  proximal and  $25\%$  distal muscle mass where *B. suillus* has slightly more proximal muscle mass compared to *H. glaber* ( $<1\%$ ). Of all the muscle groups studied, in *B. suillus* the limb retractors had the largest percentage muscle mass of the total front limb mass ( $31,93\%$ ). In contrast, in *H. glaber* the scapular retractors had the largest percentage muscle mass ( $31,75\%$ ). The muscle mass percentage of the

scapular retractors and the limb retractors were the second largest group in *B. suillus* (30,10%) and *H. glaber* (29,70%), respectively. The head extensors and hyoid bone depressors (4,46% vs. 2,77%), elbow (3,19% vs. 2,53%) and carpal flexors (2,30% vs. 2,11%), and the carpal (1,98% vs. 1,51%) and digital extensors (1,02% vs. 0,79%) had a larger percentage muscle mass of the total front limb muscle mass in *H. glaber* compared to *B. suillus* (Figure 4.2). The  $M_M$  values of the digital abductors and pronators were significantly larger in *B. suillus* compared to *H. glaber* (Table 4.1).

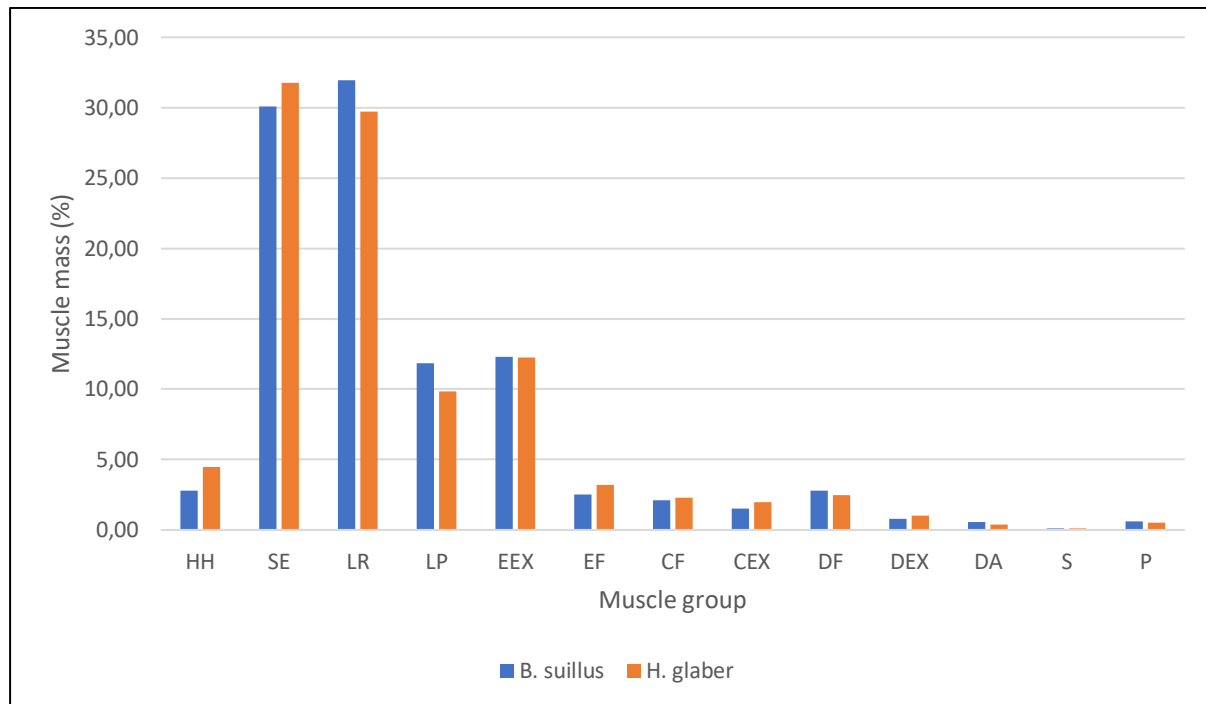


**Figure 4.2:** The muscle mass distribution of each muscle group to the total front limb muscle mass of *B. suillus* (blue) and *H. glaber* (orange). The summed muscle mass of all the individual muscles was used to calculate the total front limb mass. The muscle mass is expressed as percentages with the bars indicating the mean percentage of each muscle group. Biarticular muscles were included in more than one group (see Table 3.1). Muscle group abbreviations: HH- head extensors and hyoid bone depressors; SE- scapular elevators; LR- limb retractors; LP- limb protractors; EEX- elbow extensors' EF- elbow flexors; CF- carpal flexors; CEX- carpal extensors; DF- digital flexors; DEX- digital extensors; DB- digital abductors; S- supinators; P- pronators

### b.) Fascicle length

The fascicle length values of all the muscle groups were significantly different between the two species, with *B. suillus* having the longest fascicles and *H. glaber* the shortest (Table 4.1).

**c.) Physiological Cross-sectional Area (PCSA)**

The PCSA values of the limb retractors, elbow flexors, digital abductors and supinators were significantly larger in *B. suillus* compared to *H. glaber* (Table 4.1).

**d.) Functional space plot**

The mean PCSA (normalized to body mass,  $PCSA/M_b^{0.67}$ ) of each muscle group was plotted against the mean fascicle length (normalized to body mass,  $L_f/M_b^{0.33}$ ) per species illustrated in Figure 4.3. This figure provides an estimation of the relative muscle function by showing the functional space plot of the muscle groups. The scapular elevators and limb retractors of both species are in the upper right quadrant and indicate capabilities of high power output. The elbow extensors of both species and the limb protractors of *B. suillus* are in the upper left quadrant indicating that they have high force capabilities. The muscle groups of *B. suillus* fall within the upper left quadrant (elbow extensors and limb protractors) and have slightly higher force capabilities than the elbow extensors of *H. glaber*. Furthermore, the head extensors and hyoid bone depressors (HH) of both the species fall within the lower left quadrant. The HH group of *H. glaber* extends further towards the right, which indicates a faster shortening capability compared to the HH group of *B. suillus*.

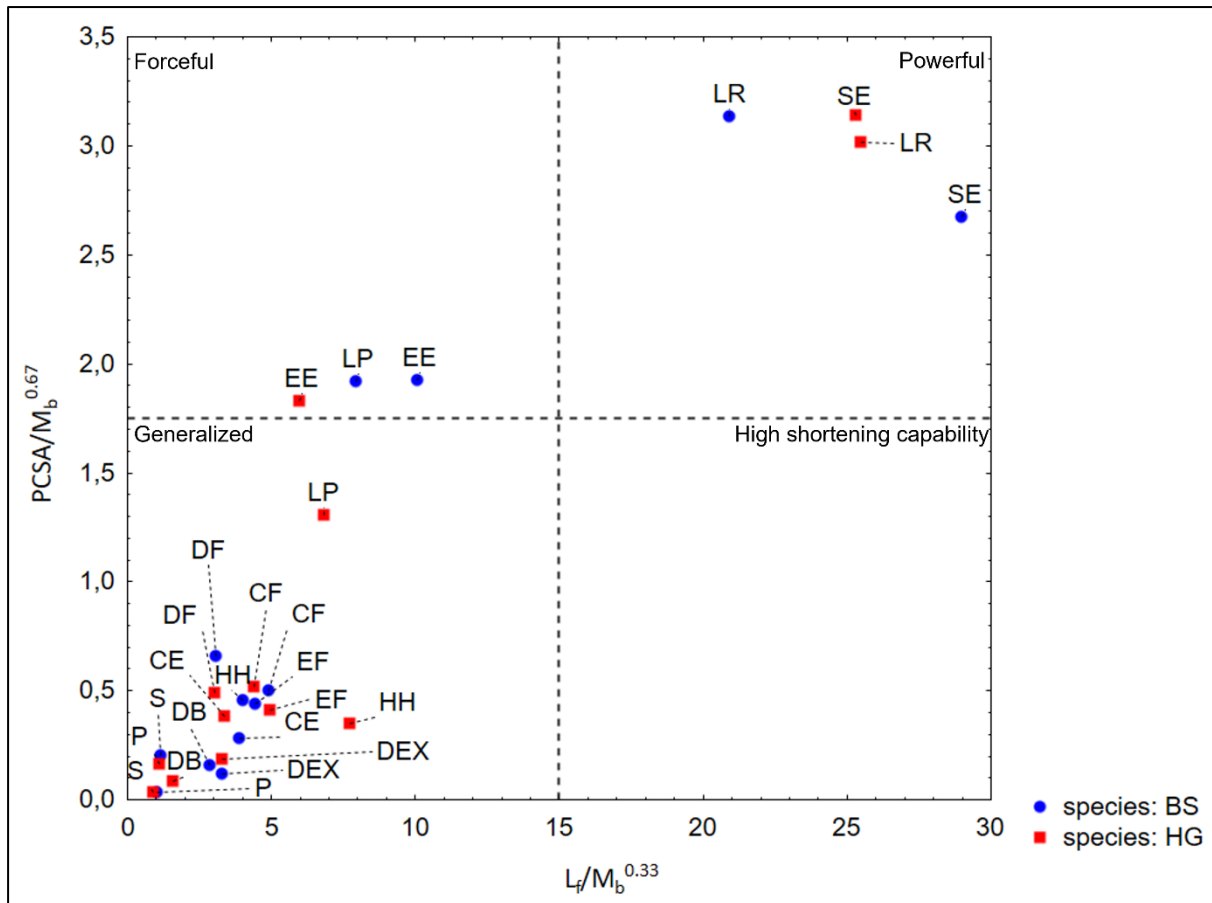


**Figure 4.3:** Physiological cross-sectional area, normalized to body mass ( $PCSA/M_b^{0.67}$ ) as a function of resting fascicle length normalized to body mass ( $L_f/M_b^{0.33}$ ) of the muscle groups in *B. suillus* (blue) and *H. glaber* (red). The force capability is represented by the horizontal dashed line (high-above line; low-below line), while the vertical dashed line separates muscles with high (right) and low (left) shortening capability. Muscles located in the upper right quadrant have both high force and high shortening capabilities and are therefore adapted for high-power outputs. HH- head extensors and hyoid bone depressors; SE- scapular elevators; LR- limb retractors; LP- limb protractors; EE- elbow extensors; EF- elbow flexors; CF- carpal flexors; CE- carpal extensors; DF- digital flexors; DEX- digital extensors; DB- digital abductors; S- supinators; P- pronators

**Table 4.1:** The analysis of covariance (ANCOVA) results of the comparisons of the muscle groups between species.

Muscle group	Muscle mass (Mm)			Fascicle length (Lf)			Physiological cross-sectional area (PCSA)		
	F	df	P	F	df	P	F	df	P
Head extensors and hyoid bone depressors	0.1	1	0.76	<b>18.29</b>	<b>1</b>	<b>p&lt;.01</b>	0.13	1	0.72
Scapular elevators	0.65	1	0.42	<b>11.61</b>	<b>1</b>	<b>p&lt;.01</b>	0.85	1	0.36
Limb retractors	2.58	1	0.11	<b>12.79</b>	<b>1</b>	<b>p&lt;.01</b>	<b>4.69</b>	<b>1</b>	<b>0.03</b>
Limb protractors	1.61	1	0.21	<b>21.42</b>	<b>1</b>	<b>p&lt;.01</b>	0.91	1	0.35
Elbow extensors	1.5	1	0.23	<b>25.81</b>	<b>1</b>	<b>p&lt;.01</b>	0.00	1	0.95
Elbow flexors	4.67	1	0.06	<b>7.74</b>	<b>1</b>	<b>0.02</b>	<b>7.12</b>	<b>1</b>	<b>0.03</b>
Carpal flexors	3.25	1	0.08	<b>14.37</b>	<b>1</b>	<b>p&lt;.01</b>	4.17	1	0.05
Carpal extensors	2.85	1	0.11	<b>15.38</b>	<b>1</b>	<b>p&lt;.01</b>	3.87	1	0.06
Digital flexors	2.05	1	0.17	<b>45.87</b>	<b>1</b>	<b>p&lt;.01</b>	0.83	1	0.37
Digital extensors	1.77	1	0.2	<b>7.38</b>	<b>1</b>	<b>0.01</b>	3.06	1	0.1
Digital abductors	<b>9.46</b>	<b>1</b>	<b>0.01</b>	<b>18.9</b>	<b>1</b>	<b>p&lt;.01</b>	<b>5.79</b>	<b>1</b>	<b>0.03</b>
Supinators	3.13	1	0.11	<b>9.85</b>	<b>1</b>	<b>0.01</b>	<b>12.32</b>	<b>1</b>	<b>0.01</b>
Pronators	<b>5.5</b>	<b>1</b>	<b>0.04</b>	<b>12.71</b>	<b>1</b>	<b>0.01</b>	1.18	1	0.3

Bold text indicates significant results  $p < 0.05$

#### 4.1.2 Muscle architecture comparison of individual muscles

The differences between the species are detailed in Table 4.4 which include the results of the ANCOVA analysis as well as the  $p$ -values. The species-specific differences are indicated in Tables 4.2 and 4.3.

##### a.) Muscle mass

Significant differences between the two species were found in the  $M_M$  of the following muscles: *mm. subclavius*, *claviculoscapularis*, *subscapularis*, *supraspinatus*, *infraspinatus*, *teres major*, *deltoideus pars acromialis*, *deltoideus pars scapularis*, *biceps brachii*, *triceps caput longus*, *triceps caput lateralis*, *palmaris longus*, *pronator teres*, *flexor digitorum superficialis*, *flexor digitorum profundus*, *flexor carpi ulnaris*, *flexor carpi radialis*, *extensor pollicis*, *extensor carpi radialis*, *extensor digitorum communis* and *abductor digiti V*. The values of these muscles were larger in *B. suillus* compared to *H. glaber*.

##### b.) Fascicle length

In most of the individual muscle the fascicle lengths were significantly longer in *B. suillus* compared to *H. glaber*. However, no significant difference was seen in *mm. rhomboideus cervicis*, *rhomboideus capitis*, *subclavius*, *teres major*, *sternohyoideus* and *palmaris longus* (Table 4.4).

##### c.) Physiological Cross-Sectional Area (PCSA)

In *B. suillus* significantly larger PCSA values were found in *mm. subclavius*, *supraspinatus*, *deltoideus pars scapularis*, *biceps brachii*, *brachialis*, *triceps caput longus*, *flexor carpi ulnaris*, *flexor carpi radialis*, *extensor digitorum communis*, *abductor digiti V* and *supinator*, in comparison with *H. glaber*. Furthermore, a significant difference was found in the PCSA of *m. sternocleidomastoideus* where *H. glaber* had the larger value compared to *B. suillus*.

##### d.) Architectural Index

Significant differences between *B. suillus* and *H. glaber* were found in the  $L_f/L_M$  ratios of *mm. subscapularis*, *teres major*, *sternocleidomastoideus* and *extensor digitorum communis* where *H. glaber* had the larger values (Figure 4.4). The  $L_f/L_M$  ratio of *m. flexor digitorum superficialis* was significantly larger in *B. suillus* compared to *H. glaber* (Table 4.4).

**Table 4.2:** The mean and standard deviation ( $\pm$ ) of the architecture parameters of the front limb muscles of *Bathyergus suillus*

Muscle	Abbr.	n	Muscle mass (M <sub>m</sub> , g)	Belly length (L <sub>M</sub> , mm)	Fascicle length (L <sub>f</sub> , mm)	Physiological cross-sectional area (PCSA, mm <sup>2</sup> )	Angle of pennation ( $\theta$ , °)	F <sub>max</sub> (N.mm <sup>-2</sup> )
<i>M. Trapezius pars cervicalis</i>	TC	4	2.7 $\pm$ 1.53	48.90 $\pm$ 10.05	36.09 $\pm$ 6.01	76.64 $\pm$ 51.23	0.00	22.99 $\pm$ 15.37
<i>M. Trapezius pars thoracis</i>	TT	4	1.21 $\pm$ 0.6	67.09 $\pm$ 11.33	58.00 $\pm$ 10.45	16.99 $\pm$ 6.98	0.00	5.1 $\pm$ 2.1
<i>M. Rhomboideus cervicis</i>	RC	3	0.73 $\pm$ 0.39	37.24 $\pm$ 12.66	30.29 $\pm$ 10.21	22.71 $\pm$ 10.4	0.00	5.11 $\pm$ 4.25
<i>M. Rhomboideus capitis</i>	RCa	3	1.17 $\pm$ 0.61	52.92 $\pm$ 17.87	42.70 $\pm$ 11.5	25.11 $\pm$ 8.72	0.00	5.65 $\pm$ 4.33
<i>M. Serratus ventralis</i>	SV	6	3.35 $\pm$ 1.51	51.63 $\pm$ 7.79	33.97 $\pm$ 5.94	70.91 $\pm$ 17.37	48.85 $\pm$ 7.55	17.73 $\pm$ 9.86
<i>M. Lattisimus dorsi</i>	LD	5	2.33 $\pm$ 1.08	74.65 $\pm$ 15.88	54.56 $\pm$ 12.45	38.72 $\pm$ 21.51	24.52 $\pm$ 9.5	9.86 $\pm$ 7.47
<i>M. Pectoralis superficialis</i>	PS	4	2.16 $\pm$ 0.99	42.08 $\pm$ 3.6	35.43 $\pm$ 4.92	59.57 $\pm$ 27.74	0.00	14.3 $\pm$ 10.76
<i>M. Subclavius</i>	SB	3	0.09 $\pm$ 0.27	19.16 $\pm$ 3.66	11.65 $\pm$ 0.8	7.01 $\pm$ 2.14	0.00	1.58 $\pm$ 1.17
<i>M. Omotransversarius</i>	OT	4	0.44 $\pm$ 0.2	32.96 $\pm$ 8.76	30.22 $\pm$ 5.88	13.81 $\pm$ 5.85	0.00	3.31 $\pm$ 2.4
<i>M. Claviculoscapularis</i>	SC	6	0.56 $\pm$ 0.22	29.82 $\pm$ 4.24	18.75 $\pm$ 3.94	29.60 $\pm$ 13.46	0.00	8.88 $\pm$ 4.04
<i>M. Subscapularis</i>	SuS	6	1.69 $\pm$ 0.55	36.18 $\pm$ 3.38	12.38 $\pm$ 2.4	118.57 $\pm$ 47.43	31.49 $\pm$ 6.99	35.57 $\pm$ 14.23
<i>M. Supraspinatus</i>	SS	6	1.38 $\pm$ 0.5	37.40 $\pm$ 2.16	20.92 $\pm$ 3.55	56.12 $\pm$ 19.31	26.37 $\pm$ 7.23	16.84 $\pm$ 5.79
<i>M. Infraspinatus</i>	IS	6	1.37 $\pm$ 0.47	39.52 $\pm$ 2.47	22.32 $\pm$ 5.52	57.59 $\pm$ 29.25	21.08 $\pm$ 3.41	17.28 $\pm$ 8.77
<i>M. Teres major</i>	TM	6	0.61 $\pm$ 0.24	34.45 $\pm$ 6.85	24.01 $\pm$ 6.05	24.85 $\pm$ 9.62	0.00	7.45 $\pm$ 2.89
<i>M. Deltoideus pars acromialis</i>	DA	6	0.48 $\pm$ 0.19	23.63 $\pm$ 2.43	16.55 $\pm$ 2.16	28.79 $\pm$ 12.6	0.00	8.64 $\pm$ 3.78
<i>M. Deltoideus pars scapularis</i>	DS	6	0.61 $\pm$ 0.24	34.65 $\pm$ 5.9	23.74 $\pm$ 5.69	24.63 $\pm$ 7.29	0.00	7.39 $\pm$ 2.19
<i>M. Sternohyoideus</i>	SH	3	0.22 $\pm$ 0.12	27.25 $\pm$ 4.79	22.95 $\pm$ 4.4	9.81 $\pm$ 6.74	0.00	1.77 $\pm$ 2.15
<i>M. Sternoclavicularomastoideus</i>	SCM	4	0.72 $\pm$ 0.33	27.88 $\pm$ 8.99	20.51 $\pm$ 5.44	33.25 $\pm$ 17.71	20.11 $\pm$ 9.02	7.98 $\pm$ 6.41
<i>M. Tensor fasciae antebrachii</i>	TFA	6	0.14 $\pm$ 0.05	22.24 $\pm$ 2.2	19.00 $\pm$ 2.44	6.10 $\pm$ 1.87	0.00	1.83 $\pm$ 0.56

Muscle	Abbr.	n	Muscle mass ( $M_m$ , g)	Belly length ( $L_M$ , mm)	Fascicle length ( $L_f$ , mm)	Physiological cross-sectional area (PCSA, $mm^2$ )	Angle of pennation ( $\theta$ , °)	$F_{max}$ ( $N \cdot mm^{-2}$ )
<i>M. Biceps brachii</i>	BB	6	0.33±0.12	33.01±5.2	17.63±1.64	18.22±6.08	0.00	5.47±1.82
<i>M. Coracobrachialis</i>	CB	6	0.15±0.07	30.42±8.44	20.97±6.43	6.14±2.5	0.00	1.84±0.75
<i>M. Brachialis</i>	Br	6	0.48±0.2	31.49±6.25	22.77±4.9	20.23±7.03	0.00	6.07±2.11
<i>M. Triceps caput longus</i>	TLo	6	2.16±0.69	36.28±2.31	24.04±3.2	83.97±24.49	13.78±1.89	25.19±7.35
<i>M. Triceps caput lateralis</i>	Tla	6	0.99±0.36	34.80±3.95	30.17±13.42	38.53±20.22	0.00	11.56±6.07
<i>M. Triceps caput medialis</i>	TMe	6	0.68±0.28	26.63±1.15	18.16±4.72	40.76±24.05	0.00	12.23±7.21
<i>M. Palmaris longus</i>	PL	6	0.18±0.06	28.39±5.6	16.74±6	10.44±3.72	19.44±5.05	3.13±1.12
<i>M. Pronator teres</i>	PT	6	0.17±0.07	23.33±2.94	10.38±3.07	17.73±8.56	0.00	5.32±2.57
<i>M. Flexor digitorum superficialis</i>	FDS	6	0.17±0.05	27.89±3.37	12.48±3.9	13.60±6.06	17.72±8.95	4.08±1.82
<i>M. Flexor digitorum profundus</i>	FDP	6	0.73±0.23	35.59±3.6	15.45±2.6	44.37±16.29	21.91±5.91	13.31±4.89
<i>M. Flexor carpi ulnaris</i>	FCU	6	0.38±0.14	31.11±4.24	13.29±2.69	25.19±7.56	21.70±8.95	7.56±2.27
<i>M. Flexor carpi radialis</i>	FCR	6	0.12±0.04	22.21±2.8	14.45±4.03	8.38±2.89	15.16±5.21	2.51±0.87
<i>M. Abductor pollicis longus</i>	APL	6	0.07±0.02	26.63±3.58	11.67±0.96	5.14±1.37	12.12±1.87	1.54±0.41
<i>M. Extensor pollicis</i>	EP	6	0.02±0.01	20.29±1.88	12.38±2	1.75±0.43	14.73±1.95	0.52±0.13
<i>M. Extensor carpi radialis</i>	ECR	6	0.33±0.12	26.43±3.22	20.68±2.62	14.67±5.24	15.06±3.12	4.40±1.57
<i>M. Extensor carpi ulnaris</i>	ECU	6	0.16±0.07	29.86±3.75	14.73±4.29	10.01±3.71	13.49±4.17	3.00±1.11
<i>M. Extensor digitorum communis</i>	EDC	6	0.16±0.04	28.81±3.59	17.57±3.41	8.54±1.82	8.91±2.22	2.56±0.55
<i>M. Abductor digiti V</i>	ADV	6	0.13±0.03	28.59±2.24	14.20±2.86	8.72±3.04	13.84±3.07	2.62±0.91
<i>M. Supinator</i>	Su	6	0.03±0.01	13.98±2.38	9.40±2.24	76.64±1.03	0.00	0.92±0.31

**Table 4.3:** The mean and standard deviation ( $\pm$ ) of the architecture parameters of the front limb muscles of *Heterocephalus glaber*

Muscle	Abbr.	n	Muscle mass ( $M_m$ , g)	Belly length ( $L_M$ , mm)	Fascicle length ( $L_f$ , mm)	Physiological cross-sectional area (PCSA, $\text{mm}^2$ )	Angle of pennation ( $\theta$ , $^\circ$ )	$F_{\max}$ ( $\text{N}\cdot\text{mm}^{-2}$ )
<i>M. Trapezius pars cervicalis</i>	TC	6	0.07 $\pm$ 0.081	16.27 $\pm$ 1.394	10.95 $\pm$ 1.102	6.12 $\pm$ 7.705	0.00	1.84 $\pm$
<i>M. Trapezius pars thoracis</i>	TT	4	0.04 $\pm$ 0.006	20.79 $\pm$ 0.791	13.55 $\pm$ 1.382	2.63 $\pm$ 0.275	0.00	0.79 $\pm$
<i>M. Rhomboideus cervicis</i>	RC	3	0.02 $\pm$ 0.003	14.20 $\pm$ 3.314	7.74 $\pm$ 0.651	2.00 $\pm$ 0.223	0.00	0.60 $\pm$
<i>M. Rhomboideus capitis</i>	RCa	5	0.06 $\pm$ 0.008	18.15 $\pm$ 2.286	14.52 $\pm$ 2.046	4.11 $\pm$ 0.689	0.00	1.23 $\pm$
<i>M. Serratus ventralis</i>	SV	6	0.13 $\pm$ 0.019	15.52 $\pm$ 1.786	11.45 $\pm$ 1.043	5.72 $\pm$ 0.965	56.77 $\pm$ 6.507	1.72 $\pm$
<i>M. Latissimus dorsi</i>	LD	6	0.12 $\pm$ 0.02	30.13 $\pm$ 2.077	25.05 $\pm$ 2.874	4.56 $\pm$ 1.01	0.00	1.37 $\pm$
<i>M. Pectoralis superficialis</i>	PS	6	0.07 $\pm$ 0.014	13.39 $\pm$ 1.578	11.26 $\pm$ 1.332	5.75 $\pm$ 0.877	0.00	1.73 $\pm$
<i>M. Subclavius</i>	SB	6	0.004 $\pm$ 0.001	5.38 $\pm$ 0.767	5.48 $\pm$ 4.12	0.86 $\pm$ 0.424	0.00	0.26 $\pm$
<i>M. Omotransversarius</i>	OT	6	0.02 $\pm$ 0.002	13.66 $\pm$ 1.431	12.10 $\pm$ 1.556	1.69 $\pm$ 0.327	0.00	0.51 $\pm$
<i>M. Claviculoscapularis</i>	SC	6	0.03 $\pm$ 0.005	11.49 $\pm$ 1.302	7.74 $\pm$ 1.361	3.63 $\pm$ 0.993	0.00	1.09 $\pm$
<i>M. Subscapularis</i>	SuS	6	0.07 $\pm$ 0.009	12.14 $\pm$ 0.755	7.24 $\pm$ 0.973	8.31 $\pm$ 0.979	22.78 $\pm$ 3.501	2.49 $\pm$
<i>M. Supraspinatus</i>	SS	5	0.04 $\pm$ 0.008	12.47 $\pm$ 1.122	8.47 $\pm$ 7.975	4.71 $\pm$ 0.749	22.304.647 $\pm$	1.41 $\pm$
<i>M. Infraspinatus</i>	IS	6	0.03 $\pm$ 0.007	13.12 $\pm$ 0.456	8.07 $\pm$ 1.99	4.08 $\pm$ 1.367	20.38 $\pm$ 2.934	1.22 $\pm$
<i>M. Teres major</i>	TM	6	0.03 $\pm$ 0.003	11.66 $\pm$ 0.967	10.77 $\pm$ 0.684	2.51 $\pm$ 0.347	0.00	0.75 $\pm$
<i>M. Deltoideus pars acromialis</i>	DA	6	0.01 $\pm$ 0.001	6.60 $\pm$ 0.695	5.05 $\pm$ 0.502	1.88 $\pm$ 0.317	0.00	0.56 $\pm$
<i>M. Deltoideus pars scapularis</i>	DS	6	0.02 $\pm$ 0.004	11.19 $\pm$ 0.749	8.02 $\pm$ 0.991	2.97 $\pm$ 0.551	0.00	0.89 $\pm$
<i>M. Deltoideus pars clavicularis</i>	DC	6	0.02 $\pm$ 0.002	10.27 $\pm$ 0.464	9.24 $\pm$ 0.77	2.13 $\pm$ 0.18	0.00	0.64 $\pm$
<i>M. Sternohyoideus</i>	SH	5	0.01 $\pm$ 0.003	15.41 $\pm$ 2.967	13.83 $\pm$ 0.79	1.01 $\pm$ 0.227	0.00	0.30 $\pm$
<i>M. Sternoclaviculomastoideus</i>	SCM	6	0.04 $\pm$ 0.009	15.71 $\pm$ 2.145	11.88 $\pm$ 1.78	3.40 $\pm$ 0.88	22.65 $\pm$ 6.051	1.02 $\pm$
<i>M. Biceps brachii</i>	BB	6	0.02 $\pm$ 0.002	10.28 $\pm$ 0.851	6.92 $\pm$ 1.426	2.30 $\pm$ 0.628	0.00	0.69 $\pm$
<i>M. Brachialis</i>	Br	6	0.03 $\pm$ 0.005	10.96 $\pm$ 0.703	9.61 $\pm$ 1.176	2.61 $\pm$ 0.383	0.00	0.78 $\pm$
<i>M. Triceps brachi caput longus</i>	TLo	6	0.09 $\pm$ 0.01	11.27 $\pm$ 1.002	6.81 $\pm$ 1.013	12.07 $\pm$ 1.321	17.61 $\pm$ 2.61	3.62 $\pm$
<i>M. Triceps brachi caput lateralis</i>	TLa	6	0.05 $\pm$ 0.004	10.85 $\pm$ 0.922	8.13 $\pm$ 1.295	5.59 $\pm$ 0.606	0.00	1.68 $\pm$

Muscle	Abbr.	n	Muscle mass ( $M_m$ , g)	Belly length ( $L_M$ , mm)	Fascicle length ( $L_f$ , mm)	Physiological cross-sectional area (PCSA, $\text{mm}^2$ )	Angle of pennation ( $\theta$ , °)	$F_{\max}$ ( $\text{N}\cdot\text{mm}^{-2}$ )
<i>M. Triceps brachii caput medialis</i>	TMe	6	0.03±0.003	9.27±0.905	5.94±1.149	4.30±0.985	0.00	1.29±
<i>M. Palmaris longus</i>	PL	4	0.01±0.001	7.86±0.761	5.90±0.853	1.01±0.25	0.00	0.30±
<i>M. Pronator teres</i>	PT	6	0.01±0.001	6.43±0.887	3.76±0.918	1.96±0.859	0.00	0.59±
<i>M. Flexor digitorum superficialis</i>	FDS	5	0.01±0.003	11.94±1.423	4.11±1.402	3.08±0.89	29.70±4.715	0.92±
<i>M. Flexor digitorum profundus</i>	FDP	5	0.02±0.002	9.25±1.638	6.2±1.706	2.67±0.339	19.98±13.848	0.8±0.102
<i>M. Flexor carpi ulnaris</i>	FCU	5	0.02±0.002	10.70±0.795	4.00±0.46	4.49±0.691	20.40±6.592	1.35±
<i>M. Flexor carpi radialis</i>	FCR	6	0.005±0.001	7.37±1.383	5.26±0.837	0.88±0.24	13.40±2.951	0.26±
<i>M. Extensor pollicis</i>	EP	4	0.004±0.001	8.58±0.906	4.03±0.581	1.02±0.181	10.71±2.39	0.31±
<i>M. Extensor carpi radialis</i>	ECR	5	0.02±0.002	9.37±0.2	8.12±0.69	1.96±0.201	19.78±3.895	0.59±
<i>M. Extensor carpi ulnaris</i>	ECU	6	0.01±0.001	9.37±0.654	3.34±1.175	2.57±0.893	19.03±2.766	0.77±
<i>M. Extensor digitorum communis</i>	EDC	6	0.01±0.002	9.59±0.761	7.08±0.468	1.17±0.216	10.02±2.079	0.35±
<i>M. Abductor digiti V</i>	ADV	3	0.01±0.001	9.31±1.015	5.34±2.243	1.00±0.428	12.98±2.589	0.30±
<i>M. Supinator</i>	Su	4	0.0014±0.001	4.78±0.827	3.12±1.014	0.43±0.162	0.00	0.13±

**Table 4.4:** The analysis of covariance (ANCOVA) results of the comparisons of the individual muscles between species.

Muscle	Muscle mass (Mm)			Fascicle length (Lf)			Physiological cross-sectional area (PCSA)			Lf/Lm		
	F	df	P	F	df	P	F	df	P	F	df	P
<i>M. Trapezius pars cervicalis</i>	0.21	1	0.66	<b>26.61</b>	<b>1</b>	<b>p&lt;.01</b>	0.35	1	0.57	0.89	1	0.38
<i>M. Trapezius pars thoracis</i>	0.41	1	0.54	<b>32.6</b>	<b>1</b>	<b>p&lt;.01</b>	2.13	1	0.2	0.72	1	0.43
<i>M. Rhomboideus cervicis</i>	0.42	1	0.56	5.82	1	0.09	1.35	1	0.33	2.81	1	0.19
<i>M. Rhomboideus capitis</i>	0.88	1	0.39	5.14	1	0.07	3.91	1	0.1	4.4	1	0.09
<i>M. Serratus ventralis</i>	3.26	1	0.1	<b>20.62</b>	<b>1</b>	<b>p&lt;.01</b>	3.21	1	0.11	0.01	1	0.93
<i>M. Lattisimus dorsi</i>	1.26	1	0.29	<b>8.46</b>	<b>1</b>	<b>0.02</b>	0.13	1	0.73	0.06	1	0.81
<i>M. Pectoralis superficialis</i>	0.17	1	0.69	<b>26.12</b>	<b>1</b>	<b>p&lt;.01</b>	0.44	1	0.53	0.2	1	0.67
<i>M. Subclavius</i>	<b>11.23</b>	<b>1</b>	<b>0.02</b>	1.89	1	0.22	<b>8.46</b>	<b>1</b>	<b>0.03</b>	0.01	1	0.92
<i>M. Omotransversarius</i>	0.53	1	0.49	<b>8.6</b>	<b>1</b>	<b>0.02</b>	0.12	1	0.74	1.09	1	0.33
<i>M. Claviculoscapularis</i>	<b>7.27</b>	<b>1</b>	<b>0.02</b>	<b>19.65</b>	<b>1</b>	<b>p&lt;.01</b>	2	1	0.19	0.29	1	0.6
<i>M. Subscapularis</i>	<b>15.69</b>	<b>1</b>	<b>p&lt;.01</b>	<b>25.37</b>	<b>1</b>	<b>p&lt;.01</b>	4.61	1	0.06	<b>6.92</b>	<b>1</b>	<b>0.03</b>
<i>M. Supraspinatus</i>	<b>10.35</b>	<b>1</b>	<b>0.01</b>	<b>11.45</b>	<b>1</b>	<b>0.01</b>	<b>6.5</b>	<b>1</b>	<b>0.03</b>	5.45	1	0.05
<i>M. Infraspinatus</i>	<b>22.39</b>	<b>1</b>	<b>p&lt;.01</b>	<b>9.9</b>	<b>1</b>	<b>0.01</b>	1.77	1	0.22	0.23	1	0.64
<i>M. Teres major</i>	<b>5.83</b>	<b>1</b>	<b>0.04</b>	4.71	1	0.06	4.48	1	0.06	<b>12.47</b>	<b>1</b>	<b>0.01</b>
<i>M. Deltoideus pars acromialis</i>	<b>6.81</b>	<b>1</b>	<b>0.03</b>	<b>92.85</b>	<b>1</b>	<b>p&lt;.01</b>	2.92	1	0.12	0.33	1	0.58
<i>M. Deltoideus pars scapularis</i>	<b>7.21</b>	<b>1</b>	<b>0.03</b>	<b>8.69</b>	<b>1</b>	<b>0.02</b>	<b>10.82</b>	<b>1</b>	<b>0.01</b>	4.2	1	0.07
<i>M. Sternohyoideus</i>	0.55	1	0.49	5.19	1	0.07	0.27	1	0.63	0.24	1	0.65
<i>M. Sternoclavicularomastoideus</i>	0.37	1	0.56	<b>15.22</b>	<b>1</b>	<b>0.01</b>	<b>54.23</b>	<b>1</b>	<b>p&lt;.01</b>	<b>6.6</b>	<b>1</b>	<b>0.04</b>
<i>M. Biceps brachii</i>	<b>11.26</b>	<b>1</b>	<b>0.01</b>	<b>41.25</b>	<b>1</b>	<b>p&lt;.01</b>	<b>23.64</b>	<b>1</b>	<b>p&lt;.01</b>	0.38	1	0.55
<i>M. Brachialis</i>	4.67	1	0.06	<b>7.74</b>	<b>1</b>	<b>0.02</b>	<b>7.12</b>	<b>1</b>	<b>0.03</b>	1.89	1	0.2
<i>M. Triceps caput longus</i>	<b>34.24</b>	<b>1</b>	<b>p&lt;.01</b>	<b>45.19</b>	<b>1</b>	<b>p&lt;.01</b>	<b>20.05</b>	<b>1</b>	<b>p&lt;.01</b>	1.15	1	0.31
<i>M. Triceps caput lateralis</i>	<b>10.12</b>	<b>1</b>	<b>0.01</b>	<b>25.00</b>	<b>1</b>	<b>p&lt;.01</b>	0.03	1	0.87	3.74	1	0.09
<i>M. Triceps caput medialis</i>	5.09	1	0.05	<b>45.45</b>	<b>1</b>	<b>p&lt;.01</b>	0.03	1	0.86	3.29	1	0.1
<i>M. Palmaris longus</i>	<b>6.63</b>	<b>1</b>	<b>0.04</b>	1.94	1	0.21	5.9	1	0.05	3.1	1	0.12

Muscle	Muscle mass (Mm)			Fascicle length (Lf)			Physiological cross-sectional area (PCSA)			Lf/Lm		
	F	df	P	F	df	P	F	df	P	F	df	P
M. Pronator teres	5.5	1	0.04	12.71	1	0.01	1.18	1	0.3	0.00	1	0.99
M. Flexor digitorum superficiales	8.7	1	0.02	33.11	1	p<.01	0.17	1	0.69	9.04	1	0.02
M. Flexor digitorum profundus	12.89	1	0.01	24.97	1	p<.01	5.63	1	0.05	0.27	1	0.62
M. Flexor carpi ulnaris	9.17	1	0.02	13.96	1	0.01	7.16	1	0.03	0.42	1	0.54
M. Flexor carpi radialis	13.8	1	p<.01	6.32	1	0.03	7.16	1	0.03	0.18	1	0.68
M. Extensor pollicis	6.08	1	0.04	65.06	1	p<.01	2.47	1	0.16	0.13	1	0.73
M. Extensor carpi radialis	10.04	1	0.01	32.37	1	p<.01	4.99	1	0.06	0.02	1	0.9
M. Extensor carpi ulnaris	2.26	1	0.17	8.13	1	0.02	1.71	1	0.22	0.58	1	0.47
M. Extensor digitorum communis	20.37	1	p<.01	15.45	1	p<.01	22.81	1	p<.01	24.56	1	p<.01
M. Abductor digiti V	39.06	1	p<.01	11.41	1	0.01	9.22	1	0.02	0.01	1	0.93
M. Supinator	3.13	1	0.11	9.85	1	0.01	12.32	1	0.01	0.26	1	0.62

Bold text indicates significant results p<0.05

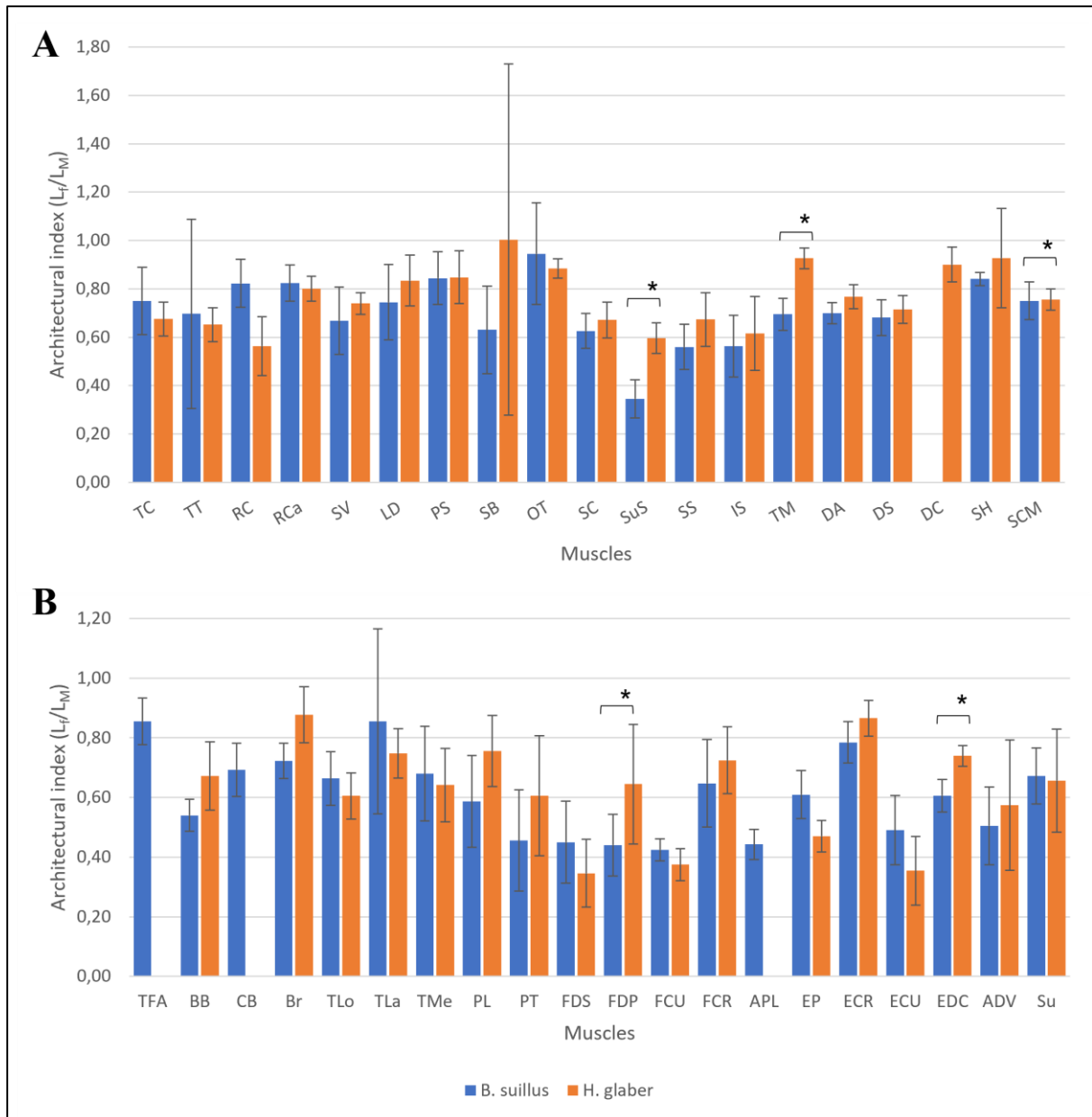


**Figure 4.4:** The mean ( $\pm$  standard deviation) architectural index of muscle fascicle length/muscle belly length (Lf/LM) for the proximal (A) and distal (B) individual muscles of *B. suillus* (blue) and *H. glaber* (orange). \* indicates a significant difference of  $p < 0.05$  between species. Muscle abbreviations as detailed in Table 4.2 and 4.3.

### e.) Functional Space Plot

The mean PCSA (normalized to body mass,  $PCSA/M_b^{0.67}$ ) of each individual muscle was plotted against the mean fascicle length (normalized to body mass,  $L_f/M_b^{0.33}$ ) per species in Figure 4.5. The *m. subscapularis* of *B. suillus* is the highest in the upper left quadrant compared to *H. glaber*, indicating that *m. subscapularis* has a higher force-output in *B. suillus*. The *m. latissimus dorsi* of both species is in the lower right quadrant with *H. glaber* having a faster shortening capability than *B. suillus* (far right in lower right quadrant), while *B. suillus* has a slightly higher force-output than *H. glaber* (upper right in lower right quadrant). The *m. sternohyoideus* (SH) of *H. glaber* is in the lower right quadrant with the *m. sternocleidomastoideus* of the head extensor and hyoid bone depressor (HH) group, situated to the left of SH. This indicates a higher shortening capacity when compared to the muscles of the HH group (*mm. sternohyoideus* and *sternocleidomastoideus*) of *B. suillus*, which are situated more to the left compared to *H. glaber*.

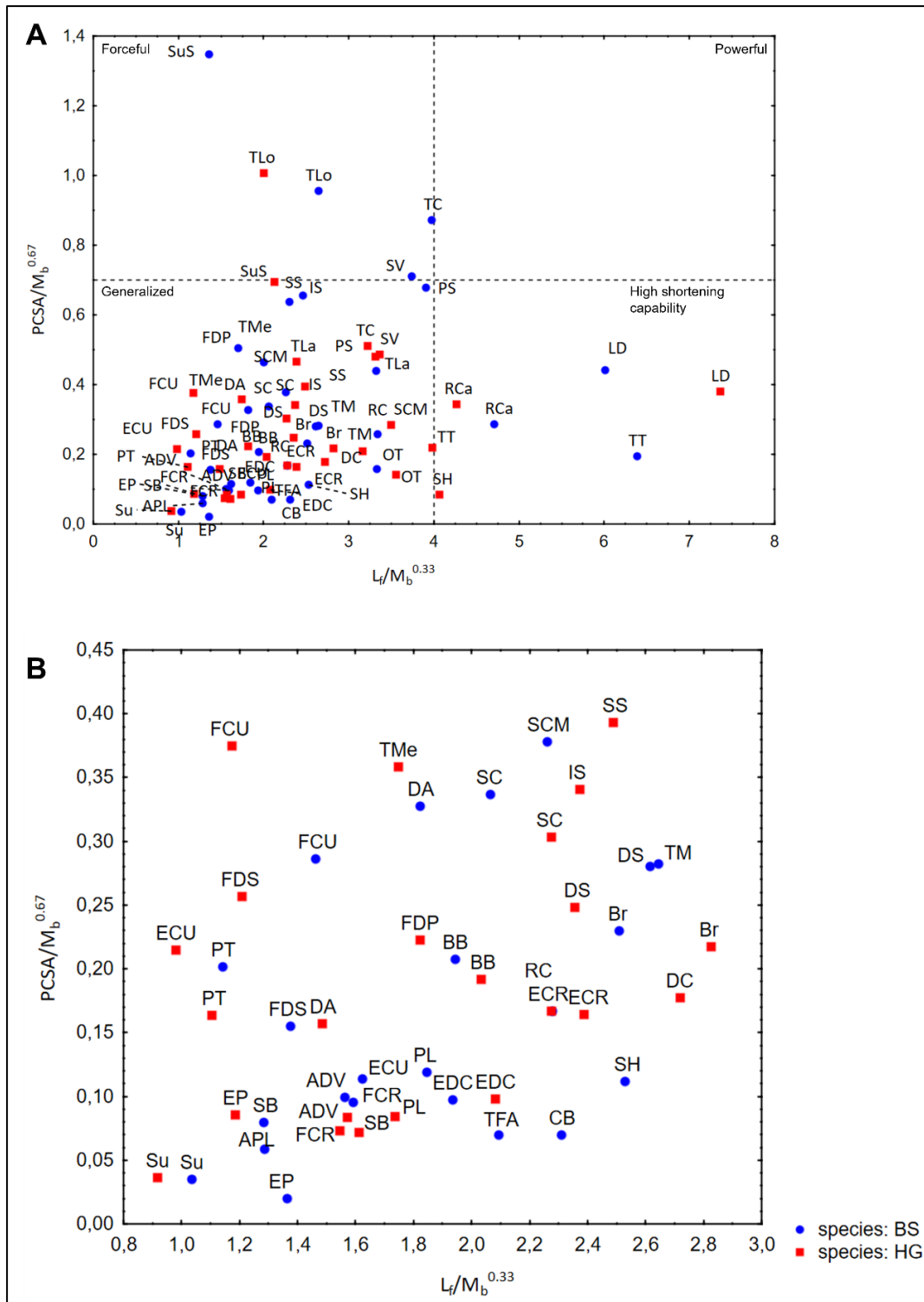


**Figure 4.5:** Physiological cross-sectional area, normalized to body mass (PCSA/Mb<sup>0.67</sup>) as a function of resting fascicle length normalized to body mass (L<sub>f</sub>/Mb<sup>0.33</sup>) of all the individual muscles (A) and an enlarged representation of the lower left quadrant of panel A (B) for *B. suillus* (blue) and *H. glaber* (red). In panel A the force capability is represented by the horizontal dashed line (high-above line; low-below line), while the vertical dashed line separates muscles with high (right) and low (left) shortening capability. For panel B the muscles are shown separately from panel A to make referencing easier. Muscle abbreviations as detailed in Table 4.2 and 4.3.

## 4.2 Muscle fibre typing

The mean percentages and standard deviation of type I and type II fibres as well as the oxidative, oxidative glycolytic and glycolytic fibres per muscle and muscle group of both species are detailed in Tables 4.5- 4.8.

### 4.2.1 Slow myosin stain: Type I and II fibres

*Bathyergus suillus* had the most type I fibres in all individual muscles when compared to *H. glaber*, except for *mm. triceps brachii caput lateralis*, *flexor digitorum profundus* and *pectoralis superficialis* which had higher type I fibre percentages in *H. glaber* (Figure 4.6).

*Bathyergus suillus* had significantly more type I fibres in *m. teres major* compared to *H. glaber* ( $p=0.03$ ; Table 4.5). Although not significant, the type I fibre percentages in *mm. triceps brachii caput medialis* and *biceps brachii* were  $\pm 20\%$  higher in *B. suillus* compared to *H. glaber*. Furthermore, *m. triceps brachii caput medialis* in *B. suillus* had the most type I fibres ( $66.17\% \pm 15.72$ ) while the *m. teres major* in *H. glaber* had the fewest slow fibres ( $7.94\% \pm 0.81$ ).

In both species the elbow extensor group had the highest type I fibre percentage when compared to the other muscle groups. *Bathyergus suillus* had the most type I fibres in all muscle groups when compared to *H. glaber* (Figure 4.7; Table 4.6).

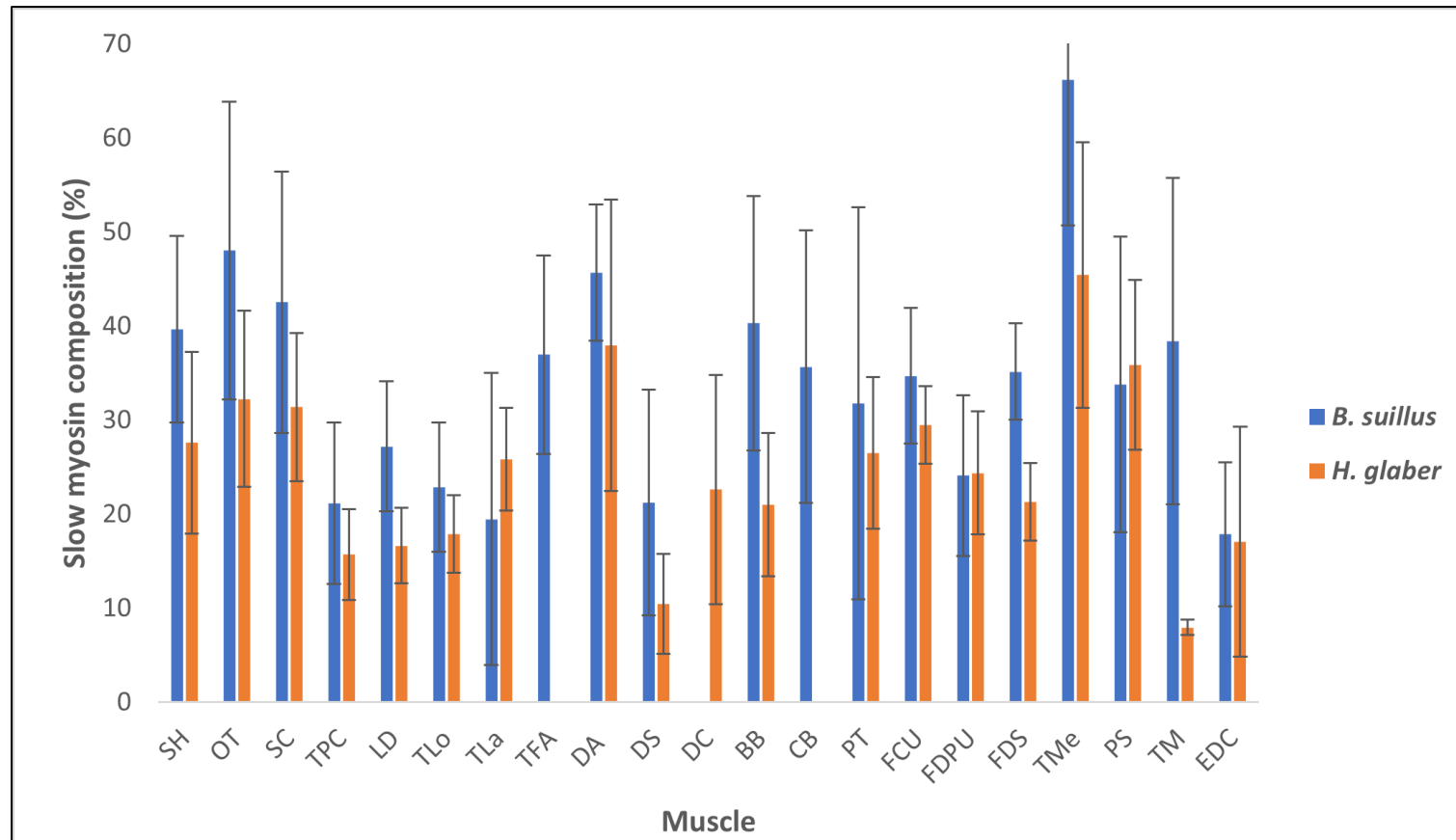


**Figure 4.6:** The mean ( $\pm$  standard deviation) of the slow myosin composition (%) of individual muscles in *Bathyergus suillus* (blue) and *Heterocephalus glaber* (orange). Muscle abbreviations: SH- *m. sternohyoideus*; OT- *m. omotransversarius*; SC- *m. claviculo-scapularis*; TPC- *m. trapezius pars cervicales*; LD- *m. latissimus dorsi*; TLo- *m. triceps brachii caput longum*; TLa- *m. triceps brachii caput lateralis*; TFA- *m. tensor fasciae antebrachia*; DA- *m. deltoideus pars acromialis*; DS- *m. deltoideus pars scapularis*; DC- *m. deltoideus pars clavicularis*; BB- *m. biceps brachii*; CB- *m. coracobrachialis*; PT- *m. pronator teres*; FCU- *m. flexor carpi ulnaris*; FDPU- *m. flexor digitorum profundus* (ulnar head); FDS- *m. flexor digitorum superficialis*; TMe- *m. triceps brachii caput medialis*; PS- *m. pectoralis superficialis*; TM- *m. teres major*; EDC- *m. extensor digitorum communis*.

**Table 4.5:** The mean percentage and standard deviation ( $\pm$ ) of the type I and type II fibres in the individual muscles of *Bathyergus suillus* and *Heterocephalus glaber*.

Muscle	<i>Bathyergus suillus</i>		<i>Heterocephalus glaber</i>	
	Type I	Type II	Type I	Type II
<i>M. Sternohyoideus</i>	39.65 $\pm$ 12.16	60.35 $\pm$ 12.16	27.6 $\pm$ 10.81	72.4 $\pm$ 10.81
<i>M. Omotransversarius</i>	48.03 $\pm$ 18.26	51.97 $\pm$ 18.26	32.25 $\pm$ 10.48	67.75 $\pm$ 10.48
<i>M. Claviculo-scapularis</i>	42.53 $\pm$ 15.19	57.47 $\pm$ 15.19	31.38 $\pm$ 9.11	68.62 $\pm$ 9.11
<i>M. Trapezius pars cervicalis</i>	21.17 $\pm$ 9.42	78.83 $\pm$ 9.42	15.69 $\pm$ 5.4	84.31 $\pm$ 5.4
<i>M. Latissimus dorsi</i>	27.21 $\pm$ 7.57	72.79 $\pm$ 7.57	16.65 $\pm$ 4.49	83.35 $\pm$ 4.49
<i>M. Triceps brachii caput longum</i>	22.86 $\pm$ 7.5	77.14 $\pm$ 7.5	17.9 $\pm$ 4.64	82.1 $\pm$ 4.64
<i>M. Triceps brachii caput lateralis</i>	19.48 $\pm$ 17.03	80.52 $\pm$ 17.03	25.81 $\pm$ 6.11	74.19 $\pm$ 6.11
<i>M. Tensor fasciae antebrachia</i>	36.95 $\pm$ 10.57	63.05 $\pm$ 10.57		
<i>M. Deltoideus pars acromialis</i>	45.7 $\pm$ 7.95	54.3 $\pm$ 7.95	37.93 $\pm$ 16.97	62.07 $\pm$ 16.97
<i>M. Deltoideus pars scapularis</i>	21.21 $\pm$ 13.15	78.79 $\pm$ 13.15	10.44 $\pm$ 5.82	89.56 $\pm$ 5.82
<i>M. Deltoideus pars clavicularis</i>			22.62 $\pm$ 12.19	77.38 $\pm$ 12.19
<i>M. Biceps brachii</i>	40.3 $\pm$ 14.81	59.7 $\pm$ 14.81	21 $\pm$ 8.32	79 $\pm$ 8.32
<i>M. Coracobrachialis</i>	35.68 $\pm$ 14.47	64.32 $\pm$ 14.47		
<i>M. Pronator teres</i>	31.76 $\pm$ 23.3	68.24 $\pm$ 23.3	26.5 $\pm$ 8.81	73.5 $\pm$ 8.81
<i>M. Flexor carpi ulnaris</i>	34.69 $\pm$ 8.33	65.31 $\pm$ 8.33	29.46 $\pm$ 4.51	70.54 $\pm$ 4.51
<i>M. Flexor digitorum superficialis</i>	35.14 $\pm$ 5.73	64.86 $\pm$ 5.73	21.32 $\pm$ 6.52	78.68 $\pm$ 6.52
<i>M. Flexor digitorum profundus (ulnar head)</i>	24.1 $\pm$ 8.55	75.9 $\pm$ 8.55	24.38 $\pm$ 6.53	75.62 $\pm$ 6.53
<i>M. Triceps brachii caput medialis</i>	66.17 $\pm$ 16.96	33.83 $\pm$ 16.96	45.43 $\pm$ 15.44	54.57 $\pm$ 15.44
<i>M. Pectoralis superficialis</i>	33.8 $\pm$ 17.58	66.2 $\pm$ 17.58	35.89 $\pm$ 9.89	64.11 $\pm$ 9.89
<i>M. Teres major</i>	<b>38.41 <math>\pm</math> 19.39</b>	<b>61.59 <math>\pm</math> 19.39</b>	<b>7.94 <math>\pm</math> 0.9</b>	<b>92.06 <math>\pm</math> 0.9</b>
<i>M. Extensor digitorum communis</i>	17.85 $\pm$ 8.37	82.15 $\pm$ 8.37	17.05 $\pm$ 13.69	82.95 $\pm$ 13.69

Bold text indicates significant results  $p < 0.05$

**Table 4.6:** The mean percentage and standard deviation ( $\pm$ ) of the type I and type II fibres in the muscle groups of *Bathyergus suillus* and *Heterocephalus glaber*.

Muscle group	<i>Bathyergus suillus</i>		<i>Heterocephalus glaber</i>	
	Type I	Type II	Type I	Type II
Scapular elevators	35.9 $\pm$ 17.8	64.1 $\pm$ 17.8	26.09 $\pm$ 11.26	73.91 $\pm$ 11.26
Limb protractors	34.34 $\pm$ 15.29	65.66 $\pm$ 15.29	22.25 $\pm$ 14.36	77.75 $\pm$ 14.36
Elbow extensors	36.37 $\pm$ 22.82	63.63 $\pm$ 22.82	29.74 $\pm$ 15.7	70.26 $\pm$ 15.7
Digital flexors	29.62 $\pm$ 9.43	70.38 $\pm$ 9.43	24.83 $\pm$ 9.03	75.17 $\pm$ 9.03

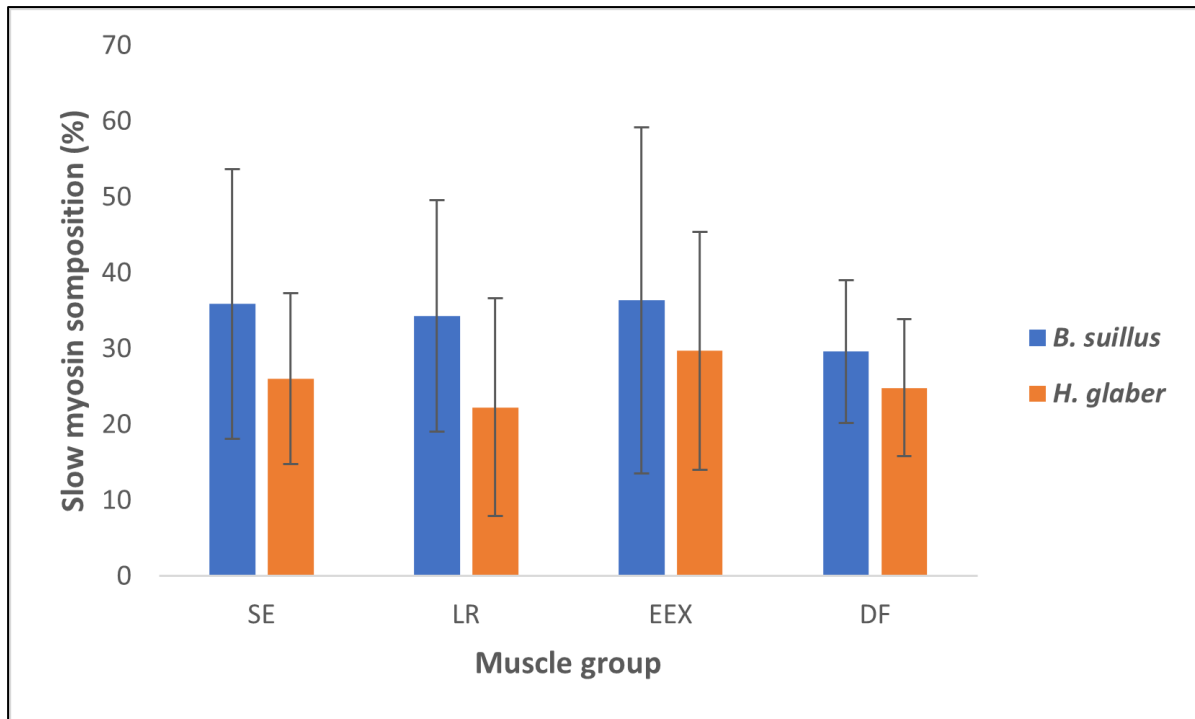


**Figure 4.7:** The mean ( $\pm$  standard deviation) of the slow myosin composition (%) of muscle groups in *Bathyergus suillus* (blue) and *Heterocephalus glaber* (orange). Muscle group abbreviations: SE- scapular elevators/stabilisers/retractors; LR- limb retractors; EEX- elbow extensors; DF- digital flexors.

Regionalisation of muscle fibres was observed in three muscles, namely, *mm. pectoralis superficialis*, *triceps brachii caput longum*, and *deltoideus pars scapularis*, in both species (Figure 4.8). Additionally, regionalisation of fibres in *m. claviculo-scapularis* was present in *B. suillus* and regionalisation in *m. triceps brachii caput medialis* in *H. glaber* (Figure 4.9).

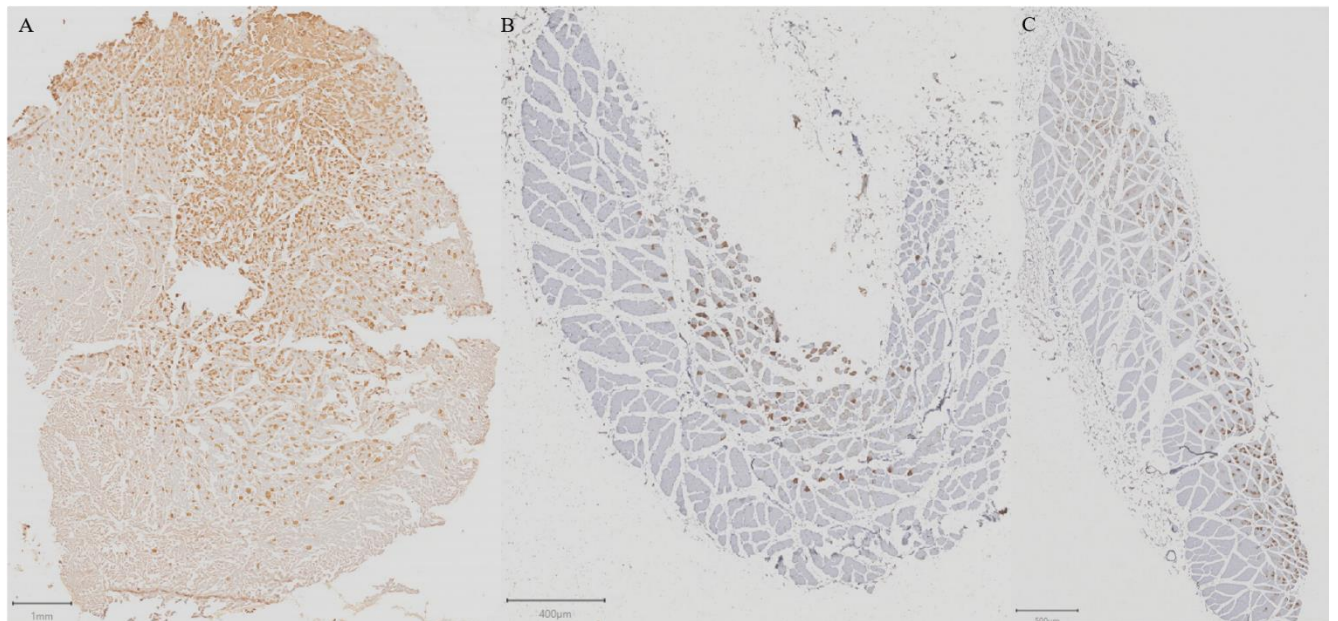


**Figure 4.8:** Regionalisation of muscle fibres (A-C) illustrated in the myosin heavy chain-stained *m. triceps brachii caput longum* of *Bathyergus suillus* (A; scale bar= 1 mm), *m. deltoideus pars scapularis* (B; scale bar=400 µm) and *m. pectoralis superficialis* (C; scale bar= 500 µm) in *Heterocephalus glaber*. Regionalisation in these three muscles were present in both species.

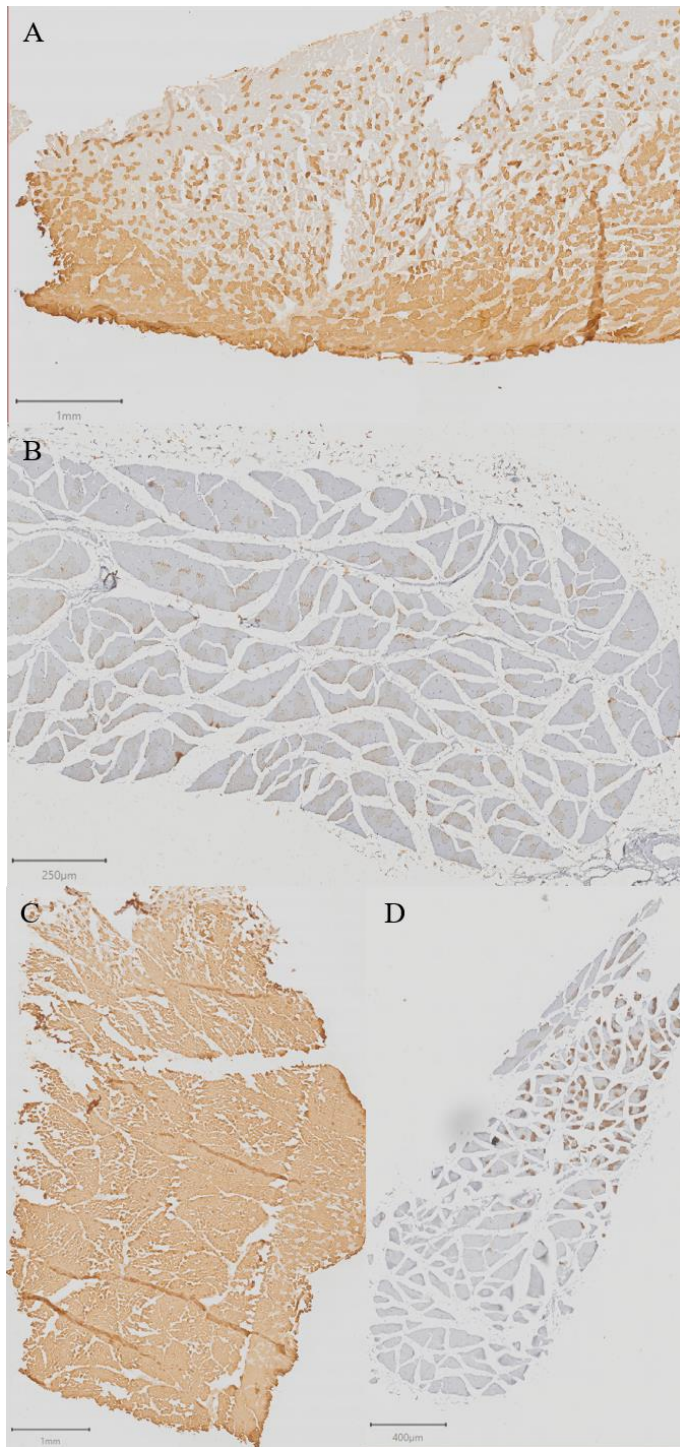


**Figure 4.9:** Myosin heavy chain-stained muscles displaying regionalisation (A & D) compared to muscles with no regionalisation (B & C) in *Bathyergus suillus* (A & C) and *Heterocephalus glaber* (B & D). *Musculus claviculo-scapularis* (A & B) with regionalisation of fibres in *B. suillus* (A; scale bar= 1mm) and no regionalisation in *H. glaber* (B; scale bar= 250 µm). *Musculus triceps brachii caput medialis* (C & D) with no regionalisation in *B. suillus* (C; scale bar= 1 mm) and regionalisation of fibres in *H. glaber* (D; scale bar= 400 µm).

#### 4.2.2 NADH and PAS stains: Oxidative, oxidative glycolytic and glycolytic fibres

Fibres that had a dark NADH and PAS staining intensity did not necessarily stain positive for slow myosin. Therefore, the fibres that stained positively for slow myosin did not correlate with a high oxidative capacity or glycogen content of fibres (Figures 4.10, 4.11).

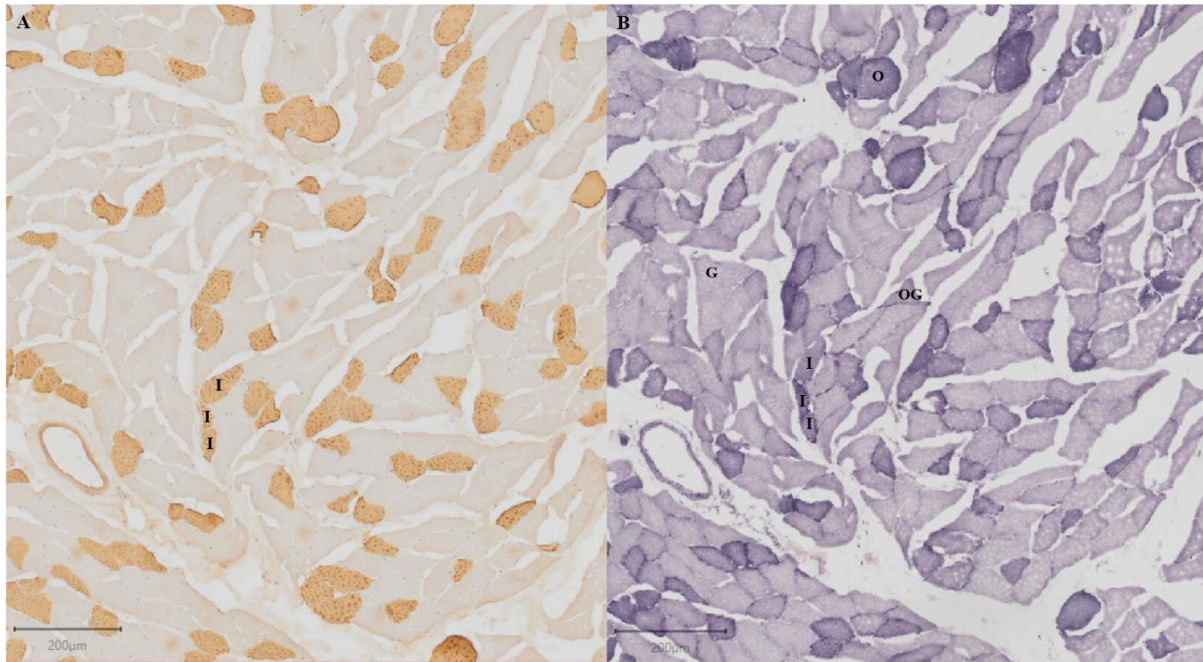


**Figure 4.10:** Two serial sections of the *m. latissimus dorsi* of *Bathyergus suillus* (A & B) stained with MHCs (A) and NADH (B) illustrates that the MHC-positive fibres did not necessarily have a high oxidative capacity (darkly stained fibres with NADH) but were rather stained with a medium to dark intensity. Type I muscle fibre (I); oxidative fibres (O); oxidative glycolytic fibres (OG); glycolytic fibres (G). Scale bar= 200 μm.

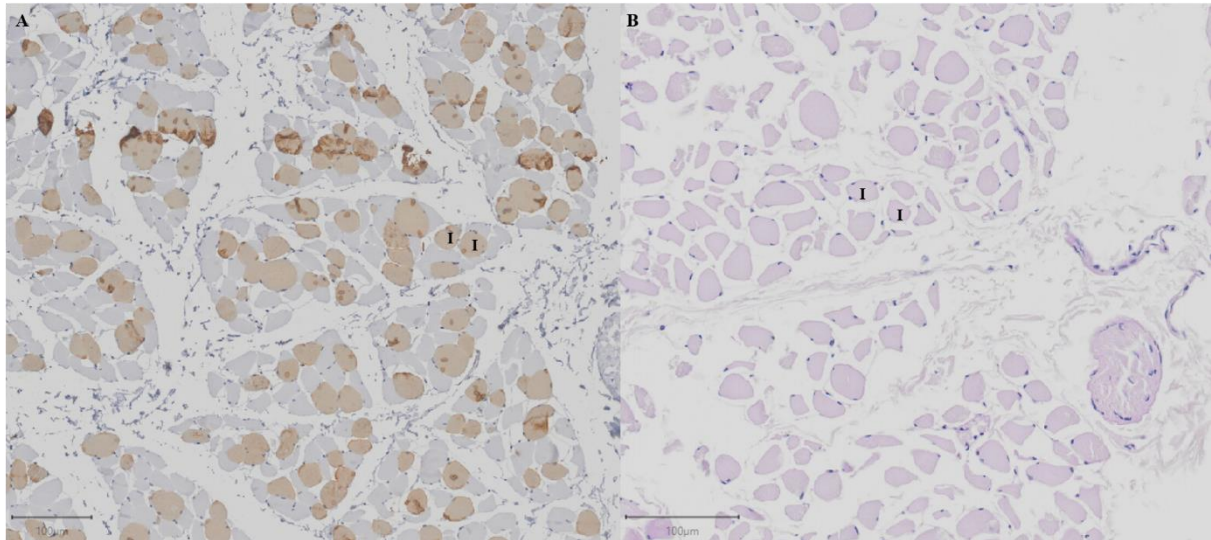


**Figure 4.11:** Two serial sections of *m. latissimus dorsi* of *Bathyergus suillus* stained with MHCs with heat-induced epitope retrieval (A) and PAS (B). Type I muscle fibre (I). Scale bar= 100 µm

The results of the oxidative, oxidative glycolytic and glycolytic fibre composition of the NADH- and PAS staining were consistent and accurate (Figure 4.12). Comparison of the frozen NADH and fixed PAS *B. suillus* tissue sections of *mm. latissimus dorsi*, *triceps brachii caput medialis* and *flexor carpi ulnaris* provided results with a difference of less than or equal to ten percent.

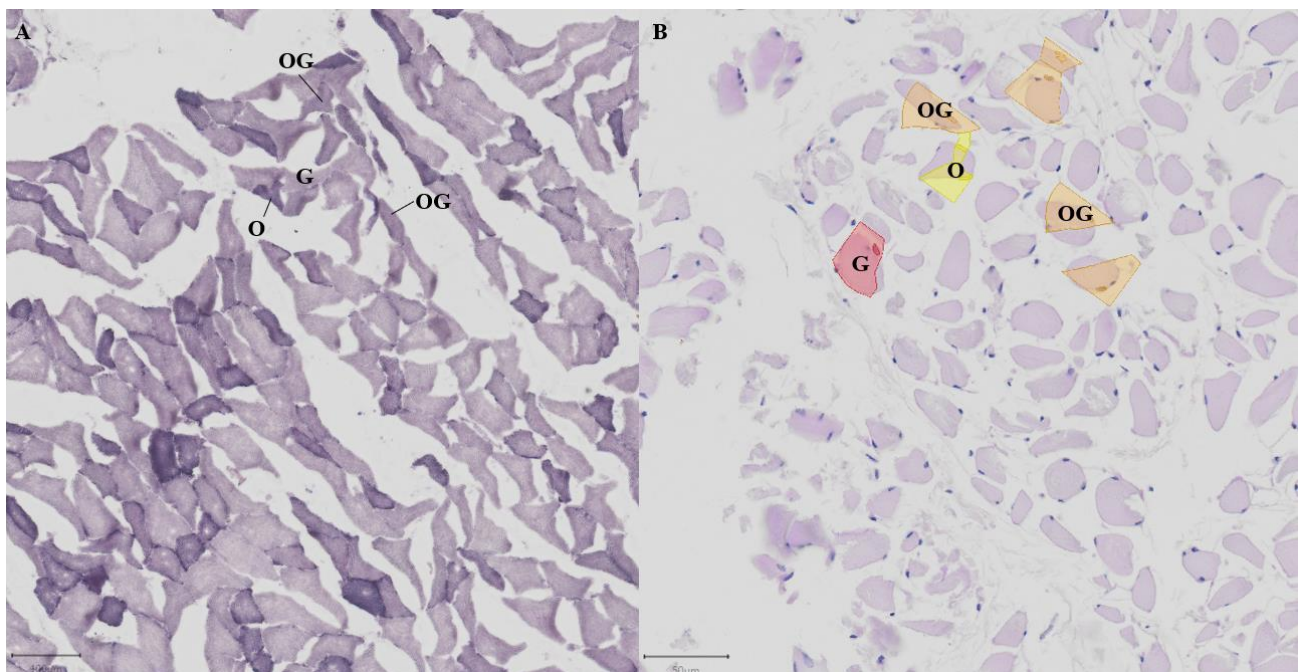


**Figure 4.12:** Frozen NADH-stained (A; scale bar= 400 µm) and fixed PAS-stained (B; scale bar=50 µm) sections of *m. latissimus dorsi* of *Bathyergus suillus* (A & B). O- oxidative fibres (yellow); OG- oxidative glycolytic fibres (orange); G- glycolytic fibres (red).

The percentage of oxidative fibres in *mm. sternohyoideus*, *trapezius pars cervicalis* and *flexor digitorum profundus* was significantly higher in *H. glaber* compared to *B. suillus* (Table 4.7). In *B. suillus* the percentage of glycolytic fibres was significantly higher in the *mm. sternohyoideus*, *claviculo-scapularis*, *trapezius pars cervicalis*, *triceps brachii caput longum et lateralis*, *deltoideus pars scapularis* and *flexor digitorum profundus* compared to the same muscles in *H. glaber*. (Figure 4.13). Although not statistically significant, between the two species *m. latissimus dorsi* in *B. suillus* had the most glycolytic fibres ( $55.6\% \pm 15.19$ ) while the most oxidative and oxidative glycolytic fibres were observed in *H. glaber* in *mm. latissimus dorsi* ( $49.44\% \pm 23.17$ ) and *claviculo-scapularis* ( $44.44\% \pm 8.82$ ), respectively.

The mean and standard deviation of the oxidative, oxidative glycolytic and glycolytic fibres in the muscles groups of both species are detailed in Table 4.8. The scapular elevators (SE) and digital flexors (DF) had significantly more glycolytic fibres in *B. suillus*, whereas the same two muscle groups (SE and DF) had significantly more oxidative fibres in *H. glaber* ( $p= 0.03$ ). The digital flexors in *B. suillus* had the highest percentage of glycolytic fibres and the elbow extensors in *H. glaber* had the highest percentages of oxidative glycolytic and oxidative fibres (Figure 4.14).

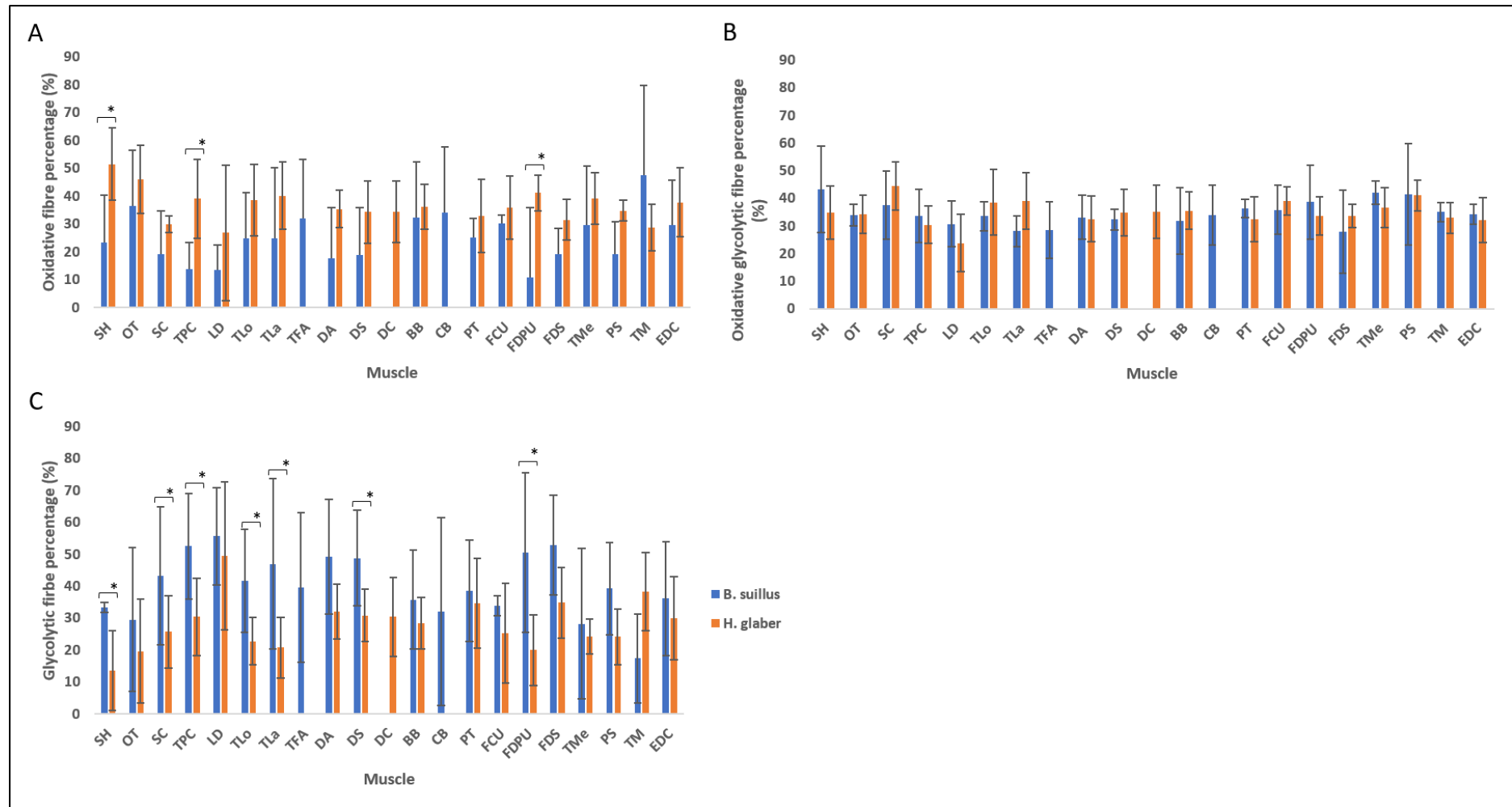


**Figure 4.13:** The mean percentages ( $\pm$  standard deviation) of the oxidative (A), oxidative glycolytic (B) and glycolytic (C) fibres in the individual muscles of *Bathyergus suillus* (blue) and *Heterocephalus glaber* (orange). Muscle abbreviations: SH- *m. sternohyoideus*; OT- *m. omotransversarius*; SC- *m. claviculo-scapularis*; TPC- *m. trapezius pars cervicales*; LD- *m. latissimus dorsi*; TLo- *m. triceps brachii caput longum*; TLa- *m. triceps brachii caput lateralis*; TFA- *m. tensor fasciae antebrachia*; DA- *m. deltoideus pars acromialis*; DS- *m. deltoideus pars scapularis*; DC- *m. deltoideus pars clavicularis*; BB- *m. biceps brachii*; CB- *m. coracobrachialis*; PT- *m. pronator teres*;

FCU- *m. flexor carpi ulnaris*; FDP- *m. flexor digitorum profundus* (ulnar head); FDS- *m. flexor digitorum superficialis*; TMe- *m. triceps brachii caput medialis*; PS- *m. pectoralis superficialis*; TM- *m. teres major*; EDC- *m. extensor digitorum communis*. \* indicates significant difference between two species  $p < 0.05$ .

**Table 4.7:** The mean percentage and standard deviation ( $\pm$ ) of the oxidative, oxidative glycolytic and glycolytic stained fibres in the individual muscles of *Bathyergus suillus* and *Heterocephalus glaber*.

Muscle	<i>Bathyergus suillus</i>			<i>Heterocephalus glaber</i>		
	Glycolytic	Oxidative glycolytic	Oxidative	Glycolytic	Oxidative glycolytic	Oxidative
<i>M. Sternohyoideus</i>	<b>33.34 <math>\pm</math> 1.55</b>	43.17 $\pm$ 15.66	<b>23.49 <math>\pm</math> 17</b>	<b>13.72 <math>\pm</math> 12.48</b>	34.75 $\pm$ 9.56	<b>51.53 <math>\pm</math> 12.97</b>
<i>M. Omotransversarius</i>	29.59 $\pm$ 22.46	34 $\pm$ 3.9	36.41 $\pm$ 20.17	19.71 $\pm$ 16.22	34.18 $\pm$ 6.99	46.1 $\pm$ 12.19
<i>M. Claviculo-scapularis</i>	<b>43.27 <math>\pm</math> 21.5</b>	37.5 $\pm$ 12.29	19.23 $\pm$ 15.61	<b>25.7 <math>\pm</math> 11.35</b>	44.44 $\pm$ 8.82	29.86 $\pm$ 3.03
<i>M. Trapezius pars cervicalis</i>	<b>52.51 <math>\pm</math> 16.57</b>	33.64 $\pm$ 9.74	<b>13.85 <math>\pm</math> 9.46</b>	<b>30.5 <math>\pm</math> 12.08</b>	30.46 $\pm$ 6.7	<b>39.04 <math>\pm</math> 14.2</b>
<i>M. Latissimus dorsi</i>	55.6 $\pm$ 15.19	31 $\pm$ 8.36	13.4 $\pm$ 8.74	49.44 $\pm$ 23.17	23.84 $\pm$ 10.35	26.82 $\pm$ 24.25
<i>M. Triceps brachii caput longum</i>	<b>41.69 <math>\pm</math> 16.17</b>	33.52 $\pm$ 5.26	24.79 $\pm$ 16.56	<b>22.81 <math>\pm</math> 7.37</b>	38.54 $\pm$ 11.95	38.65 $\pm$ 12.79
<i>M. Triceps brachii caput lateralis</i>	<b>46.98 <math>\pm</math> 26.62</b>	28.18 $\pm$ 5.55	24.84 $\pm$ 25.5	<b>20.8 <math>\pm</math> 9.53</b>	39.05 $\pm$ 10.11	40.15 $\pm$ 12.15
<i>M. Tensor fasciae antebrachia</i>	39.64 $\pm$ 23.37	28.46 $\pm$ 10.3	31.9 $\pm$ 21.2			
<i>M. Deltoideus pars acromialis</i>	49.28 $\pm$ 17.96	33.16 $\pm$ 8.07	17.56 $\pm$ 18.39	32.1 $\pm$ 8.56	32.51 $\pm$ 8.19	35.39 $\pm$ 6.67
<i>M. Deltoideus pars scapularis</i>	<b>48.82 <math>\pm</math> 15</b>	32.29 $\pm$ 3.83	18.9 $\pm$ 16.89	<b>30.85 <math>\pm</math> 8.2</b>	34.86 $\pm$ 8.43	34.29 $\pm$ 11.15
<i>M. Deltoideus pars clavicularis</i>				30.41 $\pm$ 12.34	35.13 $\pm$ 9.53	34.46 $\pm$ 11.05
<i>M. Biceps brachii</i>	35.82 $\pm$ 15.46	31.46 $\pm$ 6.85	32.42 $\pm$ 20	28.38 $\pm$ 8.05	35.47 $\pm$ 6.77	36.15 $\pm$ 8.06
<i>M. Coracobrachialis</i>	32.03 $\pm$ 29.35	33.85 $\pm$ 12.04	34.12 $\pm$ 23.63			
<i>M. Pronator teres</i>	38.61 $\pm$ 15.86	36.25 $\pm$ 10.84	25.14 $\pm$ 6.99	34.65 $\pm$ 14.13	32.41 $\pm$ 8.15	32.94 $\pm$ 13.06
<i>M. Flexor carpi ulnaris</i>	33.19 $\pm$ 3.19	36.2 $\pm$ 3.36	30.61 $\pm$ 2.94	25.22 $\pm$ 15.57	39 $\pm$ 5.2	35.78 $\pm$ 11.33
<i>M. Flexor digitorum superficialis</i>	52.9 $\pm$ 24.94	27.94 $\pm$ 8.84	19.16 $\pm$ 24.93	34.85 $\pm$ 11	33.65 $\pm$ 6.83	31.5 $\pm$ 6.39
<i>M. Flexor digitorum profundus (ulnar head)</i>	<b>50.53 <math>\pm</math> 15.55</b>	38.63 $\pm$ 13.39	<b>10.83 <math>\pm</math> 9.16</b>	<b>20.04 <math>\pm</math> 11.12</b>	33.68 $\pm$ 4.32	<b>41.18 <math>\pm</math> 7.37</b>
<i>M. Triceps brachii caput medialis</i>	27.69 $\pm$ 23.48	41.35 $\pm$ 15.08	30.97 $\pm$ 21.05	24.22 $\pm$ 5.44	36.74 $\pm$ 7.17	39.04 $\pm$ 9.24
<i>M. Pectoralis superficialis</i>	39.28 $\pm$ 14.48	41.48 $\pm$ 4.31	19.24 $\pm$ 11.67	24.19 $\pm$ 8.72	41.03 $\pm$ 5.57	34.78 $\pm$ 3.7
<i>M. Teres major</i>	17.42 $\pm$ 13.88	35.04 $\pm$ 18.32	47.54 $\pm$ 32.2	38.35 $\pm$ 12.17	33 $\pm$ 5.56	28.65 $\pm$ 8.39
<i>M. Extensor digitorum communis</i>	36.11 $\pm$ 17.84	32.28 $\pm$ 3.53	29.61 $\pm$ 16.14	30.09 $\pm$ 13.02	32.1 $\pm$ 8.07	37.81 $\pm$ 12.43

Bold text indicates significant results  $p < 0.05$

**Table 4.8:** The mean percentage and standard deviation ( $\pm$ ) of the oxidative, oxidative glycolytic and glycolytic stained fibres in the individual muscles of *Bathyergus suillus* and *Heterocephalus glaber*.

Muscle group	<i>Bathyergus suillus</i>			<i>Heterocephalus glaber</i>		
	Glycolytic	Oxidative glycolytic	Oxidative	Glycolytic	Oxidative glycolytic	Oxidative
Scapular elevators	<b>44.3 <math>\pm</math> 20.17</b>	35.09 $\pm$ 9.42	<b>20.61 <math>\pm</math> 15.86</b>	<b>24.96 <math>\pm</math> 13.5</b>	36.22 $\pm$ 9.18	<b>38.82 <math>\pm</math> 12.4</b>
Limb retractors	44.35 $\pm$ 18.16	33.59 $\pm$ 8.33	22.06 $\pm$ 18.91	32.84 $\pm$ 5.73	33.86 $\pm$ 3.68	33.3 $\pm$ 6.42
Elbow extensors	38.42 $\pm$ 20.88	33.53 $\pm$ 9.56	28.05 $\pm$ 18.71	22.61 $\pm$ 6.39	38.11 $\pm$ 8.68	39.28 $\pm$ 9.82
Digital flexors	<b>51.71 <math>\pm</math> 12.4</b>	33.29 $\pm$ 4.62	<b>15 <math>\pm</math> 14.34</b>	<b>27.44 <math>\pm</math> 8.73</b>	33.66 $\pm$ 5.11	<b>36.34 <math>\pm</math> 6.19</b>

Bold text indicates significant results  $p < 0.05$

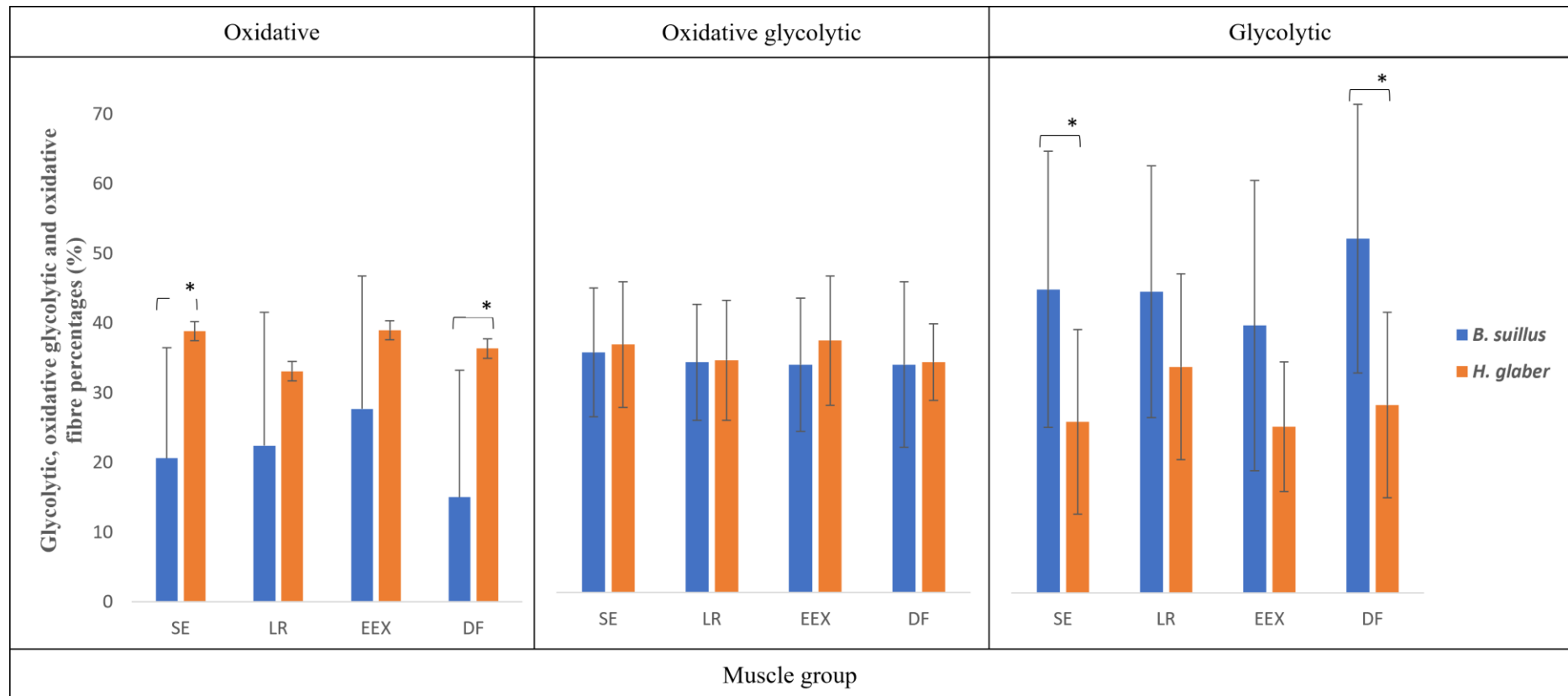


**Figure 4.14:** The mean ( $\pm$  standard deviation) of the oxidative, oxidative glycolytic and glycolytic stained fibres as an indication of oxidative capacity in the functional muscle groups of *Bathyergus suillus* (blue) and *Heterocephalus glaber* (orange). Muscle group abbreviations: SE- scapular elevators/stabilisers/retractors; LR- limb retractors; EEX- elbow extensors; DF- digital flexors. \* indicates significant difference between two species  $p < 0.05$ .

### 4.3 Cutaneous mechanoreceptors

The basic structure of the three analysed mechanoreceptors was similar in both *Bathyergus suillus* and *Heterocephalus glaber* (Figure 4.15 A-C). The means and standard deviation for the densities of the mechanoreceptors in *B. suillus* and *H. glaber* are detailed in Table 4.9. Merkel cells were the most abundant mechanoreceptor in both species while Meissner corpuscles were the least observed (Figure 4.16).

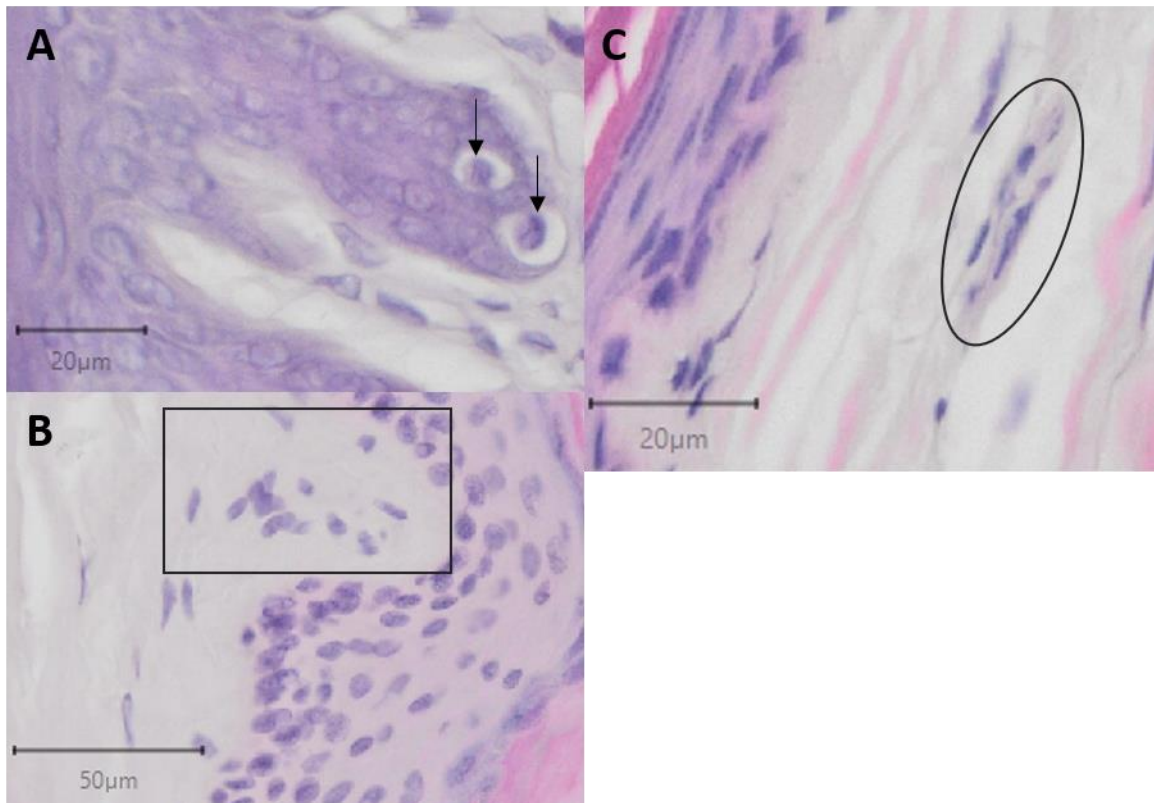


**Figure 4.15:** General structure of Merkel cells in the forefeet of *Heterocephalus glaber* (A), Meissner corpuscle (B) and a Ruffini corpuscle (C) in the forefeet of *Bathyergus suillus*. Arrows= Merkel cells; Square= Meissner corpuscle; Oval= Ruffini corpuscle. Scale bars: A= 20µm; B= 50µm; C= 20µm.

#### 4.3.1 Merkel cell density

There were no statistically significant differences in the Merkel cell densities between *B. suillus* and *H. glaber* in the total front- ( $1.465 \pm 0.03$  vs.  $1.762 \pm 0.531$  Merkel cells. $\text{mm}^2$ ) and hind limb ( $1.825 \pm 0.215$  vs.  $1.707 \pm 0.428$  Merkel cells. $\text{mm}^2$ ). However, *B. suillus* had a slightly higher density in the hind limb whereas *H. glaber* had a higher density of Merkel cells in the front limb when compared to the other species. The density of Merkel cells in the distal right forefeet of *B. suillus* was significantly lower compared to *H. glaber* ( $p= 0.02$ ). Although not statistically significant, *H. glaber* had higher densities of Merkel cells in both

the left and right forefeet as well as the proximal sections of the left and right hindfeet, when compared to *B. suillus* (Table 4.9).

#### 4.3.2 Ruffini corpuscles (RC) density

Although not statistically significant, the RC densities in *B. suillus* were higher in the sections of the fore- ( $1.251 \pm 0.216$  vs.  $1.022 \pm 0.169428$  Ruffini corpuscles. $\text{mm}^2$ ) and hindfeet ( $1.787 \pm 0.275$  vs.  $1.113 \pm 0.307$  RCs. $\text{mm}^2$ ) when compared to *H. glaber* (Figure 4.16). The density of Ruffini corpuscles in the distal sections of the left forefeet ( $p=0.04$ ) and right hindfeet ( $p=0.04$ ) in *B. suillus* was significantly higher compared to *H. glaber* (Table 4.9).

#### 4.3.3 Meissner corpuscle (MC) density

Similar to the trend observed in the densities of RC, the densities of MC in *B. suillus* were higher in the front- ( $0.225 \pm 0.214$  vs.  $0.214 \pm 0.094$  Meissner corpuscles. $\text{mm}^2$ ) and hindfeet ( $0.286 \pm 0.224$  vs.  $0.06 \pm 0.068$  MCs. $\text{mm}^2$ ) when compared to *H. glaber* (Table 4.9). Although not statistically significant, the density of MC in the forefeet of *H. glaber* was higher compared to its hindfeet whereas the density of MCs was slightly higher in the hindfeet of *B. suillus* compared to its forefeet (Figure 4.16). The distal sections of the left and right hindfeet in *B. suillus* had significantly higher densities of MC compared to *H. glaber* ( $p < 0.01$ )

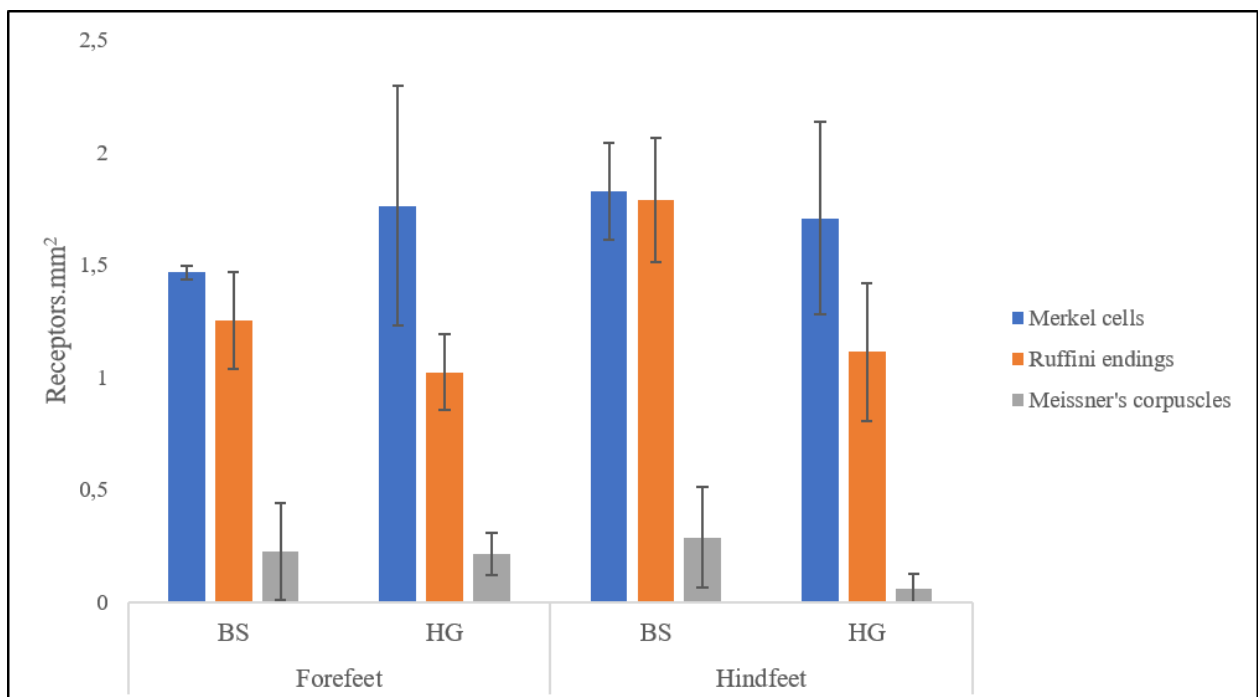


**Figure 4.16:** Total mechanoreceptor densities in the fore- and hindfeet of *Bathyergus suillus* and *Heterocephalus glaber*. BS-*Bathyergus suillus*; HG- *Heterocephalus glaber*

#### 4.3.4 Pacinian corpuscles

Pacinian corpuscles (PCs) were not observed in *Bathyergus suillus*. Only one PC was found in the right distal forefoot and two in the right distal hindfoot of two different *Heterocephalus glaber* specimens (Figure 4.17 A & B). These PCs were located deep within the dermis at the level of sweat glands in the subcutaneous layer of the glabrous skin. Density calculations and statistical comparison between the two species was impossible.

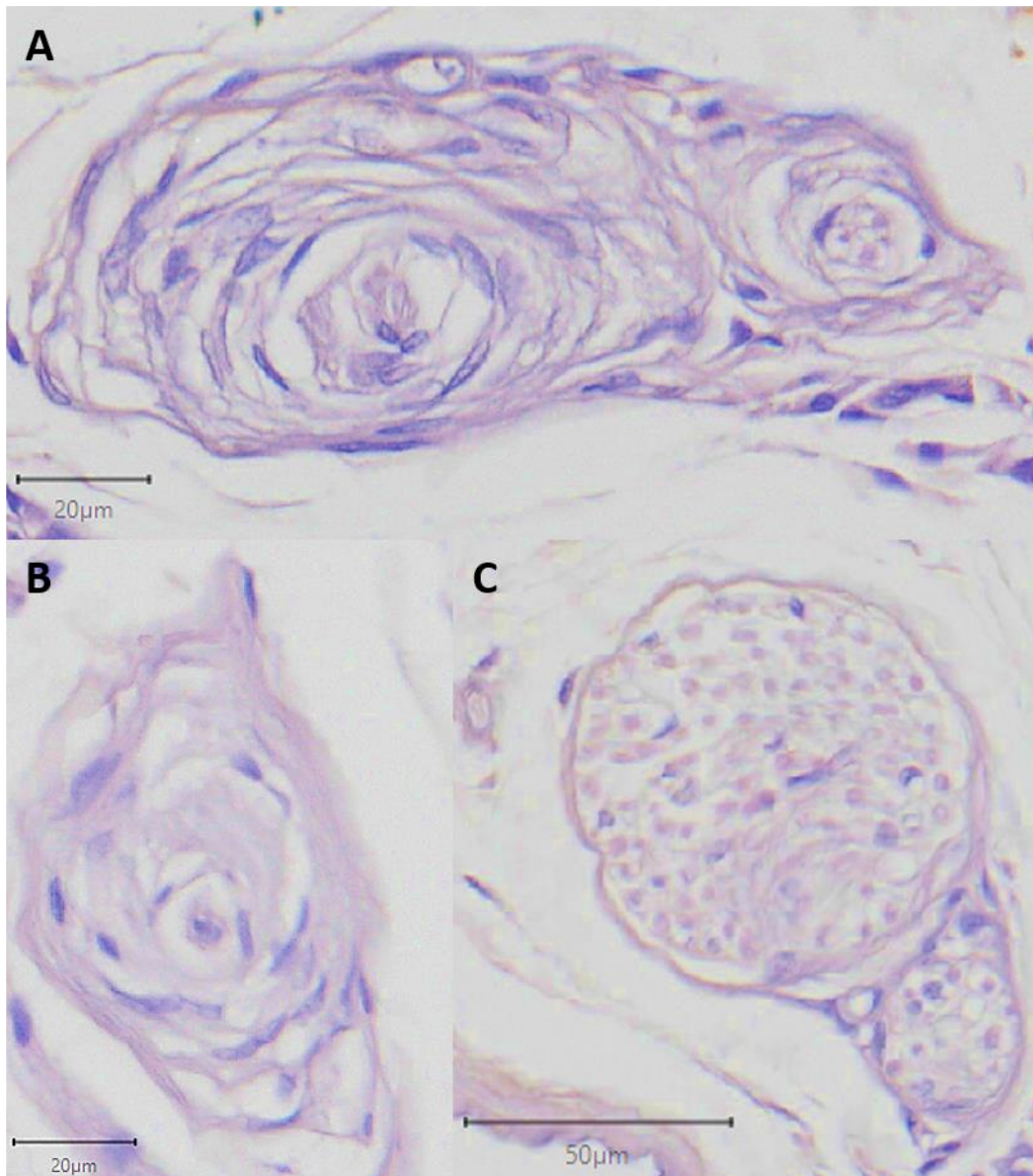


**Figure 4.17:** Pacinian corpuscles (A and B) and peripheral nerve (C) observed in the glabrous skin of the distal sections of the hindfeet (A, C) and forefeet (B) in *Heterocephalus glaber*. Scale bars: A, B= 20μm; C= 50μm.

**Table 4.9:** Average mechanoreceptor densities ( $\pm$  standard deviation) quantified in the footpads of *Bathyergus suillus* (BS) and *Heterocephalus glaber* (HG)

Area	Merkel cells (Ms.mm <sup>2</sup> )		Ruffini corpuscles (REs.mm <sup>2</sup> )		Meissner corpuscles (MCs.mm <sup>2</sup> )	
	<i>Bathyergus suillus</i>	<i>Heterocephalus glaber</i>	<i>Bathyergus suillus</i>	<i>Heterocephalus glaber</i>	<i>Bathyergus suillus</i>	<i>Heterocephalus glaber</i>
Left front proximal	0.337 $\pm$ 0.095	0.427 $\pm$ 0.067	0.267 $\pm$ 0.061	0.286 $\pm$ 0.115	0.053 $\pm$ 0.049	0.034 $\pm$ 0.039
Left front distal	0.369 $\pm$ 0.112	0.417 $\pm$ 0.063	<b>0.374<math>\pm</math>0.162</b>	<b>0.269<math>\pm</math>0.09</b>	0.052 $\pm$ 0.081	0.063 $\pm$ 0.047
Right front proximal	0.346 $\pm$ 0.032	0.384 $\pm$ 0.232	0.268 $\pm$ 0.055	0.201 $\pm$ 0.076	0.058 $\pm$ 0.053	0.037 $\pm$ 0.033
Right front distal	<b>0.334<math>\pm</math>0.049</b>	<b>0.463<math>\pm</math>0.253</b>	0.334 $\pm$ 0.137	0.211 $\pm$ 0.088	0.051 $\pm$ 0.07	0.079 $\pm$ 0.062
Front proximal	0.745 $\pm$ 0.104	0.811 $\pm$ 0.269	0.564 $\pm$ 0.026	0.486 $\pm$ 0.111	0.096 $\pm$ 0.112	0.072 $\pm$ 0.048
Front distal	0.682 $\pm$ 0.108	0.895 $\pm$ 0.287	0.688 $\pm$ 0.176	0.496 $\pm$ 0.135	0.113 $\pm$ 0.104	0.146 $\pm$ 0.095
Total front	1.465 $\pm$ 0.03	1.762 $\pm$ 0.531	1.251 $\pm$ 0.216	1.022 $\pm$ 0.169	0.225 $\pm$ 0.214	0.214 $\pm$ 0.094
Left hind proximal	0.445 $\pm$ 0.091	0.503 $\pm$ 0.199	0.433 $\pm$ 0.068	0.342 $\pm$ 0.097	0.059 $\pm$ 0.047	0.03 $\pm$ 0.048
Left hind distal	0.545 $\pm$ 0.144	0.341 $\pm$ 0.119	0.499 $\pm$ 0.1	0.278 $\pm$ 0.143	<b>0.043<math>\pm</math>0.069</b>	<b>0.01<math>\pm</math>0.023</b>
Right hind proximal	0.386 $\pm$ 0.087	0.426 $\pm$ 0.116	0.445 $\pm$ 0.154	0.268 $\pm$ 0.103	0.081 $\pm$ 0.051	0.037 $\pm$ 0.067
Right hind distal	0.443 $\pm$ 0.106	0.47 $\pm$ 0.161	<b>0.43<math>\pm</math>0.035</b>	<b>0.236<math>\pm</math>0.087</b>	<b>0.098<math>\pm</math>0.124</b>	<b>0.00<math>\pm</math>0.00</b>
Hind proximal	0.8 $\pm$ 0.136	0.929 $\pm$ 0.255	0.859 $\pm$ 0.196	0.61 $\pm$ 0.157	0.136 $\pm$ 0.083	0.067 $\pm$ 0.063
Hind distal	1.025 $\pm$ 0.183	0.834 $\pm$ 0.228	0.928 $\pm$ 0.145	0.536 $\pm$ 0.219	<b>0.15<math>\pm</math>0.184</b>	<b>0.00<math>\pm</math>0.00</b>
Total hind	1.825 $\pm$ 0.215	1.707 $\pm$ 0.428	1.787 $\pm$ 0.275	1.113 $\pm$ 0.307	0.286 $\pm$ 0.224	0.06 $\pm$ 0.068

Bold text indicates significant results  $p < 0.05$

#### 4.4 Sensory hairs

The row of course hairs on the manus and pes in both species were robust in structure with hair roots that extended deep into the dermis of the skin. These course hairs were abundant in *B. suillus* and multiple hairs were observed that were separated by connective tissue (Figure 4.18A). In contrast, sparse singular hairs were observed in *H. glaber* in the corresponding position, with a maximum of one hair identified per tissue section (Figure 4.18B). A Pacinian corpuscular-like structure was observed in the epithelium of a hair follicle in *B. suillus* stained with H&E (Figure 4.19A); however, after staining a serial slide with Masson's trichrome stain it was identified as a sebaceous gland (Figure 4.19B).

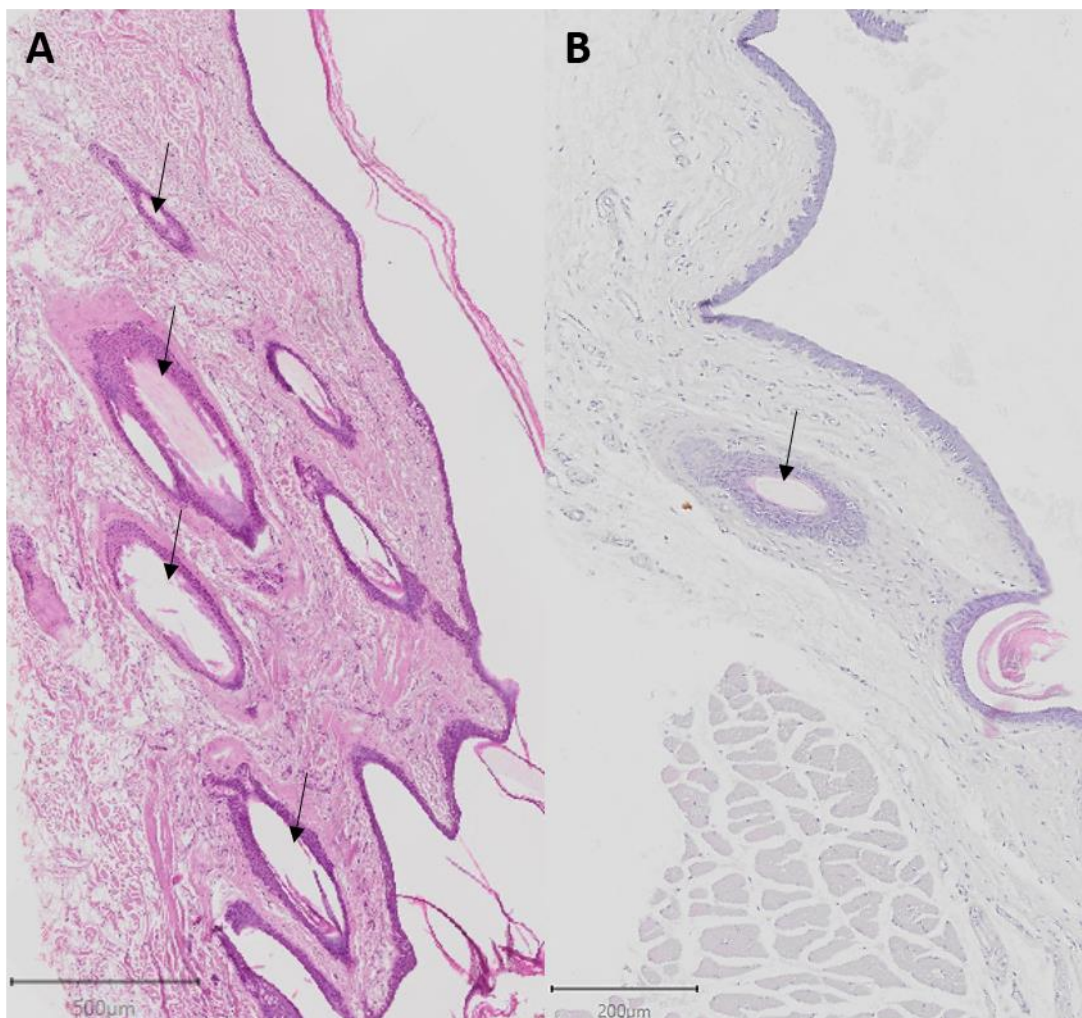


**Figure 4.18:** Sections from the lateral aspect of the skin of the feet in *Bathyergus suillus* (A) and *Heterocephalus glaber* (B) stained with H&E. Multiple hair follicles observed in the pes of *B. suillus* (A) and a single hair follicle in the pes of *H. glaber* (B). Hair follicles indicated with arrows. Scale bars: A= 500µm; 200µm.

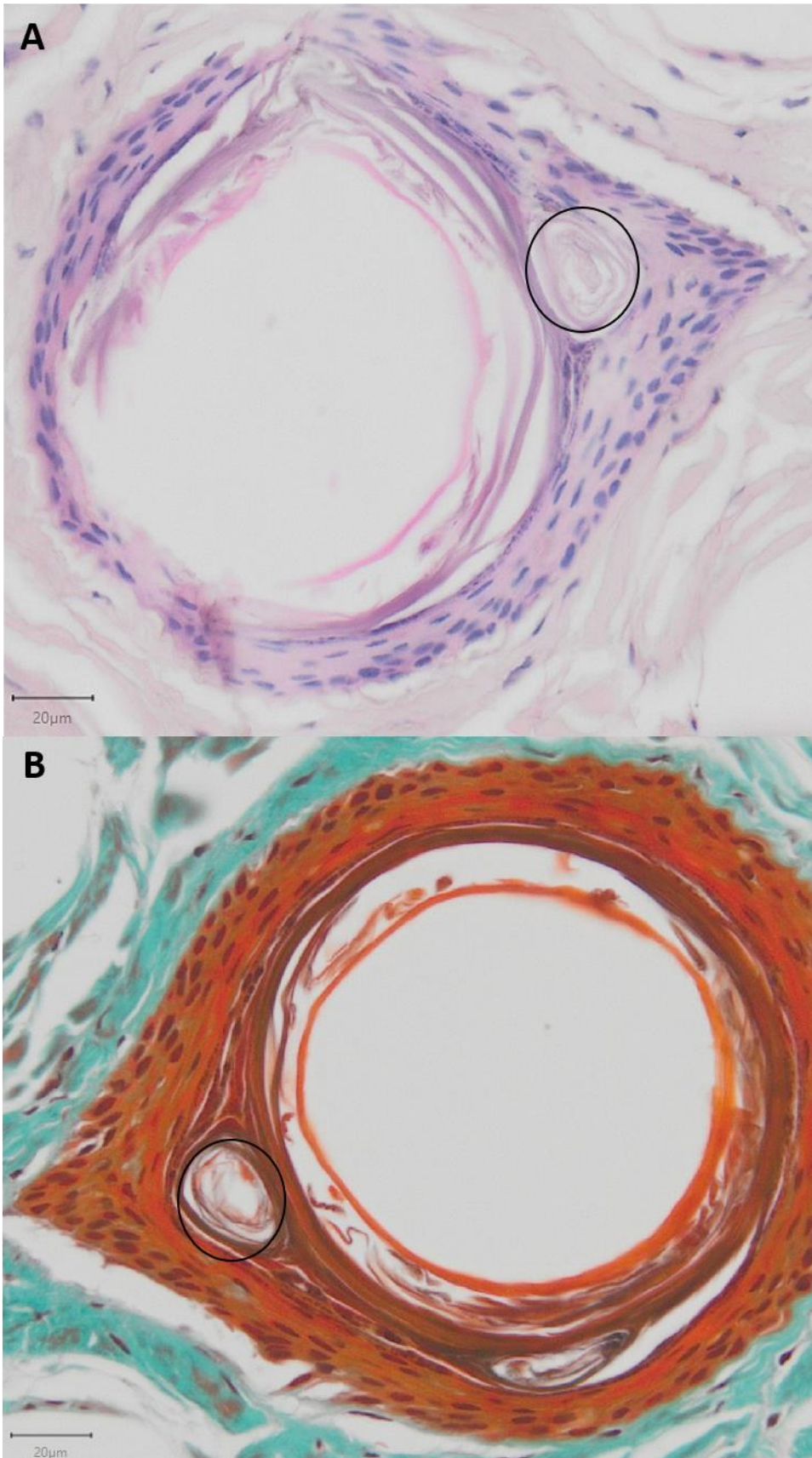


**Figure 4.19:** Haematoxylin and Eosin (A) and Masson's trichrome (B) stain of a cross section of a sensory hair follicle in *Bathyergus suillus* with a sebaceous gland indicated in black. Scale bars= 20µm

Merkel cells were identified in the basal layer of epithelium of the hair follicle in both species (Figure 4. 20D and E) and numerous cross sections of nerve fibres could be seen around the hair follicles. In *B. suillus* there were multiple hairs within a tissue section that were not surrounded with cross sections of nerve fibres (Figure 4.20 A and B), whereas in *H. glaber* the hair follicles observed in all of the specimens were encircled with nerve fibres (Figure 4. 20C). Furthermore, Merkel cells were relatively more densely situated in the outer root sheath, compared to *B. suillus* (Figure 4.20D and E). The absence of a distinct follicle-sinus complex, typically seen in sensory hairs, indicated that none of the hairs observed in both species could be classified as sensory hairs (Figure 4.21A and B).

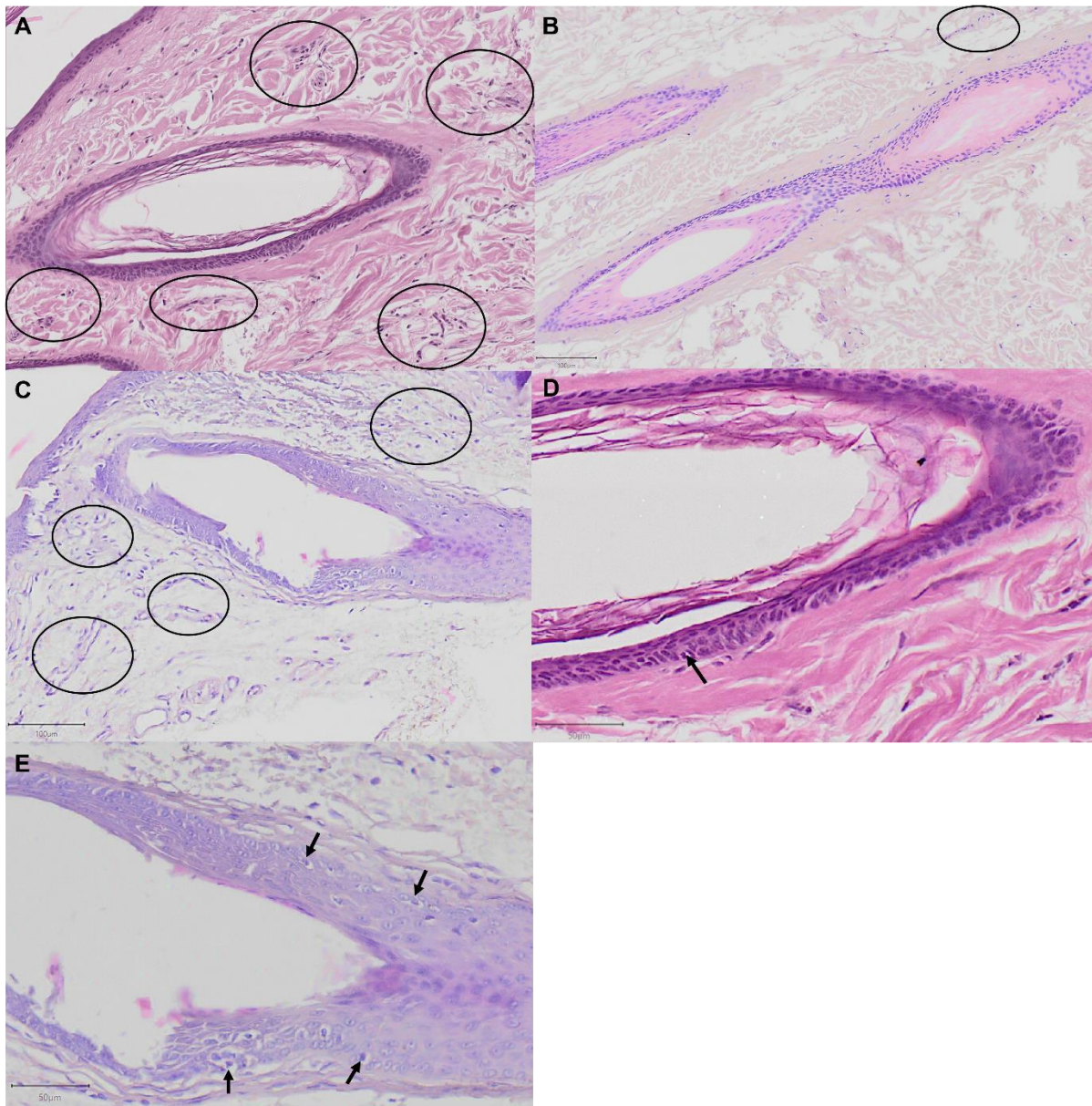


**Figure 4.20:** Nervous tissue observed surrounding the hairs of the skin on the lateral aspect of the pes of *Bathyergus suillus* (A, B, D) and *Heterocephalus glaber* (C, E); stained with H&E. A hair follicle from the manus of *B. suillus* (B) surrounded by a single section of nervous tissue. Images D and E are enlarged sections from images A and C, respectively. Merkel cells are indicated by the arrows and accumulation of nerve tissue is indicated by the circles. Scale bars: A, D, E= 50µm; B, C= 100µm

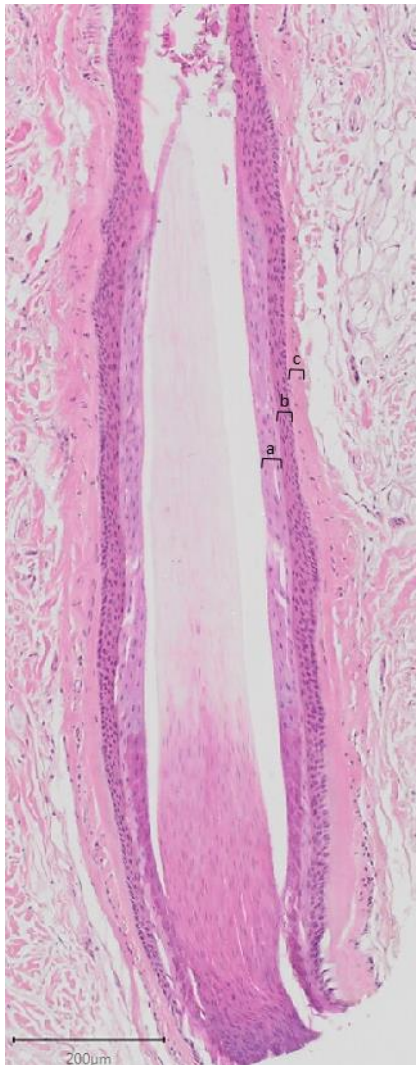


**Figure 4.21:** Haematoxylin and Eosin stain of a longitudinal section of a hair follicle on the lateral aspect of the hindfeet of *Bathyergus suillus* as representative of both species. Note the absence of a cavernous and ring sinus in between the outer root sheath and dermal capsule, which are both typically seen in sensory hairs. A= inner root sheath; b= outer root sheath; c= dermal capsule. Scale bar= 200 μm.

## 5 DISCUSSION

The aim of the present study was to investigate the muscle architecture and muscle fibre types in the forelimb of two African mole-rat species, *Bathyergus suillus* and *Heterocephalus glaber*. The results obtained reflect possible adaptations of the forelimb muscles in these mole-rat species that utilise different digging and communication methods. *Bathyergus suillus* produces seismic signals through hind foot-drumming and it was hypothesised that histological evidence of somatosensory mechanisms can be present in their feet that would detect these seismic signals. Therefore, the footpads and the lateral aspect of the skin in the fore- and hindfeet of both species were histochemically analysed for possible somatosensory mechanisms.

### 5.1 Muscle architecture and muscle fibre typing

Skeletal muscles produce force depending on the length and velocity of contraction (Lieber & Ward, 2011). Therefore, the muscle architecture parameters and muscle fibre type compositions determined in the current study, provide insight into the relationship between homologous muscles and synergistic muscle groups, as well as the functional specialisation in the scratch-digging *Bathyergus suillus* and chisel-tooth digging *Heterocephalus glaber*.

In both fossorial mole-rat species studied here, a proximal-to-distal reduction in front limb muscle mass was seen. This is a feature seen in the forelimbs of highly cursorial mammals such as the hare (*Lepus europeus*; Williams, Payne & Wilson, 2007), cheetah (*Acinonyx jubatus*; Hudson, Corr, Payne, Clancy, Lane & Wilson, 2011), Greyhounds (*Canis lupus familiaris*; Pasi & Carrier, 2003) and horse (Brown, Kawcak, McIlwraith & Pandy, 2003) as well as the fossorial Eastern mole (*Scalopus aquaticus*; Rose, Sandefur, Huskey, Demler & Butcher, 2013), where limb muscle mass is concentrated proximally (Hildebrand & Goslow, 2001). Contrary to this pattern, primates and the arboreal pine marten (*Martes martes*), have higher distal limb mass (approximately 40%; Isler, Payne, Gunther, Thorpe, Li, Savage & Crompton, 2006; Raichlen, 2006; Böhmer, Fabre, Herbin, Peigné & Herrel 2018). This indicates that higher distal limb mass may be advantageous for climbing and object manipulation whereas high proximal forelimb muscle mass may be an adaptation for running (Böhmer *et al.*, 2018). The limb muscle mass distribution of both *B. suillus* and *H. glaber* (~75% proximally and ~25% distally) is not just similar to that of highly cursorial mammals but also similar to the fossorial Eastern mole (Rose *et al.*, 2013) and may reflect the functional need of fossorial animals to rapidly move within their burrow systems.

Studies on the comparison of the fibre type compositions in different anatomical regions in the same animal species are limited. The study by Ichikawa *et al.* (2019) on the two subterranean mole species found no differences in fibre type composition between the forelimb and hindlimb, regardless of the fact that these animals use their forelimbs to dig burrows. However, the percentage slow fibres in the forelimb muscles of *B. suillus* in the present study was higher compared to the hindlimb muscles of *B. suillus* as observed by Sahd and colleagues (2021) where the same techniques were used. The high percentages of fast fibres in the muscles of the hindlimb may facilitate the fast hind foot-drumming (Sahd *et al.*, 2021), whereas more slow fibres in the muscles of the forelimb in the present study may provide sustained isometric contractions to stabilise the forelimb during hind foot drumming.

According to Kikuchi (2010), physiological cross-sectional area (PCSA) values typically increase with increasing body mass and since an increase in PCSA was observed in all muscles of *B. suillus*, body mass was used as a covariate to compare the two species. Similar to other scratch-digging mammals (Moore *et al.*, 2013; Olson *et al.*, 2016; Rose *et al.*, 2013; Rupert, Rose, Organ & Butcher, 2015), the PCSA values of the muscles (limb retractor muscle group) involved in the power stroke of scratch-digging were significantly higher in *B. suillus* compared to *H. glaber*. In addition to the limb retractors, the scapula elevators/stabilisers are one of the main muscle groups involved in the power stroke of scratch-digging (Martin, Warbouton, Travouillon & Fleming, 2019). Therefore, in *B. suillus*, although not statistically significant, the slightly higher force output of the limb retractors and slightly higher shortening capacity of the scapula elevators (Figure 4.3) could potentially provide the required force and velocity of contraction during the power stroke of digging. This feature was also seen in other scratch-digging animals such as the American badger (*Taxidea taxus*; Moore *et al.*, 2013), groundhogs (*Marmota monax*, Rupert *et al.*, 2015) and the Nine-banded Armadillo (*Dasypus novemcinctus*; Olson *et al.*, 2016). The importance of the limb retractors during scratch-digging is further indicated by its higher muscle mass percentage of the total front limb in *B. suillus*, when compared to *H. glaber* (Figure 4.3). Furthermore, the fascicle lengths of the major extrinsic muscles involved in scratch-digging, such as the *mm. latissimus dorsi* and *pectoralis major*, were significantly greater in *B. suillus* when compared to *H. glaber*, providing a higher shortening capacity (Table 4.4). The longer fascicles allow these extrinsic muscles to retract the forelimb through a large range of motion during the power stroke (Martin *et al.*, 2013; Rupert *et al.*, 2015).

The *m. subscapularis* (SuS) of *B. suillus* had the highest force output compared to the other muscles in both species. Although SuS had a slow shortening capacity in *B. suillus* (short fascicle length), the high PCSA and isometric  $F_{\max}$  of the muscle are responsible for high force production typically seen in scratch-diggers, such as the American badger (*Taxidea taxus*; Moore et al, 2013) and the Nine-banded Armadillo (*Daspys novemcinctus*; Olson et al., 2016). The high force output of the SuS functions to counter the resistance of the soil against limb retraction during scratch-digging (Moore et al., 2013). Furthermore, the high force output of SuS may provide a stabilising function (Moore et al., 2013) to support the large body mass of *B. suillus* which requires relatively large forces for locomotion, scratch-digging and balance during hind foot drumming (Williams et al., 2007; Lamas, Main & Hutchinson, 2014; Randall, 2014; Martin et al., 2019).

Architectural indices or  $L_f/L_M$  ratios higher than 0.5 indicate that a muscle has a large range of contraction to move over a joint as well as a high muscle shortening capacity (Rose et al., 2013; Rupert et al., 2015; Olson et al., 2018). The  $L_f/L_M$  ratios of both *mm. subscapularis* (SuS), *teres major* (TM) and *sternocleidomastoideus* (SCM) were significantly smaller in *B. suillus* compared to *H. glaber*. Furthermore, these three muscles (SuS, TM, SCM) had higher force outputs in *B. suillus* compared to *H. glaber* (Figure 4.4). The low contraction velocity combined with the higher force output of SuS and TM may indicate a stabilisation function of the shoulder joint rather than fast movements in *B. suillus* (Von Meiring & Fischer, 1999; Moore et al., 2013). The stabilisation function of the TM muscle is further reflected in the significantly higher percentage of slow fibres in *B. suillus* compared to *H. glaber* and may point towards the larger body mass (Kikuchi, 2010) of *B. suillus* that needs to be supported on the forelimbs during hind foot drumming.

Interestingly, the PCSA value of SCM was significantly higher in *H. glaber* compared to *B. suillus*. Therefore, large values of both the  $L_f/L_M$  ratio and PCSA of the SCM seems to be an adaptation for more forceful and faster contralateral movements of the head (Cain, Reynolds & Sarko, 2019) in the chisel-tooth digging *H. glaber*. The SCM of *H. glaber* seems to support its functional requirements for chisel-tooth digging whereas the slightly larger force output of SCM in *B. suillus* may be contributed to its large body mass and the need to stabilise and move its large head contralaterally. Although muscle fibre typing was not performed on the SCM, the percentage of oxidative fibres in the *m. sternohyoideus* (SH) of *H. glaber* was significantly higher compared to *B. suillus*. The SH in *H. glaber* may play a role in endurance movements of the jaw during long periods of digging. The large muscle mass percentage

(Figure 4.2) and fast shortening capacity (Figure 4.2) of the head extensor and hyoid bone depressor (HH) muscle group of the total front limb mass (Figure 4.2) further emphasize the importance of the neck muscles in the chisel-tooth digging *H. glaber*.

The *m. claviculo-scapularis* (SC) in *B. suillus* was regionalised with type I fibres ( $38.41\% \pm 19.39$ ) more concentrated in the deep regions of the muscles. In comparison type I fibres ( $7.94\% \pm 0.90$ ) in SC of *H. glaber* were observed scattered throughout the superficial, central and deep regions. Muscle fibre studies that include the SC muscle are underreported and future research may further provide insight on the functional significance of regionalisation in the SC muscle. Wang & Kernell (2001) suggest multiple factors as to why type I fibres might accumulate in the deep regions of muscles. One of these factors is that a regionalised muscle may provide a biomechanical advantage for the shortening contractions of fast fibres and therefore providing long moment arms. The central parts of a muscle are expected to become more heated than superficial regions during strong contractions (Bergh & Ekblom, 1979; Sargeant, 1987). The warmer muscle fibres become, the more their shortening speed and power increase relative to the surrounding muscle fibres. Therefore, the localisation of type I fibres in the deep regions of a muscle contributes to the effectiveness of the shortening contractions of a muscle (Wang & Kernell, 2001). Furthermore, since slow fibres have low activation thresholds (Goldspink, Larson & Davies, 1970), motor units or muscle regions consisting of slow fibres would be the first fibres recruited for isometric contractions (for stabilisation, postural control and walking), providing an energy-saving function to the muscle (Hoffer, Loeb, Sugano, Marks, O'Donovan & Pratt, 1987; Walmsley, Hodgson & Burke, 1978; Von Meiring & Fischer, 1999). In addition to the regionalisation of SC in *B. suillus*, muscle architecture results indicate that this muscle is slightly more forceful with a slower contraction speed compared to the SC of *H. glaber*. Therefore, SC in *B. suillus* can be described as a multi-functional muscle, providing stabilisation to the scapula for postural control and walking in addition to the fast contractions for scapular elevation and/or retraction during fast digging movements. In comparison, the SC in *H. glaber* could mainly serve to produce fast movements for walking and running.

The *m. triceps brachii* heads function as strong and powerful elbow extensors in other subterranean and scratch-digging mammals (Rose *et al.*, 2013; Olson *et al.*, 2016; Martin *et al.*, 2019). The *m. triceps brachii caput medialis* (TMe) had more type I fibres in the terrestrial cui (*Galea musteloides*) and arboreal tree shrew (*Tupaia belangeri*; Von Meiring & Fischer, 1999) compared to both *B. suillus* and *H. glaber*. The terrestrial scratch-digging

armadillo (*Daspys novemcinctus*; Olson *et al.*, 2013) had a lower percentage of type I fibres in the TMe compared to the two species studied here. Although no significant differences were observed in the muscle architecture of the TMe between *B. suillus* and *H. glaber*, regionalisation and a higher percentage of type II fibres were observed in *H. glaber*. Regionalisation of type I fibres in TMe was also absent in the common yellow-toothed cavy (*Galea musteloid*) and the Northern treeshrew (*Tupaia belangeri*; Von Mering & Fischer, 1999), similar to *B. suillus*. As the body mass of *B. suillus* is larger and sustained contractions are needed during the power stroke of digging, the high percentage of type I fibres in TMe may reflect the need to support the body mass as well as the sustained scratch-digging in *B. suillus*. In comparison, the regionalisation and high type II fibre percentage in the TMe of *H. glaber*, suggest a dual function where the TMe may provide sustained contractions for daily locomotion as well as fast elbow extension for running within the burrows.

In the current study, the differences observed in the muscle fibre type composition of the forelimb muscles may not be due to functional strains or environmental demands but rather the phylogeny of the species (Alvarez & Perez, 2019). Ichikawa and colleagues (2019) discovered the absence of type IIb fibres within the muscles of two species of subterranean true moles (Eulipotyphla) whereas all subtypes of type II fibres were present in the semi-fossorial, terrestrial and semi-aquatic Eulipotyphla species. This suggests that the subterranean habitat may have an influence on the type II fibre compositions in species belonging to the same phylogenetic order. Terrestrial animals have to maintain body equilibrium and produce maximum speed to avoid predators or hunt prey whereas subterranean mammals have no need to support their body weight to move at similar speeds within their tunnels (Nevo, 1979). However, the fast movements produced for digging in subterranean mammals may influence the percentages of the subtypes of type II fibres. Furthermore, Ichikawa and colleagues (2019) indicated the absence of type I fibres in two subterranean mole species within the order Eulipotyphla (Douady *et al.*, 2002). Other studies performed on species belonging to Eulipotyphla confirmed the absence of type I fibres within species with different locomotive habits and suggest that it may be due to phylogenetic effects and not locomotor adaptations (Suzuki, 1990; Peters, Kubis, Wetzel *et al.*, 1999; Savolainen & Vornanen, 1995). Recent studies have placed *H. glaber* into its own separate family, Heterocephalidae (Patterson & Upham, 2014; Patterson, 2016; Tavares & Seuánez, 2018; Burgin, Colella, Kahn & Upham, 2018; D'Elia, Fabre & Lessa, 2019), whereas previously, *B. suillus* and *H. glaber* belonged to same phylogenetic family, Bathyergidae.

Therefore, even though both of these species inhabit a subterranean environment, differences in muscle characteristics such as the architecture and fibre type composition, may be attributed to phylogeny and not sociality or digging methods.

An increased resistance to fatigue and larger cross-sectional areas of individual muscle fibres were observed in the muscles of rats that underwent long-term and heavy resistance exercise regimes (Glaser, You, Zhang & Medler, 2009). No increases in gross muscle mass or muscle fibre type proportions were evident. Furthermore, other studies have shown the transformation of glycolytic fibres to oxidative fibres in both humans and rodents that underwent endurance training (Yan, Okutsu, Akhtar & Lira, 2011). In the current study, the scapular elevators and digital flexors had significantly higher percentages of glycolytic fibres in *B. suillus* compared to *H. glaber*. This may indicate that various functional demands, such as vigorous bouts of scratch-digging in *B. suillus*, may lead to the transformation of oxidative fibres to glycolytic fibres in muscles that are involved in the power-stroke of digging, such as the scapular elevators and digital flexors.

Animals display sexual dimorphism in their skeletal muscle mass, MHC expression and to an extent in the metabolic properties of muscle fibres (Haizlip, Harrison & Leinwand, 2015). Sexual dimorphism has been observed in the MHC expression of multiple muscles in the mouse hindlimb (Eason, Schwartz, Pavlath & English, 2000) as well as the muscle architecture in the muscles of the hindlimb of *B. suillus* (Sahd, Bennett & Kotzé, 2021). In the current study, the sex of the *B. suillus* specimens were unknown whereas all the *H. glaber* specimens were male subordinates. A study by Pinto, Jepsen, Terranoca & Buffenstein (2010) on the femora of naked mole-rats (*H. glaber*), indicated that the femora of male and female subordinates in the colony were sexually monomorphic due to suppressed puberty which eliminates the effects of sex hormones on bone and muscle. It is possible that differences in muscle architecture and muscle fibre typing between species, specifically the large standard deviations in the values of *B. suillus*, may have been influenced by sexual dimorphism in *B. suillus* (Schiaffino & Reggiani, 2011).

## **5.2 Somatosensory mechanisms in the fore- and hind feet**

### **5.2.1 Cutaneous mechanoreceptors**

Transmission of foot-drumming signals or vibrations in subterranean mole-rats take place via one of two modalities: an auditory mechanism or a somatosensory route (Narins *et al.*, 1992; Mason & Narins, 2001). Somatosensory perception of seismic signals in subterranean rodents

include bone conduction, which is seen in the mole-rat genus, *Nannospalax* (Mediterranean blind mole-rats), whereby its cheek and lower jaw are held against the burrow wall to detect vibrations (Mason & Narins, 2000). Another somatosensory route is cutaneous mechanoreceptors, such as the Meissner's corpuscles (MC), shown to be responsible for the detection of vibrations in the fingertips of humans, forepaws of mice (Schwaller, Begay, Garcia-Cargia *et al.*, 2020) and the nose pad of the *Nannospalax* mole-rat (Mediterranean blind mole-rat; Klauer, Burda & Nevo, 1997). In the current study, the density of MC in the distal plantar area of the hindlimb in *Bathyergus suillus* was significantly higher compared to *Heterocephalus glaber*. Hind foot- drumming has not been reported in *H. glaber* with acoustic and olfactory communication being the predominant methods of communication in this species, whereas hind foot-drumming is the main method of communication in *B. suillus* (Bennett & Jarvis, 1988; Lacey, Alexander, Braude, Sherman & Jarvis, 1991). Therefore, the high MC density in *B. suillus* may be an adaptation for the detection of seismic vibrations during hind foot- drumming.

In addition, MCs have been suggested to have a nociceptive function due to its immunoreactivity to pain-related neuropeptides such as substance P and calcitonin gene-related peptide (Paré, Elde, Mazurkiewicz, Smith & Rice, 2001). Nociceptors respond to noxious stimuli which is a physiological response to protect body tissues from damage (Loeser & Treede, 2008). These pain-related neuropeptides are absent in the skin innervation of *H. glaber* and are responsible for its unique reduced pain-related behaviours (Park *et al.*, 2008). However, research on the presence of these neuropeptides in *B. suillus* is lacking. From the current study, the lower densities of MCs in the hindfeet of *H. glaber* when compared to *B. suillus*, may be the result of a lack of pain-related neuropeptides. It is possible that it is related to the fact that this eusocial species does not produce and detect seismic vibrations with their hindfeet but needs to be confirmed as information in the literature on the mechanoreceptors in the feet of other non-drumming mole-rat species is scarce.

Meissner's corpuscles and Pacinian corpuscles (PCs) are both mechanoreceptors that detect vibrations; where MCs are sensitive to low frequency vibrations (10-65 Hz) and PCs detect high frequency vibrations (20-1000 Hz; Bolanowski & Zwislocki, 1984; Makous, Friedman & Vierck, 1995; Schneider, Gracheva & Bagriantsev, 2016). Unlike MCs, PCs are not immunoreactive to pain-related neuropeptides and are just responsive to vibrational stimuli. Pacinian corpuscles in the feet of the Asian elephant have been postulated to detect their vocalizations that travel through the ground as seismic waves (Bouley, Alarcon, Hildebrandt

& O'Connell-Rodwell, 2007). *Heterocephalus glaber* produce a wide range of vocalizations (200 Hz and 9 kHz) to communicate with conspecific individuals (Pepper *et al.*, 1991; Bennett & Faulkes, 2000). Therefore, the presence of PCs in the footpads of *H. glaber*, despite the low number observed in the present study, may point towards a seismic component to the detection of their vocalizations in addition to the auditory component. Furthermore, in *B. suillus*, low frequency vocalisations supplement their hind foot-drumming when males and females meet during mating, thereby eliminating the requirement to detect high frequency sounds across long distances and may explain the absence of PCs. Since *H. glaber* has recently been shown to belong to a different phylogenetic family, Heterocephalidae (Tavares & Seuánez, 2018; Burgin, Colella, Kahn & Upham, 2018; D'Elía, Fabre & Lessa, 2019), than *B. suillus* which belongs to Bathyergidae, the presence of PCs may be linked to phylogenetic differences and not sociality.

In comparison, tactile communication in *B. suillus* is limited to specific behaviours such as courtship and mating (Jarvis & Bennett, 1991; Francescoli, 2000). Epidermal Merkel cells in the outer root sheath of the whisker follicles as well as the glabrous skin of the digits of mice, and the rhinarium of cats (Abrahams, Hodgins & Downey, 1987) have been shown to be responsible for touch perception and texture differentiation (Maksimovic *et al.*, 2014). The Merkel cells in both *B. suillus* and *H. glaber* were the most abundant mechanoreceptor in their fore-and hind footpads which suggests a similar tactile perception function used for navigation in underground burrows, during foraging and digging. Furthermore, MCs also respond not just to low frequency vibrations, but also to temporary tactile stimuli (Cauna, 1956; Cauna & Ross, 1960). This indicates that MCs may facilitate tactile perception, as well as other interactive behaviour such as mating, in both *B. suillus* and *H. glaber*.

Ruffini corpuscles (RCs) exhibit prolonged responses to sustained tactile stimuli (Morimoto & Takada, 1993), dermal stretch (Paré, Smith & Rice, 2002; Taylor, 2009) and the detection of forces generated during grasping (Halata, Schulze & Hohne, 1986). Therefore, the RCs in the footpads of both *B. suillus* and *H. glaber* may function to detect forces during burrowing and moving loosened soil and is not necessarily related to detection of seismic signals.

### 5.2.2 Sensory hairs

Almost all bathyergid species, such as *B. suillus*, have longer sensory hairs standing out from the general shorter fur hairs across its head and body (Thigpen, 1940; Jarvis & Bennett, 1991). In *H. glaber* fur hairs are completely absent and longer sensory-like hairs are scattered across its head and body, especially on the face and tail, with shorter stiff hairs bordering the

lateral edges of the feet and in between digits (Jarvis & Sherman, 2002; Jarvis & Bennett, 1991). The hairs observed on the lateral aspect of both the front- and hindfeet in *B. suillus* and *H. glaber* in the current study, did not have the follicle-sinus complex (FSC) typically seen in sensory hairs (Fundin, Arvidsson & Rice, 1995) and therefore cannot be classified as vibrissae. A study performed on the hairs of the naked mole-rat confirmed that the structure and innervation of their body and facial hair follicles are similar to that of large guard hair follicles (Rice, Kinnman, Aldskogius, Johansson & Arvidsson, 1993; Fundin, Arvidsson & Rice, 1997; Park, Comer, Carol, Lu, Hong & Rice, 2003). Guard hairs are the largest of the fur hairs and are densely distributed between the vibrissae on the face and across the body. The vibrissae on the face of *H. glaber* have been confirmed to consist of a FSC and therefore are different from the rest of the guard hairs across the face and body (Park *et al.*, 2003). In the present study, the hairs on the lateral edges of the feet in *H. glaber* and *B. suillus* had a similar structure and therefore can be classified as guard hairs and not sensory hairs. Nevertheless, stimulation of all guard and sensory hairs across the body and face in *H. glaber* evoked behavioural responses, leading to the assumption that the guard hairs must have a somatosensory mechanism for spatial orientation (Crish, Rice, Park & Comer, 2003).

Burgess and Perl (1973) suggest that the innervation of the receptors around the hair follicle as well the innervation of the hair follicle itself, determines the quality of spatial response. Therefore, the Merkel cells within the outer root sheath of the analysed hairs as well as the nervous tissue surrounding the hair follicles in both species studied here, may be responsible for a sensory function. However, no behavioural studies have been performed in *B. suillus* that indicate that a spatial reaction is elicited in response to seismic vibrations or other tactile stimuli in the vibrissae-like hairs on the outer edges of the feet. Therefore, it cannot be confirmed that these hairs in *B. suillus* elicit a spatial response even though the hair follicle structure is similar to that of *H. glaber*. Consequently, in both *B. suillus* and *H. glaber* these hairs possibly play an important role in tactile communication between colony members. In addition to the detection of seismic vibrations, these hairs may play a role in moving loosened soil in the solitary *B. suillus* (Jarvis & Bennett, 1991).

### **5.3 Limitations, strengths and future research**

The current study yielded multiple limitations based on the animal specimens used. Information on the health, sex, breeding status and capture sites of some of the *Bathyergus suillus* mole-rat specimens were not available. Factors like health status and sex have an influence on muscle morphology and fibre type expression due to hormonal effects of

oestrogen. On the other hand, the *Heterocephalus glaber* specimens were all males that are subordinates and have not gone through puberty, therefore cancelling the effect of hormones on the muscle morphology and fibre type composition. These hormonal effects in *B. suillus* may have led to inconsistent results due to effects of hormones but also because both males and females were used in the sample.

The naked mole-rat specimens used were already fixed in 10% buffered formalin and therefore the staining protocols and techniques used for fibre typing had to be adapted for fixed tissue in order to compare with the fresh *B. suillus* specimens. If the specimens of both species were fresh, the stains could be compared and analysed more accurately. For example, the NADH stain was only applied to the fresh *B. suillus* and had to be compared to a PAS stain of the *H. glaber* tissue, that stained different metabolic substances within the muscle fibres. A stain comparison test was performed on specific fixed *B. suillus* muscles to confirm that the results would be comparable with the fixed *H. glaber* muscles. However, to compensate for this problem, a slow-myosin and PAS stain were applied on the fixed *B. suillus* muscles and yielded similar results to the same fresh muscles stained with a slow-myosin and NADH stain.

Kohn, Hoffman and Myburgh (2007) observed regionalisation of fibre types from proximal to distal in the quadratus femoris muscle group of the rat. Therefore, variation of fibre type composition between species may have been interpreted inaccurately if cross-sections were taken more distally or proximally to the origin or insertion. However, to counteract this, the present study used sections from the mid-bellies of the muscles and not from the proximal or distal sections.

Multiple Ruffini corpuscles (RCs) were observed in both *B. suillus* and *H. glaber*, however, no RCs were observed in the glabrous skin of the feet in *M. fascicularis* (macaque monkey; Darian-Smith, 1984; Paré *et al.*, 2002), raccoon (Rice & Rasmusson, 2000) as well as ground and tree squirrels (Brenowits, 1980). Paré *et al.* (2002) observed that sectioned portions of innervated blood vessels often appeared to have a typical Ruffini-like structure and therefore, misinterpretation of Ruffini corpuscles is possible. Therefore, the RCs observed in *B. suillus* and *H. glaber*, may possibly have been sectioned blood vessels or a longitudinal section of a peripheral nerve. The inclusion of a silver staining technique would have produced a higher accuracy in identifying not just RCs but the other mechanoreceptors as well. Due to time-

constraints caused by the COVID-19 pandemic, a silver stain was not used in the current study and may have led to inaccurate results of the RC densities.

The present study employed a multimodal approach to understand specific behaviours in these two mole-rat species. The combined results and use of multiple techniques of the muscle architecture, muscle fibre typing, and mechanoreceptors provided a holistic perspective on the functional morphology within the two species. Additionally, the methodology of the three sections of the study can be duplicated in studies with other species in order to understand behavioural or phylogenetic differences and/or adaptations. Multiple methods of measuring muscle architecture were applied to formulate more conducive results. One of the strengths of the current study is that different staining methods were applied to analyse the fibre type compositions; metabolic (NADH and PAS) and MHC-expression indicators. Furthermore, the Masson's trichrome stain was used to confirm the presence of nerve tissue and specific mechanoreceptors within the same serial sections stained with H&E. Additionally, the comparability between the fixed and fresh tissue allows for more replicable studies.

Further investigations on the subtypes of type II fibres in scratch-digging and chisel-tooth digging mole-rat species may provide a better understanding on how their digging methods or sociality may influence fibre type composition. Additionally, analysing the fibre type composition of other forelimb muscles such as the scapular muscles (*mm. subscapularis*, *supraspinatus* and *infraspinatus*) and *m. sternocleidomastoideus* may support the possible functional adaptations of the muscle architecture in these muscles in both species.

## 6 CONCLUSION

The present research study analysed the muscle architecture and muscle fibre type composition of the forelimb in *Bathyergus suillus* and *Heterocephalus glaber*. Additionally, somatosensory mechanisms such as tactile hairs and mechanoreceptors were examined in the footpads and lateral edges of the fore- and hindfeet of both species. The initial hypothesis was that the differences in these results between species, would reflect adaptations for their different digging and communication methods. *Bathyergus suillus* is a scratch-digging species and communicates mainly with seismic signals produced by hind foot-drumming. *Heterocephalus glaber* is a chisel-tooth digger and produces a wide range of vocalizations for interspecific communication.

The limb muscle mass distribution of both *B. suillus* and *H. glaber* (~75% proximally and ~25% distally) was similar to other fossorial and cursorial animals and may reflect the functional need of fossorial animals to rapidly move within their burrow systems. Higher percentages of type I fibres observed in the forelimb muscles in *B. suillus*, when compared to the hindlimb muscles, may provide sustained isometric contractions to stabilise the forelimb during hind foot-drumming. Muscle mass percentage, force output and shortening capacity of muscles involved in the power stroke of scratch-digging, were higher in *B. suillus* compared to *H. glaber*, and may reflect adaptations for scratch-digging in *B. suillus*. Low contraction velocity and high force output of *mm. subscapularis* (SuS) and *teres major* (TM) in *B. suillus* may counter the resistance of soil against limb retraction during scratch-digging and also stabilize its large body mass during locomotion, digging and hind foot-drumming. A significantly high percentage of slow fibres in TM further supports a stabilisation function of the scapula in *B. suillus*.

The muscle architecture and fibre type compositions of the neck muscles in *H. glaber* suggest adaptations for chisel-tooth digging. The high percentage of oxidative fibres in *m. sternohyoideus* (SH), large values of  $L_f/L_M$  ratio and physiological cross-sectional area (PCSA) in *m. sternocleidomastoideus* (SCM), and fast shortening capacity of both SH and SCM in *H. glaber*, may provide forceful and sustained movements of the head and jaw during chisel-tooth digging.

Although myosin heavy chain (MHC)-expression of muscle fibres are possibly not influenced by functional and environmental strains, metabolic transformation of oxidative and glycolytic fibres take place due to functional strains (Glaser, You, Zhang & Medler, 2009; Yan, Okutsu,

Akhtar & Lira, 2011). Significantly higher glycolytic fibres in the scapular elevators and digital flexors, which are dominant muscle groups in scratch-digging, in *B. suillus* may be a result of the functional demands of vigorous scratch-digging and not phylogeny. Regionalisation in the *m. clavícula-scapularis* of *B. suillus* points towards a multifunctional purpose to stabilise the scapula during locomotion as well as to provide fast movements during digging.

Higher densities of Meissner corpuscles in the footpads of *B. suillus* may function to detect seismic vibrations during hind foot-drumming. The presence of a few Pacinian corpuscles (PC) in the footpads of *H. glaber* can be attributed to either phylogeny or the detection of a seismic component to their high frequency vocalizations, while in *B. suillus*, PCs were not detected. High densities of Merkel cells in the footpads of both *B. suillus* and *H. glaber* suggest a tactile perception function for navigation in their burrows when they dig or forage for food.

The hairs observed on the lateral aspect of the feet in *B. suillus* and *H. glaber* did not have the distinct follicle-sinus complex typically seen in sensory hairs. However, the presence of Merkel cells within the outer root sheath as well as the nervous tissue surrounding these hairs in both species studied here, point towards a sensory function.

There are multiple aspects of the muscle architecture and fibre type compositions in the forelimb muscles of *B. suillus* that reflect possible adaptations for scratch-digging and hind foot-drumming. Additionally, specific mechanoreceptors within the footpads of *B. suillus* further point towards the detection of seismic signals produced during hind foot-drumming. However, the possibility still remains that these differences can be attributed to phylogeny. Future research can be performed on other African mole-rat species that are closely related to *B. suillus* and *H. glaber*.

## 7 REFERENCES

- Acosta, L. & Roy, R.R. 1987. Fiber-type composition of selected hindlimb muscles of a primate (cynomolgus monkey). *The Anatomical Record*, 218(2): 136-141.
- Álvarez, A. & Pérez, M. 2019. Deep changes in masticatory patterns and masseteric musculature configurations accompanied the eco-morphological evolution of cavioid rodents (Hystricognathi, Caviomorpha). *Mammalian Biology*, 96: 53–60. <https://doi.org/10.1016/j.mambio.2019.03.009>
- Armstrong, R.B., Saubert, C.W., Seeherman, H.J. & Taylor, C.R. 1982. Distributions of fibre types in locomotory muscles of dogs. *American Journal of Anatomy* 163:87–98
- Arnold, E.M., Ward, S.R., Lieber, R.L. & Delp, S.L. 2010. A model of the lower limb for analysis of human movement. *Annals of Biomedical Engineering* 38, 269–279. doi:10.1007/s10439-009-9852-5
- Avram, A. S., Avram, M. M., & James, W. D. 2005. Subcutaneous fat in normal and diseased states: 2. Anatomy and physiology of white and brown adipose tissue. *Journal of the American Academy of Dermatology* 53: 671-683.
- Bankhead, P., Loughrey, M.B., Fernández, J.A., Dombrowski, Y., McArt, D.G., Dunne, P.D., McQuaid, S., Gray, R.T., Murray, L.J., Coleman, H.G. & James, J.A. 2017. Open source software for digital pathology image analysis. *Scientific Reports*, 7:16878. <https://doi.org/10.1038/s41598-017-17204-50>.
- Behan, W.M.H., Cossar, D.W., Madden, H.A., & McKay, I.C. 2002. Validation of a simple, rapid, and economical technique for distinguishing type 1 and 2 fibres in fixed and frozen skeletal muscle. *Journal of Clinical Pathology* 55(5): 375-380.
- Bell, J., Bolanowski, S. & Holmes, M.H., 1994. The structure and function of Pacinian corpuscles: a review. *Progress in neurobiology*, 42(1): 79-128.
- Bennett, N.C. & Faulkes, C.G. 2000. African mole-rats: ecology and eusociality. Cambridge University Press, United Kingdom.
- Bennett, N.C. & Jarvis, J.U.M. 1988. The reproductive biology of the Cape mole-rat, *Georychus capensis* (Rodentia, Bathyergidae). *Journal of Zoology* 214:95–106.

- Bennett, N.C., Faulkes, C.G., Hart, L. & Jarvis, J.U.M. 2009. *Bathyergus suillus* (Rodentia: Bathyergidae). *Mammalian Species* 828:1-7
- Bergh, U. & Ekblom, B. 1979. Influence of muscle temperature on maximal muscle strength and power output in human skeletal muscles. *Acta physiologica scandinavica*, 107(1): 33-37.
- Blausen.com staff. 2014. "[Medical gallery of Blausen Medical 2014](#)". *WikiJournal of Medicine* 1 (2). DOI:10.15347/wjm/2014.010.
- Bloemberg, D., & Quadrilatero, J. 2012. Rapid determination of myosin heavy chain expression in rat, mouse, and human skeletal muscle using multicolor immunofluorescence analysis. *PloS one*, 7(4): e35273.
- Bodine, S.C., Roy, R.R., Meadows, D.A., Zernicke, R.F., Sacks, R.D., Fournier, M. & Edgerton, V.R. 1982 Architectural, histochemical, and contractile characteristics of a unique biarticular muscle: the cat semitendinosus. *Journal of Neurophysiology* 48, 192–201.
- Böhmer, C., Fabre, A.-C., Herbin, M., Peigné, S., & Herrel, A. 2018. Anatomical basis of differences in locomotor behaviour in martens: A comparison of the forelimb musculature between two sympatric species of *Martes*. *The Anatomical Record*, 301(3): 449–472.
- Bolanowski, S., & Zwislocki, J. J. 1984. Intensity and frequency characteristics of Pacinian corpuscle. II. Receptor potentials. *Journal of Neurophysiology*, 51: 812–830.
- Boulais, N & Misery, L. 2008. The epidermis: a sensory tissue. *European Journal of Dermatology*, 18: 119-27.
- Bouley, D.M., Alarcón, C.N., Hildebrandt, T. & O'Connell-Rodwell, C.E. 2007. The distribution, density and three-dimensional histomorphology of Pacinian corpuscles in the foot of the Asian elephant (*Elephas maximus*) and their potential role in seismic communication. *Journal of Anatomy* 211: 428-435.
- Brandner, J.M., Haftek, M & Niessen C.M. 2010. Adherens Junctions, Desmosomes and Tight Junctions in Epidermal Barrier Function. *The Open Dermatology Journal* 4: 14-20.
- Braude, S. 1991. Which naked mole-rats volcano? In: P. W. Sherman, J. U. M. Jarvis, and R. D. Alexander (eds.), *The biology of the naked mole-rat*, pp: 185- 194, Princeton University Press, New Jersey.

- Braude, S., Schilder, K. & Muli, J. 1999. Interspecific interactions between ants and naked mole-rats. *African Journal of Ecology* 37:241-245.
- Braverman, I. M. 2000. The Cutaneous Microcirculation. *Journal of Investigative Dermatology Symposium Proceedings* 5:3-9
- Brenowitz, G.L. 1980. Cutaneous mechanoreceptor distribution and its relationship to behavioural specialisations in squirrels. *Brain Behavioural Evolution* 17: 432-453.
- Brett, R. A. 1991. The population structure of naked mole-rat colonies. In “The Biology of the Naked Mole-Rat” Ed by PW Sherman, JUM Jarvis, RD Alexander.
- Brooke, M.H. & Kaiser, K.K. 1970. Muscle fiber types: how many and what kind? *Archives of Neurology* 23: 369-379.
- Brown, N., Kawcak, C.E., McIlwraith, C.W. & Pandey, M. 2003. Architectural properties of distal forelimb muscles in horses, *Equus caballus*. *Journal of Morphology* 258:106–114.
- Burgess, P. T. & Perl, E. R., 1973. Cutaneous mechanoreceptors and nociceptors. In: *Somatosensory system*, pp. 29-78, Springer, Berlin, Heidelberg.
- Burgin, C. J., Colella, J. P., Kahn, P. L. & Upham, N. S. 2018. How many species of mammals are there?. *Journal of Mammalogy*, 99(1): 1-14.
- Burke, R.E., 2011. Motor units: anatomy, physiology, and functional organization. *Comprehensive Physiology*, 345-422.
- Cain, B. W., Reynolds, T. & Sarko, D. K. 2019. Superficial, suprahyoid, and infrahyoid neck musculature in naked mole-rats (*Heterocephalus glaber*): Relative size and potential contributions to independent movement of the lower incisors. *Journal of Morphology*, 280(8): 1185-1196.
- Catania, K.C. & Kaas, J.H. 1995. Organization of the somatosensory cortex of the star-nosed mole. *Journal of Comparative Neurology* 351:549–567.
- Cauna, N. & Ross, L.L. 1960. The fine structure of Meissner's touch corpuscles of human fingers. *The Journal of Cell Biology*, 8(2): 467-482.
- Cauna, N. 1956. Nerve supply and nerve endings in Meissner's corpuscles. *American Journal of Anatomy* 99:315–327.

- Cauna, N. 1965. The effects of aging on the receptor organs of the human dermis. In: *Advances in the Biology of Skin*, Vol H: Aging, 63-96.
- Chambers, M.R., Andres, K.H., Duering, M. & Iggo, A. 1972. The structure and function of the slowly adapting type II mechanoreceptor in hairy skin. *Quarterly Journal of Experimental Physiology* 57:417-445.
- Charles, J.P., Cappellari, O., Spence, A.J., Hutchinson, J.R., & Wells, D.J. 2016. Musculoskeletal geometry, muscle architecture and functional specialisations of the mouse hindlimb. *PLoS One* 11(4).
- Chouchkov, H.N. 1971. Ultrastructure of Pacinian corpuscles in men and cats. *Zeitschrift fur Mikroskopisch-anatomische Forschung* 83:17-32.
- Crish, S.D., Rice, F.L., Park, T.J. & Comer, C.M. 2003. Somatosensory Organization and Behavior in Naked Mole-Rats I: Vibrissa-Like Body Hairs Comprise a Sensory Array That Mediates Orientation to Tactile Stimuli. *Brain Behavioural Evolution* 62: 141-151. <https://doi.org/10.1159/000072723>
- da Silva, A.P., Machado, A.S., Le Bas, A.E., Silva, R.G., dos Anjos Silva, E. & Hernandez-Blazquez, F.J., 2020. The skin structures and their role in the thermoregulation of the South American fur seal (*Arctocephalus australis*). *The Anatomical Record*, 303(12): 3155-3167.
- D'Elía, G., Fabre, P. H. & Lessa, E.P. 2019. Rodent systematics in an age of discovery: recent advances and prospects. *Journal of Mammalogy*, 100: pp.852-871.
- Darian-Smith, I. 1984. The sense of touch: performance and peripheral neural processes. In: Brookhart, J. M., Mountcastle, V.B. (eds), *The nervous system*, vol III: Sensory processes, part 2. pp 739-788, Bethesda, MD: American Physiological Association.
- Description, Dartmouth.edu. 2021. [online] Available at: <<http://anatomy.host.dartmouth.edu/CTO/homepage/Lab%204/Lab4%20Virtual/Lab4Histo.html?>> [Accessed 10 July 2021].
- Davies, K.C. & Jarvis, J.U.M. 1986. The burrow systems and burrowing dynamics of the mole-rats *Bathyergus suillus* and *Cryptomys hottentotus* in the fynbos of the southern-western Cape, South Africa. *Journal of Zoology* 209, 125-147.

- Davis, A.K., Brummer, S.P. & Shivik, J. 2010. Sexual differences in hair morphology of coyote and white-tailed deer: Males have thicker hair. *Annales Zoologici Fennici* 47: 411–416.
- Dellmann, H.D. & Eurell, J. 1998. Textbook of Veterinary Histology. 5<sup>th</sup> Edition., pp, 450, Philadelphia, Lea and Febiger.
- Douady, C.J., Chatelier, P.I., Madsen, O., de Jong, W.W., Catzeflis, F., Springer, M.S. & Stanhope, M.J., 2002. Molecular phylogenetic evidence confirming the Eulipotyphla concept and in support of hedgehogs as the sister group to shrews. *Molecular phylogenetics and evolution*, 25(1): 200-209.
- Doubell, N. S., Sahd, L. & Kotzé, S. H. 2020. Comparative forelimb morphology of scratch-digging and chisel-tooth digging African mole-rat species. *Journal of Morphology* 281(9): 1029-1046.
- Eason, J. M., Schwartz, G. A., Pavlath, G. K. & English, A. W. 2000. Sexually dimorphic expression of myosin heavy chains in the adult mouse masseter. *Journal of Applied Physiology*, 89(1): 251-258.
- Edin, B.B. & Abbs, J.H. 1991. Finger movement responses of cutaneous mechanoreceptors in the dorsal skin of the human hand. *Journal of Neurophysiology* 65:657–669.
- Edin, B.B. 1992. Quantitative analysis of static strain sensitivity in human mechanoreceptors from hairy skin. *Journal of Neurophysiology* 67:1105–13.
- Eng, C.M., Smallwood, L.H., Rainiero, M.P., Lahey, M., Ward, S.R. & Lieber, R.L. 2008. Scaling of muscle architecture and fiber types in the rat hindlimb. *Journal of Experimental Biology* 211: 2336–2345 DOI: 10.1242/jeb.017640
- English, A.W. 1984. An electromyographic analysis of compartments in cat lateral gastrocnemius muscle during unrestrained locomotion. *Journal of Neurophysiology* 52:114–125
- English, A.W. 1993 Compartmentalization of muscles and their motor nuclei: the partitioning hypothesis. *Physical Therapy* 3: 857– 867
- English, A.W., Eason, J., Schwartz, G., Shirley, A. and Carrasco, D.I. 1999. Sexual dimorphism in the rabbit masseter muscle: myosin heavy chain composition of neuromuscular compartments. *Cells Tissues Organs*, 164(4): 179-191.

- Erdoğan, B., 2017. Anatomy and physiology of hair. *Hair and Scalp Disorders*, 13.
- Eroschenko, V.P. 2008. Difiore's Atlas of histology with functional correlations 11<sup>th</sup> Edition Lippincott Williams & Wilkins 212-234.
- Erovic, I. & Erovic, B.M., 2013. Merkel cell carcinoma: the past, the present, and the future. *Journal of Skin Cancer*, 2013.
- Eulep.pdn.cam.ac.uk. 2021. *Skinbase - Mutant Mouse Skin Database*. [online] Available at: <[http://eulep.pdn.cam.ac.uk/~skinbase/2015\\_mutant\\_images.php?mutant=Anatomic\\_hair\\_types](http://eulep.pdn.cam.ac.uk/~skinbase/2015_mutant_images.php?mutant=Anatomic_hair_types)> [Accessed 10 July 2021].
- Faqi, A. S. 2017. A Comprehensive Guide to Toxicology in Nonclinical Drug Development, Second Edition. Elsevier, Cambridge. Chapter 1: Introduction
- Faulkes, C. G., Abbott, D. H. & Jarvis, J. U. 1991. Social suppression of reproduction in male naked mole-rats, *Heterocephalus glaber*. *Reproduction*, 91: 593–604.
- Faulkes, C.G. & Abbott, D.H. 1997. The physiology of a reproductive dictatorship: Regulation of male and female reproduction by a single breeding female in colonies of naked mole-rats. In Solomon, N.G. & French, J.A. (eds.), *Cooperative Breedings in Mammals*, pp 302–334, Cambridge Univ Press, Cambridge, UK.
- Feldhamer, G.A., Drickamer, L.C., Vessey, S.H., Merritt, J.F. & Krajewski, C. 2007. *Mammalogy: adaptation, diversity, ecology*. JHU press.
- Fransescoli, G. 2000. Sensory capabilities and communication in subterranean rodents. In *Life Undergroun: The Biology of Subterranean Rodents*, E. A. Lacey, J. L. Patton and G. N. Cameron (eds.), 111-144. Chicago, USA. The University of Chicago Press.
- Fundin, B.T., Arvidsson, J. and Rice, F.L., 1995. Innervation of nonmystacial vibrissae in the adult rat. *Journal of Comparative Neurology*, 357(4): 501-512.
- Fundin, B.T., Arvidsson, J., Aldskogius, H., Johansson, O., Rice, S.N. & Rice, F.L. 1997. Comprehensive immunofluorescence and lectin binding analysis of intervibrissal fur innervation in the mystacial pad of the rat. *Journal of Comparative Neurology*, 385(2): 185-206.
- Gans, C. & Bock, W.J. 1965. The functional significance of muscle architecture: a theoretical analysis. *Advances in Anatomy, Embryology and Cell Biology* 38: 115–142.

- Gans, C. & De Vries, F. 1987. Functional bases of fiber length and angulation in muscle. *Journal of Morphology*, 192: 63–85.
- Glaser, B. W., You, G., Zhang, M. & Medler, S. 2010. Relative proportions of hybrid fibres are unaffected by 6 weeks of running exercise in mouse skeletal muscles. *Experimental physiology*, 95(1): 211-221.
- Goldspink, G., Larson, R. E. & Davies, R. E. 1970. The immediate energy supply and the cost of maintenance of isometric tension for different muscles in the hamster. *Zeitschrift für vergleichende Physiologie*, 66(4): 389-397.
- Gregory, J.E., McIntyre, A.K. & Proske, U. 1986. Vibration-evoked responses from lamellated corpuscles in the legs of kangaroos. *Experimental brain research* 62: 648–653.
- Griffin, A.S., 2008. Naked mole-rat. *Current Biology*, 18(18): R844-R845.
- Haizlip, K. M., Harrison, B. C., & Leinwand, L. A. 2015. Sex-based differences in skeletal muscle kinetics and fiber-type composition. *Physiology*, 30(1): 30-39.
- Halata, Z., Schulze, W. & Hohne, K. H. 1986. The ultrastructure and computer-aided three-dimensional aspect of Ruffini corpuscles in human skin of the prepuce and pig skin of the nose. *Anatomical Record* 214:48A.
- Hamann, W. 1995. Mammalian cutaneous mechanoreceptors. *Progress in Biophysics & Molecular Biology* 64(1): 81-104.
- Hart, L., Chimimba, C. T., Jarvis, J. U. M., O’Riain, J. & Bennett, N. C. 2007. Craniometric sexual dimorphism and age variation in the South African Cape dune mole-rat, *Bathyergus suillus*. *Journal of Mammalogy* 88:657–666.
- Hausman, L. A. 1920. Structural characteristics of the hair in mammals. *The American Naturalist*, 5: 496-523.
- Hildebrand, M. & Goslow, G. E. 2001. Digging, and crawling without appendages. In: McFadden, P. (ed.), pp 455–474. *Analysis of Vertebrate Structure*. New York: Wiley.
- Hildebrand, M. 1985. Digging of quadrupeds. In: Hildebrand, M., Bramble, D. M., Liem, K. F. & Wake, D. B. (eds), *Functional Vertebrate Morphology* pp. 90–108. Cambridge: Belknap Press of Harvard University.

- Hoffer, J. A., Loeb, G. E., Sugano, N., Marks, W. B., O'Donovan, M. J. & Pratt, C. A. 1987. Cat hindlimb motoneurons during locomotion. III. Functional segregation in sartorius. *Journal of Neurophysiology* 57:554–562
- Honeycutt, R. L., Allard, M. W., Edwards, S. V. & Schlitter, D. A. 1991. Systematics and evolution of the family Bathyergidae, in Sherman, P. W., Jarvis, J. U. M. & Alexander, R. D. (eds.), *The Biology of the Naked mole-rat*. New Jersey: Princeton University Press, pp. 45-65.
- Hudson, P. E., Corr, S. A., Payne-Davis, R. C., Clancy, S. N., Lane, E. & Wilson, A. M. 2011. Functional anatomy of the cheetah (*Acinonyx jubatus*) forelimb. *Journal of Anatomy* 218:375–385.
- Hunt, C. C. 1961. On the nature of vibration receptors in the hind limb of the cat. *Journal of Physiology* 155: 175– 186.
- Hyvärinen, H., Kangasperko, H. & Peura, R., 1977. Functional structure of the carpal and ventral vibrissae of the squirrel (*Sciurus vulgaris*). *Journal of Zoology*, 182(4): 457-466.
- Ichikawa, H., Matsuo, T., Higurashi, Y., Nagahisa, H., Miyata, H., Sugiura, T. & Wada, N. 2019. Characteristics of muscle fibre type distribution in moles. *Anatomical Record* 302: 1010-1023.
- Iggo, A. & Muir, A.R., 1969. The structure and function of a slowly adapting touch corpuscle in hairy skin. *The Journal of physiology*, 200(3): 763-796.
- Iggo, A. & Ogawa, H. 1977. Correlative physiological and morphological studies of rapidly adapting mechanoreceptors in cat's glabrous skin. *Journal of Physiology* 266: 275–296.
- Isler, K., Payne, R. C., Gunther, M. M., Thorpe, S. K., Li, Y., Savage, R. & Crompton, R.H. 2006. Inertial properties of hominoid limb segments. *Journal of Anatomy* 209:201–218
- Jarvis, J. U. 198. Eusociality in a mammal: Cooperative breeding in naked mole-rat colonies. *Science* 212:571–573.
- Jarvis, J. U. M. & Bennett, N. C. 1991. Ecology and behavior of the family Bathyergidae. In P.W. Sherman, J. U. M. Jarvis, and R.D. Alexander (eds.), *The biology of the naked mole-rat*, pp. 66– 96. Princeton Univ. Press, Princeton
- Jarvis, J. U. & Sale, J. B. 1971. Burrowing and burrow patterns of East African mole-rats *Tachyoryctes*, *Heliophobius* and *Heterocephalus*. *Journal of Zoology*, 163(4): 451-479.

- Jarvis, J. U. M. & Sherman, P. W. 2002. *Heterocephalus glaber*. *BioOne*. 706: 1-9
- Jarvis, J. U. M. 1978. Energetics of survival in *Heterocephalus glaber* (Rüppell) the naked mole-rat (Rodentia: Bathyergidae). *Bulletin of the Carnegie Museum of Natural History* 6:81–87.
- Jarvis, J.U.M. 1969. The breeding season and litter size of African mole-rats. *Journal of Reproduction and Fertility Suppl.* 6:237-248.
- Kalmar, B., Blanco, G. & Greensmith, L. 2012. Determination of muscle fiber type in rodents. *Current Protocols in Mouse Biology* 2: 231-243.
- Kanitakis, J. 2002. Anatomy, histology and immunohistochemistry of normal human skin. *European Journal of Dermatology*. 12: 390-401.
- Kikuchi, Y. 2010. Comparative analysis of muscle architecture in primate arm and forearm. *Anatomia, Histologia, Embryologia* 39: 93–106.
- Kikuchi, Y., & Kuraoka, A. 2014. Differences in muscle dimensional parameters between non-formalin-fixed (freeze-thawed) and formalin-fixed specimen in gorilla (*Gorilla gorilla*). *Mammalian Study* 39(1): 65-72.
- Klauer, G., Burda, H. & Nevo, E. 1997. Adaptive differentiations of the skin of the head in a subterranean rodent, *Spalax ehrenbergi*. *Journal of Morphology* 233: 53–66.
- Knecht, L. 2012. The use of hair morphology in the identification of mammals. *Wildlife forensics: methods and applications*, 8:29-43.
- Kohn, T. A., Hoffman, L. C., & Myburgh, K. H. 2007. Identification of myosin heavy chain isoforms in skeletal muscle in four southern African wild ruminants. *Comparative Biochemistry and Physiology*, 148: 399–407.
- Kotzé, S. H., Van der Merwe, E. L., Ndou, R., O'Riain, M. J. & Bennett, N. C. 2009. The colonic groove or furrow: A comparative morphological study of six species of African mole-rats (Rodentia, Bathyergidae). *Journal of morphology*, 270(8): 966-975.
- Kotzé, S. H., Van der Merwe, E. L., Bennett, N. C. & O'Riain, M. J. 2010. The comparative anatomy of the abdominal gastrointestinal tract of six species of African mole-rats (Rodentia, Bathyergidae). *Journal of Morphology*, 271(1): 50-60.

- Lacey, E. A., Alexander, R. D., Braude, S. H., Sherman, P. W. & Jarvis, J. U. M. 1991. An ethogram for the naked mole-rat: Non-vocal behaviours. In *The biology of the naked mole-rat*, P. W. Sherman, J. U. M. Jarvis and R. D. Alexander (eds.), 209-242. Princeton, NJ: Princeton University Press.
- Lamas, L. P., Main, R. P., & Hutchinson, J. R. 2014. Ontogenetic scaling patterns and functional anatomy of the pelvic limb musculature in emus (*Dromaius novaehollandiae*). *PeerJ*, 2: e716.
- Leem, J. W., Willis, W. D., Weller, S. C. & Chung, I. M. 1993. Differential activation and classification of cutaneous afferents in the rat. *Journal of Neurophysiology* 70: 2411-2424.
- Lehmann, W.H. 1963. The forelimb architecture of some fossorial rodents. *Journal of Morphology*. 113: 59-76.
- Lessa, E. P. & Stein, B. R. 1992. Morphological constraints in the digging apparatus of pocket gophers (Mammalia: Geomyidae). *Biological Journal of the Linnean Society*. 47(4): 439-453.
- Lieber, R. L. & Ward, S. R. 2011. Skeletal muscle design to meet functional demands. *Philosophical Transactions of the Royal Society B* 366: 1466-1476.
- Lieber, R. L. 1992. Skeletal muscle structure and function: implications for physical therapy and sports medicine, pp. 300. Williams & Wilkins, Baltimore
- Loeser, J. D., Treede, R. D. 2008. The Kyoto protocol of IASP Basic Pain Terminology. *Pain* 137(3): 473–7.
- Loo, S. K. & Halata, Z. 1991. Innervation of hairs in the facial skin of marsupial mammals. *Journal of Anatomy* 174: 207-219.
- Makous, J. C., Friedman, R. M., & Vierck, C. J. 1995. A critical band filter in touch. *Journal of Neuroscience*, 15 (4): 2808–2818.
- Marotte, L. R., Rice, F. L., & Waite, P. M. E. 1992. The morphology and innervation of facial vibrissae in the tammarwallaby, *Macropuseugenii*. *Journal of Anatomy*. 180: 401–417.
- Marshall, C. D., Amin, H., Kovacs, K. M. & Lydersen, C. 2006. Microstructure and innervation of the mystacial vibrissal follicle-sinus complex in bearded seals, *Erignathus barbatus* (Pinnipedia: Phocidae). *The Anatomical Record Part A: Discoveries in Molecular,*

*Cellular, and Evolutionary Biology: An Official Publication of the American Association of Anatomists*, 288(1): 13-25.

Martin, M. L., Warbouton, N. M., Travouillon, K. J. & Fleming, P. A. 2019. Mechanical similarity across ontogeny of digging muscles in an Australian marsupial (*Isoodon fusciventer*). *Journal of Morphology* 280: 423-435.

Mason, M. J. & Narins, P. M. 2001. Seismic signal use by fossorial mammals. *American Zoology* 41: 1171-1184.

McConathy, D., Giddings, C. J. & Gonyea, W. J. 1983. Structure-function relationships of the flexor carpi radialis muscle compared among four species of mammals. *Journal of Morphology* 175: 279-292.

McIntosh, J. S., Ringqvist, M. & Schmidt, E. M. 1985. Fiber type composition of monkey forearm muscle. *The Anatomical Record* 211: 403-409.

Medler, S. 2002. Comparative trends in shortening velocity and force production in skeletal muscles. *American Journal of Physiology-Regulatory, Integrative and Comparative Physiology* 283: 368–378

Mendez, J. & Keyes, A. 1960. Density and composition of mammalian muscle. *Metabolism* 9:184–188.

Merzenich, M. M. & Harrington, T. 1969. The sense of flutter-vibration evoked by stimulation of the hairy skin of primates: Comparison of mechanoreceptive afferents innervating the hairy skin of monkeys. *Experimental Brain Research* 9: 236–260.

Meyer, W. 2009. Hair follicles in domesticated mammals with comparison to laboratory animals and humans. *Hair loss disorders in domestic animals*. Wiley-Blackwell, Ames, IA, 43-64.

Miller, M. R., Ralston, H. J. & Kasahara, M. 1958. The pattern of cutaneous innervation of the human hand. *American Journal of Anatomy* 102: 183–217.

Moore, A. L., Budny, J. E., Russell, A. P. & Butcher, M. T. 2013. Architectural specialisation of the intrinsic thoracic limb musculature of the American badger (*Taxidea taxus*). *Journal of Morphology* 274:35-48.

- Morgan, C. C. & Verzi, D. H. 2011. Carpal-metacarpal specializations for burrowing in South American octodontoid rodents. *Journal of Anatomy* 219: 167–175.
- Morimoto, T. & Takada, K., 1993. The sense of touch in the control of ingestion. In *Neurophysiology of Ingestion* , pp. 79-97. Pergamon Press, Oxford.
- Munger, B. L. 1971. Patterns of organization of peripheral sensory receptors. In Loewenstein, W. R. (ed.), *Handbook of Sensory Physiology, Chapter 1: Principles of Receptor Physiology*, pp. 523-556. Springer, Berlin.
- Munger, B. L., Page, R. B. & Pubols, B. H. 1979. Identification of specific mechanosensory receptors in glabrous skin of dorsal root ganglionectomized primates. *Anatomical Record* 193: 630-631
- Narins, P. M., Reichman, O. J., Jarvis, J. U. M & Lewis, E.R. 1992. Seismic signal transmission between burrows of the Cape mole-rat, *Georychus capensis*. *Journal of Comparative Physiology*, 170: 13-21.
- Nevo, E., 1979. Adaptive convergence and divergence of subterranean mammals. *Annual review of ecology and systematics*, 10(1): 269-308.
- Nowak, R. M. & Paradiso, J. L. 1983. *Walker's Mammals of the World*. 4th ed. Baltimore, The Johns Hopkins University Press, pp: 1362.
- Nowak, R. M. 1999. *Walker's mammals of the world*. 6th ed. The Johns Hopkins University Press, Baltimore.
- Ollausson, H., Wessberg, J. & Kakuda, N. 2000. Tactile directional sensibility: peripheral neural mechanisms in man. *Brain Research* 866: 178–187.
- Olson, R. A., Womble, M. D., Thomas, D. R., Glenn, Z. D. & Butcher, M. T. 2016. Functional morphology of the forelimb of the nine-banded armadillo (*Dasypus novemcinctus*): Comparative perspectives on the myology of Dasypodidae. *Journal of Mammalian Evolution*. 23:49-69. DOI 10.1007/s10914-015-9299-4.
- Otberg, N., Richter, H., Schaefer, H., Blume-Peytavi, H., Sterry, W. & Lademann, J. 2004. Variations of Hair Follicle Size and Distribution in Different Body Sites *Journal of Investigative Dermatology* 122:14 –19.

- Ounjian, M., Roy, R. R., Eldred, E., Garfinkel, A., Payne, J. R., Armstrong, A., Toga, A. W. & Edgerton, V. R. 1991. Physiological and developmental implications of motor unit anatomy. *Journal of Neurobiology* 22: 547–559.
- Oznurlu, Y., Celik, I., Sur, E., Telatar, T. & Ozparlak, H. 2009. Comparative skin histology of white new zealand and Angora rabbits: Histometrical and immunohistochemical evaluations. *Journal of animal and veterinary advances*. 8: 1694-1701.
- Paré, M., Smith, A. M. & Rice, F. L. 2002. Distribution and terminal arborizations of cutaneous mechanoreceptors in the glabrous finger pads of the monkey. *Journal of Comparative Neurology*. 445: 347-359.
- Park, T. J., Comer, C., Carol, A., Lu, Y., Hong, H. S. & Rice, F. L. 2003. Somatosensory organization and behavior in naked mole-rats: II. Peripheral structures, innervation, and selective lack of neuropeptides associated with thermoregulation and pain. *Journal of comparative neurology*, 465(1): 104-120.
- Park, T. J., Lu, Y., Jüttner, R., Smith, E. S. J., Hu, J., Brand, A., Wetzel, C., Milenkovic, N., Erdmann, B., Heppenstall, P. A. & Laurito, C. E. 2008. Selective inflammatory pain insensitivity in the African naked mole-rat (*Heterocephalus glaber*). *PLoS biology*, 6(1): p.e13.
- Pascalau, R. & Kuruvilla, R. 2020. A Hairy End to a Chilling Event. *Cell*, 182(3): 539-541.
- Pasi, B. M. & Carrier, D. R. 2003. Functional trade-offs in the limb muscles of dogs selected for running vs. fighting. *Journal of Evolutionary Biology* 16: 324-332.
- Patterson, B. D. 2016. Family Heterocephalidae (naked molerats). *Handbook of mammals of the world*, pp.342-351.
- Patterson, B. D. & Upham, N. S. 2014. A newly recognized family from the Horn of Africa, the Heterocephalidae (Rodentia: Ctenohystrica). *Zoological Journal of the Linnean Society*, 172(4): 942-963.
- Pawlina, W. & Ross, M. H. 2018. Histology: a text and atlas: with correlated cell and molecular biology. Lippincott Williams & Wilkins.
- Payne, R. C., Hutchinson, J. R., Robilliard, J. J., Smith, N. C. & Wilson, A. M. 2005. Functional specialization of pelvic limb anatomy in horses (*Equus caballus*). *Journal of Anatomy* 206:557–574.

- Pepper, J. W., Braude, S. H, Lacey, E. A. & Sherman, P. W. 1991. Vocalizations of the naked mole-rat. In P. W. Sherman, J. U. M. Jarvis, and R. D. Alexander (eds.), *The biology of the naked mole-rat*, pp. 243–274. Princeton Univ. Press, Princeton.
- Peter, J. B., Barnard, R. J., Edgerton, V. R., Gillespie, C. A. & Stempel, K. E. 1972. Metabolic profiles on three fiber types of skeletal muscle in guinea pigs and rabbits. *Biochemistry* 11, 2627-2733.
- Peters T, Kubis HP, Wetzel P, Sender S, Asmussen G, Fons R, Jürgens KD. 1999. Contraction parameters, myosin composition and metabolic enzymes of the skeletal muscles of the Etruscan shrew *Suncus etruscus* and of the common European white-toothed shrew *Crocidura russula* (Insectivora: soricidae). *Journal of Experimental Biology* 202: 2461–2473.
- Peters, S. E. & Rick, C. 1977. The actions of three hamstring muscles of the cat: a mechanical analysis. *Journal of Morphology*. 152 (3): 315-28. DOI: 10.1002/jmor.1051520304
- Pinto, M., Jepsen, K. J., Terranova, C.J. & Buffenstein, R. 2010. Lack of sexual dimorphism in femora of the eusocial and hypogonadic naked mole-rat: a novel animal model for the study of delayed puberty on the skeletal system. *Bone*, 46(1): 112-120.
- Powell, P. L., Roy, R. R., Kanim, P., Bello, M. & Edgerton, V. R. 1984. Predictability of skeletal muscle tension from architectural determinations in guinea pig hindlimbs. *Journal of Applied Physiology* 57: 1715–1721.
- Raichlen, D. A. 2006. Effects of limb mass distribution on mechanical power outputs during quadrupedalism. *Journal of Experimental Biology*. 209: 633-644.
- Randall, J. A. 2001. Evolution and function of drumming as communication in mammals. *American Zoology* 41: 1143-1156.
- Randall, J. A. 2014 Vibrational communication: spiders to kangaroo rats. In: Witzany, G. (ed) *Biocommunication of Animals*. pp 103–133, Springer, Dordrecht,
- Rein, S., Hanisch, U., Zwipp, H., Fieguth, A., Lwowski, S. & Hagert, E. 2013. Comparative Analysis of Inter-and Intraligamentous Distribution of sensory Nerve Endings in Ankle Ligaments: A Cadaver Study. *American Orthopaedic Foot & Ankle Society*. 20(10): 1-8.

- Rice, F. L. & Munger, B. L. 1986. A comparative light microscope analysis of the sensory innervation of the mystacial pad. II. The common fur between the vibrissae. *Journal of Comparative Neurology* 252:186-205.
- Rice, F. L., Kinnman, E., Aldskogius, H., Johansson, O. & Arvidsson, J. 1993. The innervation of the mystacial pad of the rat as revealed by PGP 9.5 immunofluorescence. *Journal of Comparative Neurology* 337: 366–385.
- Rice, F. L. & Rasmusson, D. D. 2000. Innervation of the digit on the forepaw of the racoon. *Journal of Comparative Neurology* 417:467–490.
- Rice, F. L., Fundin, B. T., Arvidsson, J., Aldskogius, H. & Johansson, O. 1997. A comprehensive immunofluorescence and lectin binding analysis of vibrissal follicle sinus complex innervation in the mystacial pad of the rat. *Journal of Comparative Neurology* 385:149–184.
- Rice, F. L., Mance, A. & Munger, B. L. 1986. A comparative light microscopic analysis of the sensory innervation of the mystacial pad. I. Innervation of vibrissal follicle-sinus complexes. *Journal of Comparative Neurology* 252:154-174.
- Rivero, J. L. 2018. Locomotor muscle fibre heterogeneity and metabolism in the fastest large-bodied rorqual: the fin whale (*Balaenoptera physalus*). *Journal of Experimental Biology*. 22;221: jeb177758. <https://doi.org/10.1242/jeb.177758>
- Rose, J. A., Sandefur, M., Huskey, S., Demler, J. L., & Butcher, M. T. 2013. Muscle architecture and out-force potential of the thoracic limb in the eastern mole (*Scalopus aquaticus*). *Journal of Morphology* 274: 1277–1287. DOI: 10.1002/jmor.20178
- Rupert, J. E., Rose, J. A., Organ, J. M. & Butcher, M. T. 2015. Forelimb muscle architecture and composition in the groundhog (*Marmota monax*). *Journal of Experimental Biology*. 218: 194-205. doi: 10.1242/jeb.107128
- Sacks, R. D. & Roy, R. R. 1982. Architecture of the hindlimb muscles of cats: functional significance. *Journal of Morphology* 173: 185–195. DOI:10.1002/jmor.1051730206
- Sahd, L., Bennett, N. C. & Kotzé, S. H. 2021. Hind foot drumming: Volumetric micro-computed tomography investigation of the hind limb musculature of three African mole-rat species (Bathyergidae). *Journal of Anatomy*.

- Sargeant, A. J. 1987. Effect of muscle temperature on leg extension force and short-term power output in humans. *European journal of applied physiology and occupational physiology*, 56(6): 693-698.
- Savolainen, J. & Vornanen, M. 1995. Fiber types and myosin heavy chain composition in muscles of common shrew (*Sorex araneus*). *Journal of Experimental Zoology*, 271(1): .27-35.
- Schiaffino, S. & Reggiani, C. 2011. Fiber types in mammalian skeletal muscles. *Physiological reviews*, 91(4): 1447-1531.
- Schneider, C. A., Rasband, W. S. & Eliceiri, K. W. 2012. NIH Image to ImageJ: 25 years of image analysis. *Nature Methods* 9: 671–675
- Schneider, E. R., Gracheva, E. O. & Bagriantsev, S. N. 2016. Evolutionary specialization of tactile perception in vertebrates. *Physiology*, 31(3):193-200.
- Sharir, A., Milgram, J. & Shahar, R. 2006. Structural and functional anatomy of the neck musculature of the dog (*Canis familiaris*). *Journal of anatomy*, 208(3): 331-351.
- Skinner, J. D., & Smithers, R. H. N. 1990. The mammals of the southern African subregion. Cape and Transvaal Printers, Pretoria, South Africa.
- Smith, K. R. 1970. The ultrastructure of human “Haarscheibe” and Merkel cell. *Journal of Investigative Dermatology* 54: 150–159.
- Sokolov, V. E. 1982. Mammal skin, pp. 1-695. University of California Press, Berkeley.
- Suzuki, M. 1990. Fractal decomposition of exponential operators with applications to many-body theories and Monte Carlo simulations. *Physics Letters A*, 146(6): 319-323.
- Stains, H. J. 1958. Field key to guard hair of Middle Westerns furbearers. *The Journal of Wildlife Management*, 22: 95-97.
- Talbot, J. & Maves, L. 2016. Skeletal muscle fibre type: using insights from muscle developmental biology to dissect targets for susceptibility and resistance to muscle disease. *Wiley Interdisciplinary Reviews-Developmental Biology* 5(4): 518-534
- Tavares, W. C. & Seuánez, H. N. 2018. Changes in selection intensity on the mitogenome of subterranean and fossorial rodents respective to aboveground species. *Mammalian Genome*, 29(5): 353-363.

- Taylor, J. L. 2009. Proprioception. In Bloom, F. E., Spitzer, N. C., Gage, F., & Albright, T (eds.), *Encyclopedia of Neuroscience*, pp.1143–1149. Academic Press, Massachusetts.
- Thigpen, L. W. 1940. Histology of the skin of a normally hairless rodent, *Journal of Mammalogy*. 21:449-456.
- Thompson, S. W. & Hunt, R. D. 1966. Selected histochemical and histopathological methods.
- Tridico, S. 2005. Examination, analysis, and application of hair in forensic science- animal hair. *Forensic Science Review*, 17: 18-28.
- Von Mering, F. & Fischer, M. S. 1999. Fibre type regionalization of forelimb muscles in two mammalian species, *Galea musteloides* (Rodentia, Caviidae) and *Tupaia belangeri* (Scandentia, Tupaiidae) with comments on postnatal myogenesis. *Zoomorphology* 119: 117-126.
- Wallace, M. L., Chen, C. H., Chorev, E. & Brecht, M. 2013. Structure, function, and cortical representation of the rat submandibular whisker trident. *Journal of Neuroscience*, 33(11): 4815-4824.
- Walmsley, B., Hodgson, J. A. & Burke, R. E. 1978. Forces produced by medial gastrocnemius and soleus muscles during locomotion in freely moving cats. *Journal of Neurophysiology* 41: 1203–1216
- Wang, L.C. & Kernell, D. 2001. Fibre type regionalisation in lower hindlimb muscles of rabbit, rat and mouse: a comparative study. *The Journal of Anatomy*, 199(6): 631-643.
- Ward, S. R. & Lieber, R. L. 2005 Density and hydration of fresh and fixed skeletal muscle. *Journal of Biomechanics* 38: 2317– 2320 doi:10.1016/j.jbiomech.2004.10.001
- Williams, S. B., Payne, R. C. & Wilson, A. M. 2007. Functional specialization of the thoracic limb of the hare (*Lepus europeus*). *Journal of Anatomy* 210: 491–450.
- Windhorst, U., Hamm, T. M. & Stuart, D. G. 1989. On the function of muscle and reflex partitioning. *Behavioural Brain Science* 12: 629–681
- Winters, T. M., Takahashi, M., Lieber, R. L. & Ward, S. R. 2010. Whole muscle length-tension relationships are accurately modelled as scaled sarcomeres in rabbit hindlimb muscles. *Journal of Biomechanics* 44: 109–115.

Yan, Z., Okutsu, M., Akhtar, Y. N. & Lira, V. A. 2011. Regulation of exercise induced fiber type transformation, mitochondrial biogenesis, and angiogenesis in skeletal muscle. *Journal of Applied Physiology*. 110: 264-274.

Yochem, P. K. & Stewart, B. S. 2018. Hair and fur. In *Encyclopedia of marine mammals*, pp. 447-448. Academic Press: Massachusetts

Young, B., Woodford, P. & O'Dowd, G. 2006. *Wheater's functional histology E-Book: a text and colour atlas*. Elsevier Health Sciences.

Zajac, F. E. 1992. How musculotendon architecture and joint geometry affect the capacity of muscles to move and exert force on objects: A review with application to arm and forearm tendon transfer design. *Journal of Hand Surgery* 17: 799–804.

**Addendum A: Slow myosin immunohistochemical staining procedure (adapted from Kalmar *et al.*, 2012)**

Dilution of Antibody:

MHCs 1:40 dilution

5ul of AB (incubated at 37° C) with 195ul of TRIS

Method:

1. Freeze the muscle in n-pentane cooled in liquid nitrogen.
2. Cut sections from the test muscle onto positively charged slides and a section of control muscle as a positive control.
3. Cut a negative control incubated with the Novocastra Post Primary.
4. Circle the sections with a diamond pencil to ensure the antibody is restricted to the desired area.
5. Apply 35-50 µl of the primary antibody to each of the sections for 60 minutes in a humidity chamber at 37° C. Apply TRIS buffer to the negative control.
6. Wash gently in TBS (TRIS buffered saline pH 7.6) for 5 to 10 minutes.
7. Wipe around the edges of the section and immediately apply 35-50 µl of the post-primary antibody for 15 minutes.
8. Wash gently in TBS (TRIS buffered saline pH 7.6) for 5 to 10 minutes.
9. Wipe around the edges of the section and apply 35-50 µl of the Novolink Polymer for 15 minutes.
10. Make up a 1:20 DAB solution using the Leica DAB Polymer Kit Novocastra Novolink.
  - a. Add 100 µl of DAB Chromogen to 1900 µl DAB Substrate Buffer
  - b. Filter the DAB solution into a separate tube using a syringe filter and a syringe.
11. Dry the slide around the edge and immediately apply ± 50 µl DAB solution to each section and incubate at room temperature for 4-6 minutes.
12. Wash the sections in tap water.
13. Counterstain with haematoxylin for 1 minute
14. Wash in running tap water until cleared.
15. Dehydrate, clear and mount.

**Addendum B: NADH staining protocol****Reagents:**

0.01 g NBT (Nitroblue tetrazolium salt)

0.008 g NADH (reduced phosphopyridene nucleotide)

10 ml 0.2 M TRIS buffer @ pH 7.4

<b>TRIS buffer:</b>	100ml	250ml
Hydroxylmethylamino methane	0.606 g	1,515 g
Distilled water	58 ml	145 ml
0.1M Hydrochloric acid	42 ml	105 ml

**Procedure:**

- Cut 7/8  $\mu\text{m}$  thick cryosections of the specific muscle are placed on standard histological slides and allow to air dry
- Add the NBT to the TRIS buffer
- Place all reagents on the tissue
- Place the slides in a humidity chamber at incubate 37° C for 30-45 minutes
- Rinse slides in distilled water
- Mount coverslips with glycerine jelly/ glycergel

**Results:**

NADH- will stain blue

Type I fibres – Dark blue

Type II fibres – Light blue

## **Addendum C: Periodic Acid Schiff (PAS) staining protocol**

### • Reagents

1. Haematoxylin (Gill's)
2. 1.0% Periodic Acid Solution (1gram in 100ml water)
3. Schiff's Reagent

### • Method

1. Deparaffinise and hydrate slides to distilled water
2. Oxidize in 1.9% periodic acid solution for 10 minutes
3. Rinse in distilled water
4. Place in Schiff reagent for 20 minutes (sample should become light pink during this step)
5. Wash in lukewarm tap water for 7 minutes and 30 seconds (immediately sections turn dark pink colour)
6. Counterstain in Mayer's Haematoxylin solution for 30 seconds
7. Wash in tap water for 3 minutes
8. Dehydrate and clear as usual
9. Mount samples using DPX

### • Interpretation of results

- Acid mucosubstance present blue
- Neutral polysaccharides present Magenta
- Mixture of the above will present blue/purple
- Nuclei will present blue/black

## **Addendum D: Masson's Trichrome staining protocol**

### Reagents:

1. Solution a:

- Acid fuchsin 0.5 g
- Glacial acetic acid 0.5 ml
- Distilled water 100 ml

2. Solution b:

- Phosphomolybdic acid 1 g
- Distilled water 100 ml

3. Solution c:

- Methyl blue 2 g
- Glacial acetic acid 2.5 ml
- Distilled water 100 ml

### • Method:

1. Deparaffinize sections and take to water.
2. Remove mercury pigment by iodine, sodium thiosulfate sequence.
3. Wash in tap water.
4. Stain nuclei by the celestine blue-haematoxylin method.
5. Differentiate with 1% acid alcohol.
6. Wash well in tap water.
7. Stain in acid fuchsin Solution a, 5 minutes.
8. Rinse in distilled water.
9. Treat with phosphomolybdic acid Solution b, 5 minutes.
10. Drain.

11. Stain with methyl blue Solution c, 2–5 minutes.
12. Rinse in distilled water.
13. Treat with 1% acetic acid, 2 minutes.
14. Dehydrate through ascending grades of alcohol.
15. Clear in xylene, mount in permanent mounting medium.

• Results:

Nuclei = blue/black

Cytoplasm, muscle, and erythrocytes = red

Collagen = blue

**Addendum E: Histological processing protocol**

<b>Order</b>	<b>Solution</b>	<b>Duration</b>	<b>Purpose</b>
<b>1</b>	Formaldehyde	12-24 hours	Fixation
<b>2</b>	Alcohol 70%	2.0 hours	Dehydration
<b>3</b>	Alcohol 96%	1.5 hours	Dehydration
<b>4</b>	Alcohol 96%	1.5 hours	Dehydration
<b>5</b>	Alcohol 99%	1.5 hours	Dehydration
<b>6</b>	Alcohol 99%	1.5 hours	Dehydration
<b>7</b>	Alcohol 99%	1.5 hours	Dehydration
<b>8</b>	Xylene	1.5 hours	Clearing
<b>9</b>	Xylene	1.0 hours	Clearing
<b>10</b>	Paraffin Wax	2.0 hours (60°C)	Processing
<b>11</b>	Paraffin Wax	2.0 hours (60°C)	Processing

**Addendum F: Plagiarism report**

Match Overview			×
<b>10%</b>			
<hr/>			
<			>
1	L. Sahd, N. C. Bennett, ... Publication	3%	>
2	Lauren Sahd, Narusa D... Publication	2%	>
3	Narusa S. Doubell, Laur... Publication	2%	>
4	Submitted to University... Student Paper	2%	>
5	José-Luis L. Rivero. " L... Publication	1%	>